universität wien

MASTERARBEIT

Titel der Masterarbeit

Reservoir properties of glauconite sandstones (Greifenstein Formation) in the quarry Strombauamt

Verfasserin

Raffaela Löffler BSc.

angestrebter akademischer Grad

Master of Science (MSc.)

Wien, Jänner 2013

Studienkennzahl lt. Studienblatt:	A 066815
Studienrichtung lt. Studienblatt:	Erdwissenschaften
Betreuerin / Betreuer:	Ao. Univ. Prof. Mag. Dr. Susanne Gier

Index

Acknowledgments

As part of this thesis, I would like to thank the following people who accompanied and helped me on this path.

I would like to thank my supervisor Susanne Gier, for allowing me to participate actively in this project and for always supporting me. She has always helped me with her advice.

I would also like to thank Michael Wagreich, who helped me in the field to map the profiles on the east wall and gave me valuable advice concerning the structures. Further, Kurt Decker for his help collecting the sample of the south wall and his help during my field work.

I would also like to thank Mr. Walter Strasser of the Technischen Prüfanstalt, who has taken a closer look at the porosity methods.
In addition, I also want to thank Mr. Gumpenberger at the OMV in Gänserndorf, for his explanations and help concerning the micropermeamter and for helping me with my measurements.

Special thanks to my whole family, who always built me up and always motivated me.

Of course I would like to thank my best friend Doris, for her advice and help with some methods.

I would like to thank Andrea Schicker. She always gave me good tips about my work and helped me, when I had problems.

Last but not least, I would like to thank Sabine Hruby-Nichtenberger, for her help dyeing the thin sections and her explanations concerning the handling of the various machines I used for my work.

Abstract

The reservoir properties of glauconitic sandstones of the Greifenstein Formation in the quarry Strombauamt in Lower Austria were investigated to find analogues to deep-water sandstones buried below the Neogene of the Vienna Basin. The upper Paleocene to lower Eocene Greifenstein Formation is the uppermost unit of the Greifenstein nappe, belonging to the Rhenodanubian Flysch Zone. Lithologically it contains glauconite rich, partly weathered sandstones and conglomerates, as well as typical classical turbidites. Further, siltstones and mudstones can be found.

Two sections were measured and logged in the quarry (eastern and southern quarry walls). The succession consists of thick-bedded massive sandstones with few intercalated shale layers. Few ripple layers and laminated beds were found. In the eastern, stratigraphically younger part of the section the percentage of glauconite is much higher than in the southern section. The southern section consists of conglomerates at the base, thick-bedded sandstones with turbidites in the middle and thin-bedded sandstones on the top.

Geometries and sedimentary features of the massive and thick-bedded sandstones indicate the presence of small (5-15 m wide) roughly east-west trending channels which show varying degree ofconnectivity.

The sandstones were classified after Folk (1968), all of them are glauconite rich quartz arenites. The percentage of quartz (mono- and polycrystalline) in the samples ranges between 55 and 75 %, glauconite ranges between 12 and 33 %.

The mineralogical composition of the individual samples was determined with an X-ray diffractometer. The samples contain quartz, calcite, glauconite, orthoclase, and occasionally ankerite. The calcite content evident in the x-ray patterns is based on the presence of fossils and calcite cement in the sandstone samples.

With cathodoluminescence (CL) microscopy an orange-red luminescing cement could be seen, it was identified as Fe-bearing calcite.

The porosities and permeabilites of the sandstone and conglomerate samples were determined by two methods: the determination of the net density with a pycnometer and the determination of the bulk density with immersion weighting. The results of 2 to 8 % porosity of the majority of the sandstone samples indicate that these rocks do not posses good

reservoir properties. For determining the permeability a micropermeameter was used. The results range generally between 4.5 and 6.5 mD.

The stage of maturation and the chemical composition of glauconite were determined with electron microprobe (EMP). The glauconites in samples GR 78.5 and GRO 3 are well developed and do not contain expandable clay minerals. Due to the low porosity and permeability values of the sandstone samples it can be stated, that the reservoir properties of sandstones of the exposed Greifenstein Formation are poor and that the reservoirs in the subsurface of the Vienna basin must be fracture-related. Fracture porosity and permeability will be evaluated in a next step. This project is part of a University cooperation project with OMV Exploration and Production GesmbH.

Zusammenfassung

Die Reservoireigenschaften des Glaukonitsandsteins der Greifenstein Formation im Steinbruch Strombauamt (Niederösterreich) wurden bestimmt, um diese mit analogen Sedimenten im Untergrund des Wiener Beckens zu vergleichen. Bei der Greifenstein Formation (Oberes Paleozän bis unteres Eozän) handelt es sich um die oberste Einheit der Greifensteiner Decke, die ein Teil der Rhenodanubischen Flyschzone ist. Lithologisch besteht diese aus Glaukonit-reichen Sandsteinen, die im Aufschluss stark verwittert sind, Konglomeraten, und auch aus klassischen Turbiditen. Ebenfalls sind Siltsteine und Tonsteine anzutreffen.

Im Steinbruch wurden zwei 2D Profile aufgenommen (einerseits die östliche und andererseits die südliche Steinbruchwand). Diese bestehen hauptsächlich aus dick-bankigen massiven Sandsteinen mit eingelagerten Tonschichten. Gelegentlich konnten Rippelschichtung und Laminationen angetroffen werden. Im östlichen, stratigraphisch jüngeren Teil des Aufschlusses, ist der Anteil an Glaukonit höher als in der südlichen Einheit.
Das südliche Profil besteht aus Konglomeraten an der Basis, dick-bankigen Sandsteinen mit Turbiditen im Mittelteil, und dünn-schichtigen Sandsteinen am Top. Die massiven dick-bankigen Sandsteinlagen zeigen ost-west streichende Rinnenstrukturen mit einer lateralen Ausdehnung von 5-15 m. Nach der Klassifikation von Folk (1968) können die Sandsteine als glaukonitführende Quarzarenite eingestuft werden. Der Anteil an Quarz, sei es mono- bzw. polykristallin, beträgt zwischen 55 und 75 % und der Anteil an Glaukonit 12 und 33 %.

Die mineralogische Zusammensetzung wurde mittels Röntgendiffraktometrie bestimmt. Die Proben enthalten Quarz, Calcit, Glaukonit, Orthoklas und teilweise Ankerit. Die Anwesenheit von Calcit ist auf den reichlichen Anteil an Fossilfragmenten und Kalzitzement innerhalb der Proben zurückzuführen. Mit Kathodenlumineszenz konnte, auf Grund der orangeroten Lumineszenzfarben, Kalzitzement bestimmt werden.
Die Porositäten bzw. Permeabilitäten wurden mittels zwei verschiedener Methoden bestimmt: Bestimmung der Reindichte durch die Hilfe eines Pyknometers und die Bestimmung der Rohdichte durch die Tauchwägung. Die Porositäten liegen zwischen 2 und 8 %, was darauf schließen lässt, dass es sich bei den Gesteinsproben um keine guten Speichergesteine für Erdöl bzw. Erdgas handelt.

Für die Bestimmung der Permeabilität wurde ein Mikropermeameter benutzt. Die Ergebnisse liegen zwischen 4.5 und 6.5 mD.
Mit Hilfe der Mikrosonde konnten genaue chemische Untersuchungen von Glaukoniten und des Kalzitzements gemacht werden mit dem Ergebnis, dass es sich beim Glaukonit um einen reifen Glaukonit handelt sowie, dass es sich beim Zement um einen eisenhaltigen Kalzitzement handelt.
Aufgrund der niedrigen Porositäts- und Permeabilitätswerte der Sandsteinproben kann gesagt werden, dass die Sandsteine der Greifenstein Formation schlechte Reservoireigenschaften haben und dass es sich bei den Reservoirs im Untergrund des Wiener Beckens um Kluftspeicher handelt.

Diese Arbeit ist Teil eines Projektes zwischen der Universität Wien und der OMV Exploration und Produktion GesmbH.

1. Introduction

The present MSc thesis is part of a research project in cooperation with OMV Exploration and Production GesmbH named “Flysch Vienna Basin – tectonics, stratigraphy, lithofacies, reservoir properties and clay mineralogy of the Rhenodanubic Flysch units in the subcrop of the Vienna Basin”.

The research project and the present study were initiated because of a renewed interest in the Flysch units in the subsurface of the Vienna Basin as a target for oil and gas exploration. Because of the limited availability of subsurface data, outcrop analogues are used to gain a better understanding of the Flysch in the subsurface.

The present work focussed on the reservoir properties of the sandstones of the Greifenstein Formation. To characterize reservoir properties, porosities and permeabilities were measured. Controlling factors like the mineralogical and chemical composition of the sandstones had to be established, too.

Samples were taken from the quarry Strombauamt, which is located between Höflein an der Donau and Greifenstein (Lower Austria). Two sections were measured and sampled. This was followed by laboratory work on these samples.

2. General Geology

2.1 Geology and Stratigraphy of the Flysch zone

The Greifenstein Formation is part of the Rhenodanubian Flysch zone which extends west-east, from Vorarlberg to Vienna. In the region of Vienna the zone continues below the Neogene of the Vienna Basin (Egger, 1992; Besada, 1996) (figure 1).

The Greifenstein Nappe is the northernmost and deepest of the three main tectonic units of the Wienerwald flysches and is overlain by the Laab and Kahlenberg Nappe (Götzinger, 1954; Prey, 1962).

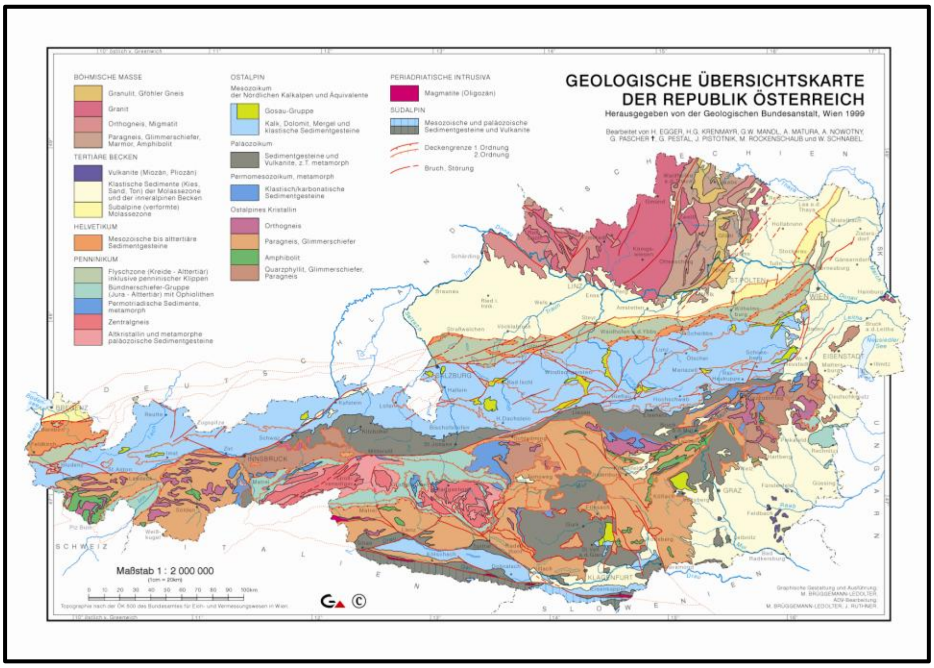

Figure 1 Geology of Austria – In green the Rhenodanubian Flysch zone (Geologische Bundesanstalt, 1996)

The depositional environments of the flysch range from submarine landslides to turbidity currents (Kuenen and Migliorini, 1950). The flysch deposits are regarded as deep-sea sediments of a submarine fan (delta-fan). These were sediments, which resedimented by tectonic movements, earthquakes, hurricanes, but also volcanic activities (Dengler and Wilde, 1983). Characteristic features are the formation and deposition of turbidites, which resulted in complete or incomplete Bouma sequences.

The Rhenodanubian Flysch zone comprises four tectonic units, which extend from north to south (Faupl, 1996; Wessely, 2006) (figure 2):

- Northern Margin Zone
- Greifenstein Nappe
- Laab Nappe
- Kahlenberg Nappe

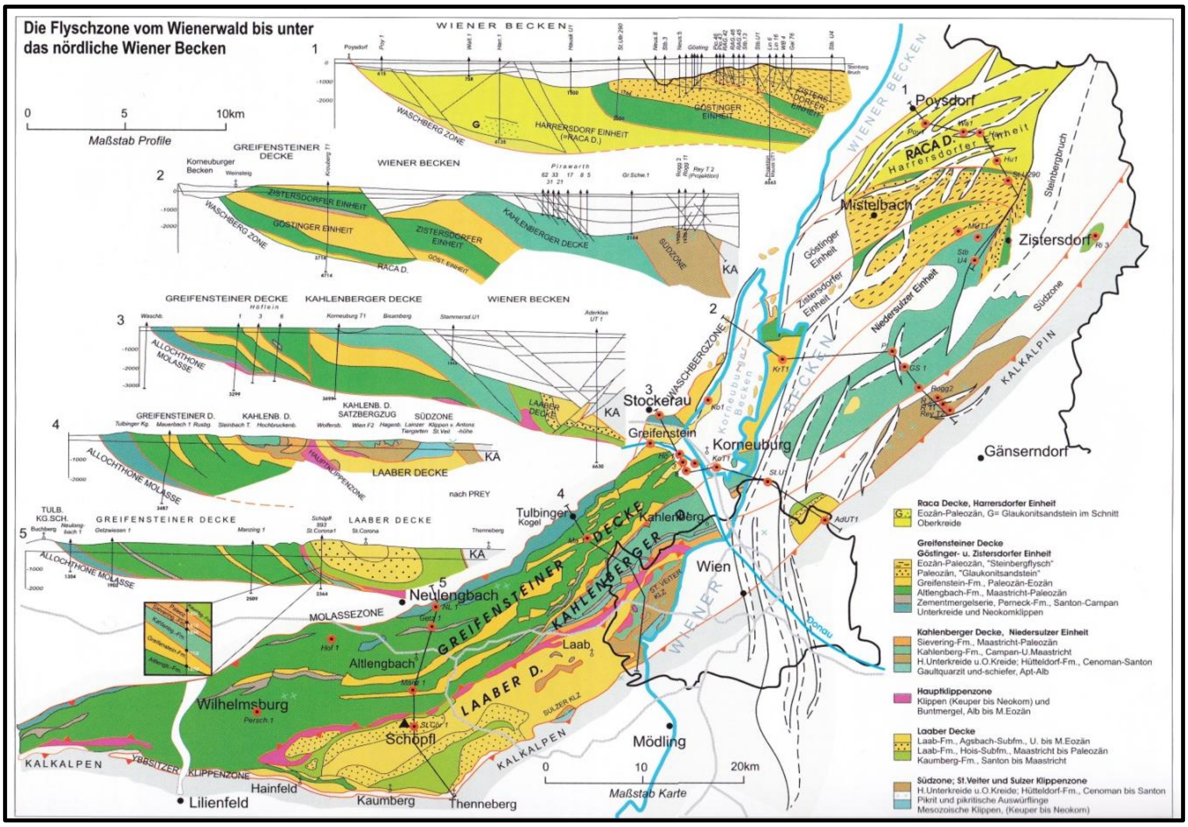

Figure 2 The Flysch zone - The Wienerwald and northern Vienna Basin: Map of the distribution of tectonic units and depth profiles (Wessely, 2006)

Figure 2 is modified after Prey (1980), Grün (1984), Rammel (1989) and Schnabel (1997).

The different tectonic units are shown in the stratigraphic chart (table 1).

The classification of the Rhenodanubian Flysch in single layer elements is always controversial and not yet fully understood. In this study, however, the latest aspects of the research are introduced (table 1).

The *Wolfpassing Fomation* belongs to the **Northern Margin Zone**. This is considered to be the stratigraphic basin of the Greifenstein Nappe (Sauer et al., 1992) or a separate tectonic unit (Faupl, 1996). Jäger (1914) referred to it as Neokomflysch, which is constituted by thin-bedded calcareous mud-turbidites.

The chronostratigraphic age of this unit ranges from the Barremian to the early Aptian/Albian (Grün et al., 1972) and it has a thickness of 100 m. The Tristel Formation is located laterally to it (table 1).

The **Greifenstein Nappe** includes several formations and members. The main lithostratigraphic units are the Röthenbach Subgroup, the Perneck Formation, the Altlengbach Formation and the Greifenstein Formation.

The *Rehbreingraben Formation* also refered to Gault-Flysch (Prey, 1950) consists of pelagic shales and sandstones. The turbidites show a typical Bouma sequence, except for the absence of the Ta sequence. The turbidites and mudstones suggest a deposition below the CCD (calcite compensation depth) from a suboxic to anoxic environment (Wortmann et al., 2004). The formation was deposited from middle Barremian to late Albian and has a thickness of about 250 m (Wagreich, 2012 (OMV Report)).

The *Ofterschwang Formation* consists of calcareous and non-calcareous marlstones with a large variety of silts. The origin of these calcareous turbidites is suggested to be below the CCD. The unit has a chronostratigraphic age from late Albian to early Cenomanian and is about 100 m thick. It is located laterally of the Untere Bunte Schiefer (Wagreich, 2012 (OMV Report)).

According to Egger and Schwerd (2008) the *Untere Bunte Schiefer* is called “Lower Varicoloured Marls”. Gray and red shales, and also marlstones alternate in this layer. The occurring sandstones are again arranged in a Bouma sequence. The marlstone is regarded to as hemipelagic sediment that was deposited below the CCD. The age ranges from late Albian to early Cenomanian and comprises a thickness of several tens of meters (Wagreich, 2012 (OMV Report)).

The next formation on the stratigraphic chart is the *Reiselsberg Formation* (table 1). It is mainly coarse-grained and consists very often of thick-bedded mica-rich sandstones.
The Reiselsberg Formation can be related to deep-sea fan environments (Mattern 2005).
The stratigraphic age range from Cenomanian to Coniacian in the Upper Cretaceous and the thickness varies extremely.

The *Seisenburg Formation*, also referred to as Obere Bunte Schiefer after Prey 1952, consists in the lower part of hemipelagic mudstones with some turbiditic layers.

The top part consists of an alternation of thin layers of turbidites and hemipelagic mudstones. The age extends from the middle Coniacian to early Campanian, and is about 50 m thick. The Formation is followed laterally by the Röthenbach Subgroup (Wagreich, 2012 (OMV Report)).

Röthenbach Subgroup ("Zementmergelserie") - The name Zementmergelserie was characterized by Prey 1950 and Faupl 1996. The lithology consists of micritic limestones and marls, which were formed by deep-water turbidites. The formation was deposited during the Coniacian to the Campanian. It is several hundreds of meters thick. The Piesenkopf Formation, Kalkgraben Formation and Hällritz Formation belong also to the Röthenbach Subgroup (Wagreich, 2012 (OMV Report)).

The Seisenburg Formation and the Röthenbach Subgroup overlap in time, but the Röthenbach Subgroup occurs earlier. While in Germany this earlier occurring period is also called Röthenbach Subgroup, in Austria the term Zementmergelserie was used (table 1).

The *Perneck Formation* consists of thin-bedded shales and siltstones. They are deep-water turbidites and non-turbiditic hemipelagic mudstones. The stratigraphic age is late Campanian. The Formation has a thickness of about 50 m (table 1).

The Perneck Formation is followed by the *Altlengbach Formation* which is also known as Altlengbacher Schichten (Götzinger and Becker, 1932). This unit is characterized by thick-bedded, coarse to medium grained turbiditic sandstones. The formation extends from the upper Cretaceous to early Paleocene (Egger, 1995). The thickness of this formation is estimated about 2000 m (Wagreich, 2012 (OMV Report)).

Greifenstein Formation - This unit consists of thick-bedded, yellow, weathered, sandstones and conglomerates, with a varying content of glauconite. Siltstones and mudstones can also be found. The sandstones display classical turbidites. The deep-sea fan deposits indicate deposits by sediment gravity flow. The thick-bedded sandstones and conglomerates show channel filling. The Greifenstein Formation represents the highest unit of the Greifenstein Nappe and has a thickness between 100 to 1000 m. This formation also includes the Gablitz Member and the Irenental Member (Wagreich, 2012 (OMV Report)).

The **Laab Nappe** includes the Kaumberg Formation and Laab Formation (table 1).
The *Kaumberg Formation* consists of thin-bedded siltstones and mudstones and forms the base of the Laab Nappe. It is not clear, whether it dates back to the Turonian or to the

Coniacian and ends in the Campanian or the Maastrichtian. Their thickness ranges within several hundred meters (Wagreich, 2012 (OMV Report)). The intermediate layers between the Kaumberg and Laab Formation could not be clarified sufficiently until now.

The lithology of the *Laab Formation* is constituted by thick, coarse-grained sandstone banks, and is visible in the Hois Member. In the Agsbach Member mudstones, siltstones, and sandstones, can be found. This formation extends from questionable Late Cretaceous to early Paleogene (Ypresian) and is about 100 m thick (Wagreich, 2012 (OMV Report)).

The tectonic top constitutes the **Kahlenberg nappe**, which consist of the Hütteldorf Formation, the Kahlenberg Formation, and the Sievering Formation (table 1).
In the *Hütteldorf Formation* three lithofacies can be recognized (Wagreich, 2008): a thick-bedded sandstone facies with amalgamation, a thin-bedded sandstone facies with lamination and a pelitic facies, which is dominated by red carbonate-free claystones.
Deep-water turbidites and mass flow transport under the CCD are responsible for this lithology. It has not yet been sufficiently clarified, whether the Hütteldorf Formation is the base of the Kahlenberg Nappe or the underlying Gault-Flysch.
Chronostratigraphically we can locate the Hütteldorf Formation in the upper Cretaceous with a layer thickness of several hundred meters (Wagreich, 2012 (OMV Report)).

The *Kahlenberg Formation* consists of calcareous marl and calcareous sandstone rocks. This unit originates only from the period of the Campanian and has a thickness of about 600 m (Wagreich, 2012 (OMV Report)).

The last formation is the *Sievering Formation*. It forms the top of the Kahlenberg Nappe and comprises thick- and thin-bedded siliciclastic sandstones in alternation with marl stones. Some of the sandstone banks can have a thickness of about 14 m. The encountered lithology was generated by the deposits of a deep-sea fan. This formation originates only in the Masstrichtian and has a layer thickness of a few hundred meter (Wagreich, 2012 (OMV Report)).

Table 1 Stratigraphic chart of the Flysch zone of the Wienerwald area (modified after Wagreich, 2012 and Sauer et al., 1992)

		Northern Margin Zone & Greifenstein Nappe	Laab Nappe	Kahlenberg Nappe
Paleogene	Eocene			
	Paleocene	Greifenstein Formation (100 – 1000 m)	Laab Formation (about 1000 m)	
Upper Cretaceous	Maastrichtian	Altlengbach Formation (about 2000 m)	Dark shales and quartzites ?	Sievering Formation
	Campanian	Perneck Formation (about 50 m); Röthenbach Subgroup („Zementmergelserie“) (about 200 – 500 m)	Kaumberg Formation (several tens of meters)	Kahlenberg Formation (about 600 m)
	Santonian	Seisenburg Formation (about 50 m)		Hütteldorf Formation (several hundreds of meters)
	Coniacian			
	Turonian	Reiselsberg Formation		
	Cenomanian	Untere Bunte Schiefer (10-50 m)/Ofterschwang Formation (about 100 m)		
Lower Cretaceous	Albian	Rehbreingraben Formation (Gault-Flysch) (about 250 m)		Gault – Flysch ?
	Aptian			
	Barremian	Wolfpassing Formation (about 100 m)		
	Hauterivian			

2.2 Sedimentology of the Flysch zone

The word “flysch” means soft flow and slide tendencies of shales and sandstones. Their origin is in deposited sediments in deep water, fed by avalanche-like turbidity currents and debris flows. These sediments were resedimented by tectonic movements, earthquakes, hurricanes, but also volcanic activities (Dengler and Wilde, 1983).

The deposits develop with different transport mechanisms, such as gravity flow and turbulent flow processes (rolling and sliding) (Besada, 1996). The sediments are first collected in rivers and then transported to the deltas (Johnson et al., 2001).Typical areas of deposition are continental margins and deep basins.

Turbidite layers are special characteristics of the Greifenstein Formation.

Turbiditic sediments are the most important and most common type of clastic sediments in the deep water area (Besada, 1996). In this thesis special attention will be paid to the classical turbidites, which can be described by the Bouma sequence.

The Bouma sequence (Figure 3) is an ideal case of a sedimentary sequence. The sections are separated by single letters (Ta, Tb, Tc, Tef and Tep). These sequences show a decrease in grain size, sedimentation rate, energy and speed of transport from bottom to top (Bouma, 1962; Besada, 1996).

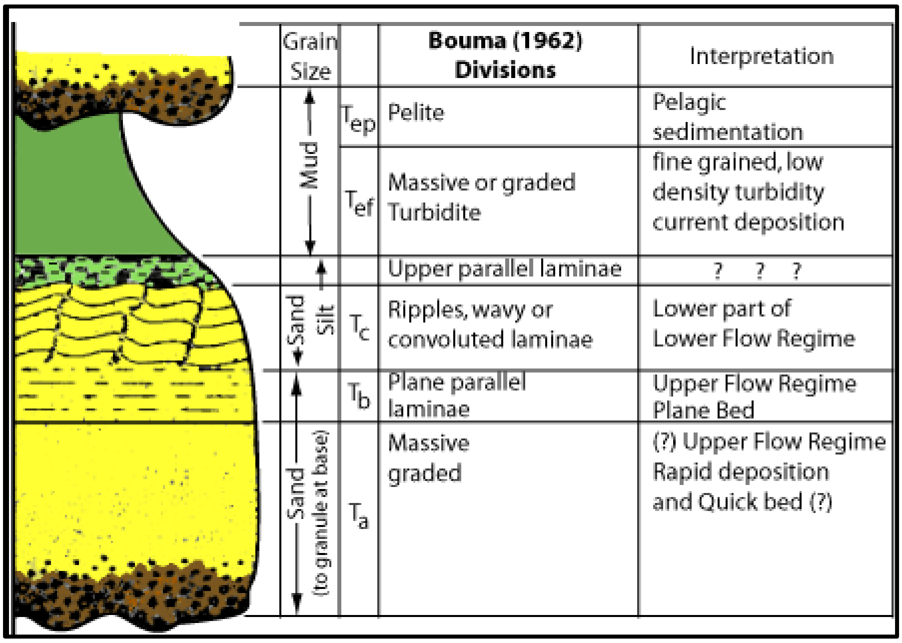

Figure 3 Bouma-Sequenz

(http://www.sepmstrata.org/Deepwater/DeepWatClasticSediments.html)

Description of the Bouma sequence (Bouma, 1962; Besada, 1996):

Section **Ta** consists of massive graded, weak stratified sandy sediments, which are formed by rapid deposition from a suspension. This section forms the basis of this sequence.

The following section **Tb**, is characterized by sandy, horizontal and parallel lamination.

In Section **Tc** asymmetric flow ripple can be found, but also convolute stratification in sandy to silty sediments are important to mention. Sections Tb and Tc are developed by slow processing and from continuously deposited sediments from the turbidity current.

Section **Tef** is formed by deposition out of the sediment cloud. In this section horizontally laminated, pelitic materials are deposited. The section Tef should be considered as slow accumulation of fine grain sizes from the tail of the turbidity current.

The last section, **Tep** consists of sediments from the suspension, pelagic material without clearly recognizable sedimentary structures.

Section Tep constitutes the following hemipelagic sediments, which may also be regarded as section F.

Often there is an absence of individual sections, with which the sequence is incomplete.

Furthermore, there are also turbiditic sequences that cannot be described by the Bouma sequence. These are called non-classical turbidites and were specified by Mutti and Ricci Lucchi (1975). These are deep-water coarse clastic sediments, which have passed through gravitational sediment flows into the deep sea. They are characterized with four main facies (A, B, E and F).

Facies **A** contains breccia and conglomerates, especially coarse-grained sandstones and conglomerates. In this case the individual layers have a thickness of 15 m. In general, they are thinnig out.

In the facies **B** mainly medium-grained to coarse-grained, ungraded sandstone banks are deposited. They are better sorted than in facies A. Special features are a coarse horizontal lamination and flat-angled cross-bedding. The layers can reach a thickness of 3 m. In facies **E** thin, ungraded, coarse- to medium-grained sandstones are deposited. They show an irregular stratification in the outcrop and thinning out. As deposition mechanism a highly concentrated gravity flow is considered.

Facies **F** consists of chaotic pebbly mudstones and of breccias. Their characteristics are submarine slump deposits, sand flows and mud flows.

On top another facies can ocassionally be found: facies **G**. The facies contains marine, hemipelagic and pelagic clays and marls. They are formed by “normal” sedimentation.

2.3 Quarry Strombauamt

Just before the turn of the 20th century the regulation of the Danube began. For this purpose building material was taken from the quarry Strombauamt at Greifenstein. These materials have been used not only for the riverbank construction, but also for various buildings in Vienna. This quarry is abandoned. Today it is used only as a dump for construction waste.

The location of this quarry is between Höflein an der Donau and Greifenstein, near Klosterneuburg (figure 4). Coordinates: degree of latitude are 48.35 and degree of longitude are 16.26 (http://www.mapcoordinates.net). In this area two walls were exactly recorded in a profile. First, 1996 by Besada. He described in his master thesis the southern wall (profile figure 26). The renewed eastern wall was recorded in 2011 and is described in this thesis. The profile of Besada (1996) showed alternations of conglomerates, sandstones (fine, medium and coarse grained, with or without grade or amalgamation) and clay clasts. In general it can be said that the grain size diminishes to the top. At the base there are conglomerates; fine-grained sandstones are found at the top.

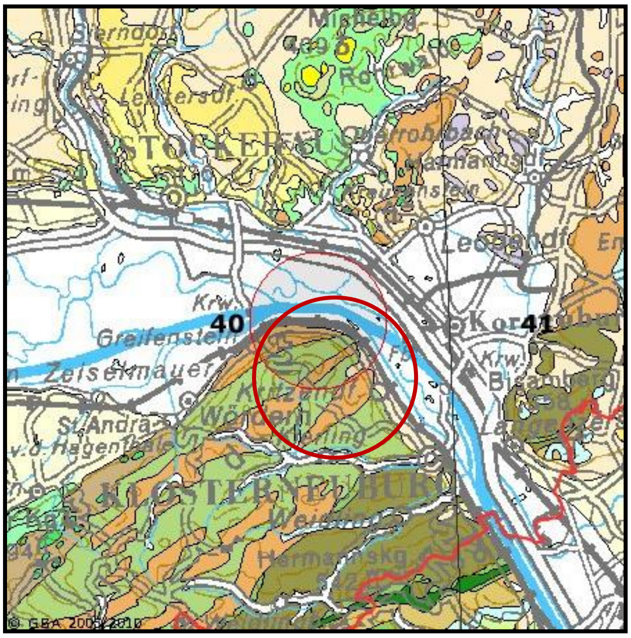

Figure 4 Geological map of Höflein an der Donau (http://geomap.geolba.ac.at/GEO/GEO_main.cfm?Init=false)

Samples were taken from different layers (sandstones, conglomerate and clay samples). The naming of the sample descriptions is based on the location (Greifenstein-GR) and the hight of the rock samples (e.g. 44 m). For example, a sample taken from Greifenstein at 44 m, will be named GR 44. In addition samples of Besada were taken to complete the south quarry wall. This contain the samples A3(2), A5(1), N4, H2, H6, H10, D3(5), D5α, D5c and X1.

In the eastern quarry wall there are mainly sandstones (fine-, medium- and coarse-grained) interbedded with clay layers. The wall shows various deposits, channels and fillings. Five sandstone samples were collected, GRO 1a, GRO 1b, GRO 3, GRO 3X and GRO 4X. These samples are named Greifenstein East (GRO) and sample number.

3. Materials and Methods

3.1 Materials:

As part of this project sandstone and conglomerate samples were collected from the quarry Strombauamt. These were analyzed using the methods described below.

From the south wall 15 samples (four conglomerates and 11 sandstones) were taken. Additionally 10 samples from the thesis of Besada were taken (table 2). In the east wall five sandstone samples were collected. It was important to ensure that the samples had a fresh surface and were not weathered.

Table 2 List of samples taken at the quarry Strombauamt (for sample positions see profiles figure 23-26)

	Sample	[m]	Lithology
Southwall	A3(2)	5,5	Sandstone
	A5(1)	9,5	Sandstone
	N4	25,5	Conglomerate
	H2	36,5	Sandstone
	H6	38,5	Sandstone
	H10	41	Sandstone
	GR 44	44	Conglomerate
	GR 46	46	Conglomerate
	GR 51	51	Sandstone
	GR 52	52	Sandstone
	D3(5)	63,5	Sandstone
	D5α	64,5	Sandstone
	D5c	65,5	Sandstone
	GR 66,7	66,7	Sandstone
	GR 68	68	Sandstone
	GR 69	69	Conglomerate
	GR 71,5	71,5	Conglomerate
	GR 73,5	73,5	Sandstone
	GR 75,5	75,5	Sandstone
	GR 78,5	78,5	Sandstone
	GR 80,5	80,5	Sandstone
	GR 83,5	83,5	Sandstone
	GR 86	86	Sandstone

	GR 93	93	Sandstone
	X1	110	Sandstone
Eastwall	GRO 1a	2,5-3	Sandstone
	GRO 1b	2,5-3	Sandstone
	GRO 3	5,4-12,4	Sandstone
	GRO 3X	5,4-12,4	Sandstone
	GRO 4X	5,4-12,4	Sandstone

3.2 Petrographic analysis:

This chapter describes various petrographic methods for the characterization of sandstones. The analyses were carried out on thin sections and powdered samples. The mineralogical composition was determined by thin section microscopy and x-ray diffraction (XRD) analysis. Further, cathodoluminescence microscopy was applied to make lattice defects, zoning and luminescence phenomena visible.

3.2.1 Point counting:

Samples were impregnated with blue resin before thin sectioning in order to indicate porosity. Before point counting, half of each thin section was stained with Kaliumhexacyanoferrat(III) and Alizarin Red S. This method is used to differentiate calcite from dolomite and their respective iron contents. In this case calcite is colored red to purple and dolomite light to dark blue. After staining, the thin sections were inspected under a microscope (Nikon Typ 104). With the help of a point counter (Prior James Swift Model F) the samples were counted easily. The samples were placed in the apparatus and moved along the microscopic lense in a pre-defined stage interval depending on grain-size. In each sample a total of 400 grains was counted for modal sandstone composition. Quartz (mono- and polycrystalline), glauconite, cement, feldspars (plagioclase and orthoclase), mica (biotite and muscovite), rock fragments and fossil fragments were counted separately.

3.2.2 Characterization of the sandstones:

The outcrop samples were analyzed macroscopically and microscopically. Sedimentary structures, color, grain size and sorting were determined from the rock samples. The samples are sandstones (fine, medium, or coarse-grained) and conglomerates. The composition and porosity were determined under a transmitted-light microscope.
Photos of the thin sections were taken with a LEICA DM 4500P Microscope.

3.2.3 Classification of the sandstones:

The sandstones were classified after Folk (1968). For this classification Folk used triplots (figure 5); the three corners represent feldspar, quartz and rock fragments. The resulting lithologies of these three corners are arkose, quarzarenit and litharenit. By plotting the results the lithology of an individual sample can be determined.

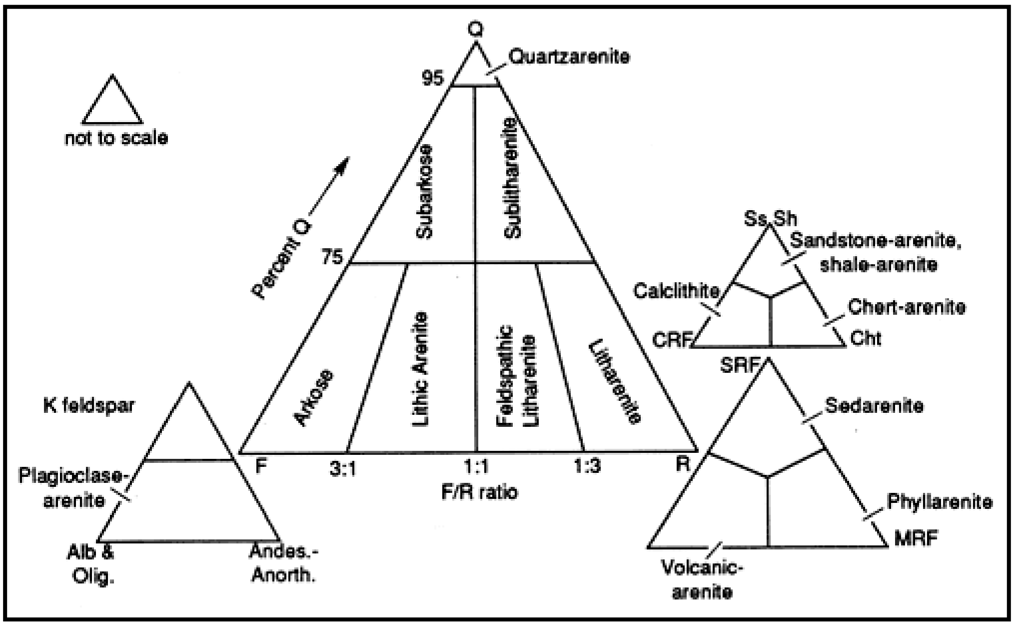

Figure 5 Classification of sandstones after Folk (1968)

3.2.4 X-ray diffraction (XRD):

XRD (figure 7 and 8) is a method to determine the mineral composition of rock samples. This requires that the samples are powdered. Therefore, the samples were ground with an agate mill. The powder is pressed into a sample holder (figure 6) and then measured with XRD. A Panalytical PW 3040/60 X'Pert PRO X-ray diffractometer (CuKα radiation, 40 kV, 40 mA, step scan, step size 0.02, 5s per step) was used for the analyses.

Figure 6 Pressed powder in sample holder

The diffractograms were interpreted according to Moore and Reynolds (1997).
The main peak positions for the minerals are: quartz (26.6 °2Theta), plagioclase (28 °2Theta), alkali feldspar (27.5 °2Theta), calcite (29.42 °2Theta) and dolomite (30.99 °2Theta) (Tucker, 1988).

Figure 7 X- ray diffractometer

Figure 8 X- ray diffractometer (detail)

3.2.5 Cathodoluminescence (CL):

With this method the luminescence of the different minerals including the carbonate cement was assessed. For this, polished thin-sections of 15 µm thickness were prepared. The thin-sections were coated with carbon before analysis for better conductivity.

For the cathodoluminescence examination (figure 9), the model Lumic LM-HC5, at 0.3 mA (milli Ampere) and 14 kV (kilo volts) was used (Marshall, 1988). The observation was carried out under the polarization microscope in a vacuum chamber (figure 10). Here, the thin section was clamped into a holder and then the vacuum was applied (1.0 x 10^{-4}). After that, an electron beam (hot cathode-ray) was directed at the sample causing luminescence. Generally, quartz shows the color dark blue or dark brown, K- feldspar light blue and carbonate cement orange (Marshall, 1988). Also zonation, lattice defects and radiation defects can be examined with this method. Out of 20 thin sections two sandstone samples GR 78.5 and GRO3 were selected for analysis. These two sandstones samples were selected, because of their particular characteristics. They contain a lot of glauconite,coarse quartz grains, calcite cement and occasionally fossil fragments.

Figure 9 Cathodoluminescence

Figure 10 Sample in vacuum chamber (open)

3.2.6 Electron microprobe (EMP):

With this method the chemical composition of cement and glauconite was assessed. A CAMECA SX100 electron microprobe at the University of Vienna was used for the analyses. Thin sections with a thickness of 55 µm were produced and coated with carbon to avoid charging and to achieve conductivity. The thin sections were clamped on the sample stage with standards in the middle (figure 11) and analyzed with an electron beam (15 kV and 20 nA) in a vacuum chamber (figure 12).

Two samples were selected for this method; GR 78.5 and GRO3. From sample GR 78.5, twenty-three points were measured and from the sample GRO 3 thirteen points. The major elements (K, Na, Ca, Al, Fe, Mg, Si, Al) were analyzed in the centre and in the outer rim of the glauconite grains.

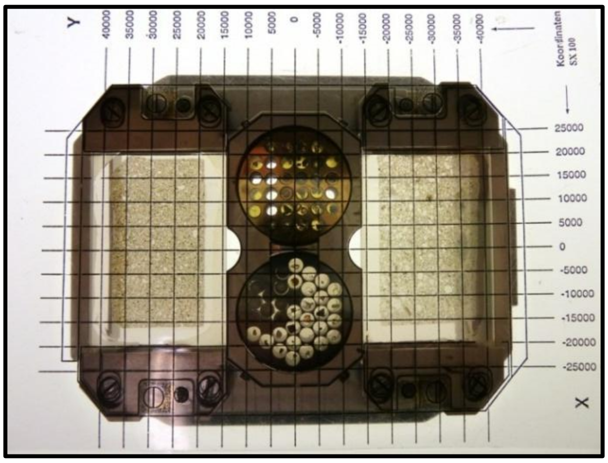

Figure 11 Holder with the two samples: GRO3 on the left side and GR 78.5 on the right side – in the middle are the standards

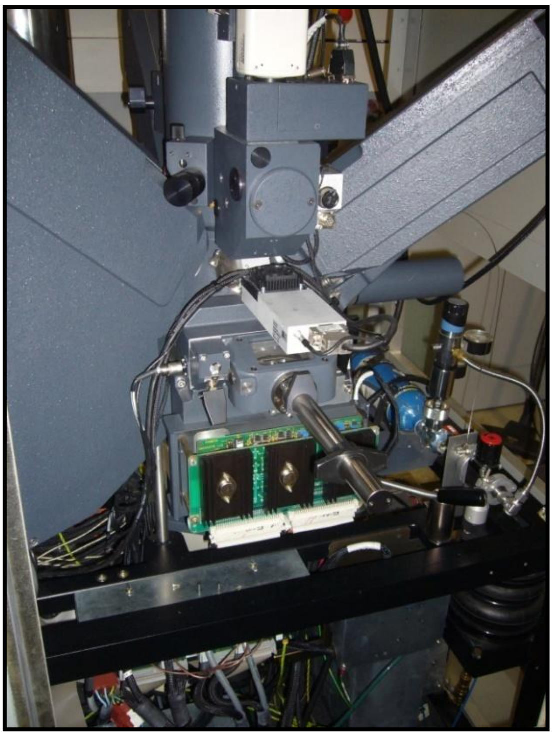

Figure 12 Electron microprobe

The analysis gives the quantitative chemical composition of the glauconites. With these the chemical-structural formula can be calculated with the Marshall method (Marshall, 1949). On the base of 10 oxygens and 2 hydroxyl-groups, which give a total negative charge of 22, the formulae of 2:1-phyllosilicates were calculated (Köster, 1977).

The tetrahedral, octahedral and interlayer charges were calculated and plotted in a charge-distribution diagram with the end members muscovite, pyrophyllite and celadonite (figure 13). With this method the stage of maturation of the glauconites and the composition of single grains were determined.

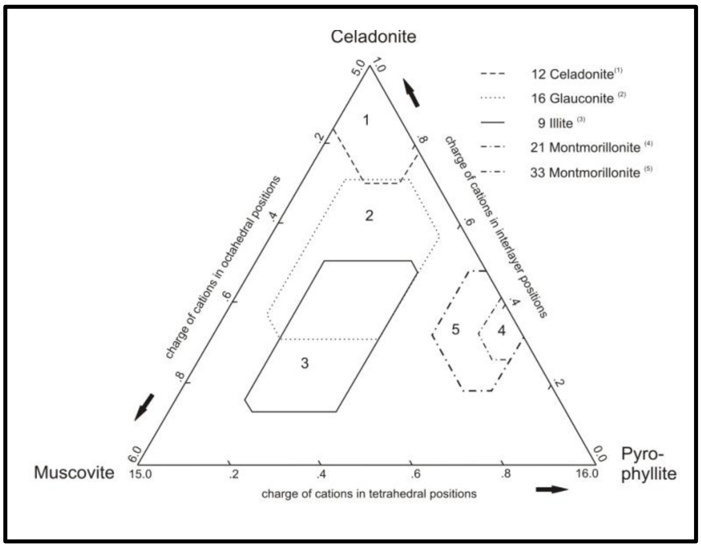

Figure 13 Charge distribution diagram with end-members celadonite, muscovite and pyrophyllite (modified from Köster, 1977)

3.3 Technical analysis:

The technical analyses were carried out on powdered samples and whole rock pieces. The porosity was determined according to ÖNORM B3121 and ÖNORM EN1936, and with additional use of a pycnometer. By determining the porosity, particular attention should be paid to the calibration of the scale and its location. The scale used for this procedure should stand free and should not be influenced by biasing factors. Furthermore, the permeability was determined using a micropermeameter.

3.3.1 Porosity:

Determination after ÖNORM B3121 (Testing of natural stone; density, apparent density, bulk density) *and ÖNORM EN 1936* (Natural stone test methods - Determination of real density and apparent density, and of total and open porosity):

With this method, the bulk density, the open porosity and the total porosity were determined.

For the operational procedure the ÖNORM B3121 was used and for the calculation of the porosity the new ÖNORM EN 1936 was applied. The samples were dried in a drying oven at 105 °C (figure 14) and weighted.

Afterwards the samples were placed in water (figure 15) until they were saturated with water. The sample is then dipped into the water from the scale and weighed again.

Figure 14 Drying oven

Figure 15 Container for rock samples

The calculation was carried out using following formula:

Open porosity:

$p_o = (m_s - m_d) / (m_s - m_h) * 100$ [%]

m_d	dry mass of the sample	[g]
m_h	mass of the body dipped in water	[g]
m_s	mass of water-saturated body	[g]
ρ_b	bulk density	[g/cm^3]
ρ_{rh}	density of water	[g/cm^3]
p_o	open porosity	[%]

Bulk density:

$\rho_b = (m_d * \rho_{rh}) / (m_s - m_h)$ [kg/m^3]

Determination with Pycnometer (ÖNORM B3121: Testing of natural stone; density, apparent density, bulk density):

With this method, the net density and the total porosity were determined. Since the density of the rock without the pore spaces was of interest, a powdered sample was used (figure 16). Samples GRO 3X and GRO 4X were determined at Technischen Prüfanstalt (TPA). First, the empty pycnometer (figure 17) is weighed, and then the sample is placed inside. Then, the pycnometer with the sample inside is weighed again. After that, the pycnometer is filled with distilled water. No air bubbles should be trapped in the flask.

The pycnometer must be filled to the top, so that water is spilled when the stopper is placed on top. Finally, the pycnometer with the sample and water was weighed. For the determination of the porosity, we used the results of the bulk density of the previous measurement (ÖNORM EN 1936).

Figure 16 Powdered sample

Figure 17 Pycnometer (http://de.wikipedia.org/w/index.php?title=Datei:Pyknometer.jpg&filetimestamp=20100427213155)

The calculation was carried out using this formula:

Porosity:

1 – (bulk density / net density) * 100 [%]

Bulk density (Results from the ÖNORM EN 1936) [g/cm³]

Net density:

$\rho = (C-A) / (B-A) - (D-C)$ [g/cm³]

A	weight of the pycnometer	[g]
B	weight of the pycnometer with water (volume)	[g/cm³]
C	weight of the pycnometer with powdered sample	[g]
D	Weight of the pycnometer with water and powdered sample	[g/cm³]

3.3.2 Permeability:

The permeability is determined by hydraulic conductivity. These measurements were performed using the micropermeameter (figure 18 and figure 19) at OMV in Gänserndorf. For this purpose, the rock sample was clamped in the micropermeameter and nitrogen was pressed onto the rocks with a pressure of 8 bar. With this method the permeability, in mD (milli Darcy) can be determined. It was important, that the rock sample was placed firmly in the machine and could not move. It was also very important that a plain and not weathered rock surface was used for this procedure.

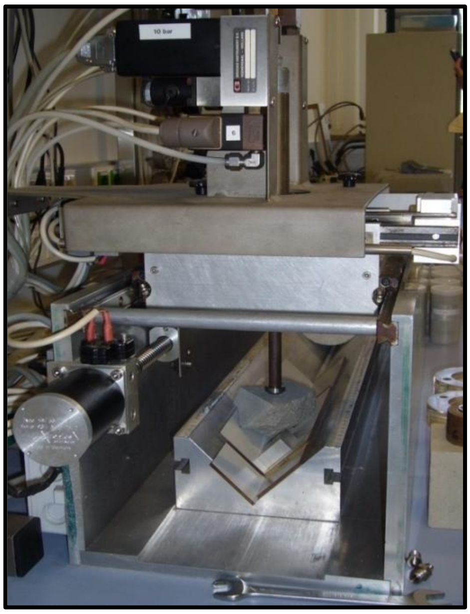

Figure 18 Micropermeameter

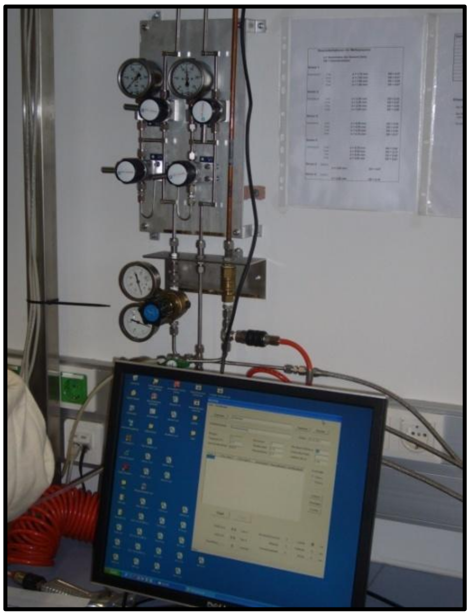

Figure 19 Nitrogen valve and PC

4. Results

4.1 Profiles:

The first two profiles were logged at the east wall of the quarry. The most frequently occurring rocks are sandstones (fine-to medium-grained) and mudstones (clay). The wall is made up of thick-bedded sandstone layers (200-400 cm). In between are clay layers of variable thicknesses.

The first part of the first profile (figure 20 and figure 23) comprises the first 700 cm and shows that the sandstone is fining upward. The sandstone beds are brown, fine- to medium-grained, and are partly heavily weathered.
Lamination can be seen ccasionally.

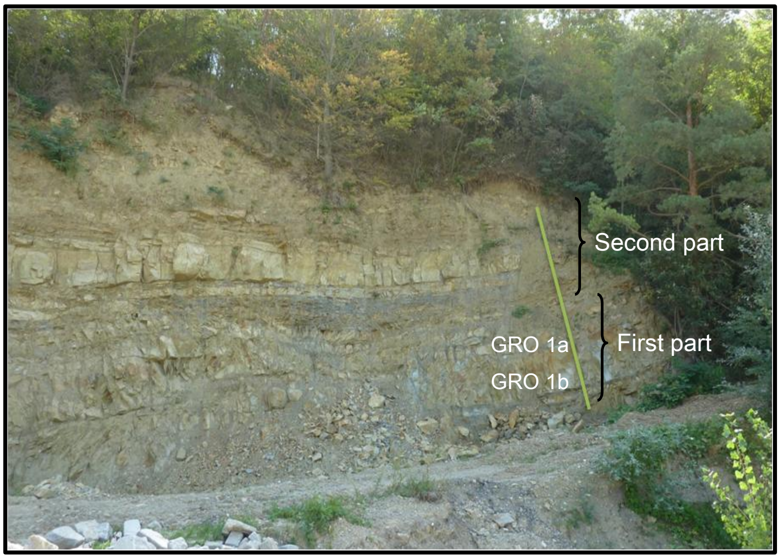

Figure 20 First profile of the east wall of the quarry

Between these sandstone beds, clay layers are intercalated.
Two sandstone samples were taken, GRO 1a and GRO1b (figure 20 and figure 23).

The second part of the first profile shows the section between 700 to 1208 cm (figure 20 and figure 24). This section consists mainly of yellow-brown sandstones. Only a few clay layers could be identified.
Lamination and ripple stratification is evident.
The top meter could not be recorded exactly.

Figure 21 Second profile of the east wall of the quarry

The second profile of the east wall (figure 21 and figure 25) consists of thick-bedded sandstone layers with two clay layers intercalated.
The sandstone beds are 300 to 500 cm thick. Predominantly medium-grained, yellow-brown, moderately to highly weathered sandstones are found.
Four samples were collected; three sandstones (GRO 3, GRO 3X and GRO 4X) and one mudstone sample. The sandstone samples were taken from the same layer, because the sandstone shows internal variation of properties.

The profile of the south wall (figure 22 and figure 26) was recorded by Besada (1996) in his thesis. The profile has a total thickness of about 126 m, starting at the base with pebbly sandstones and conglomerates and becoming more finely grained towards the top.

Figure 22 South wall of the quarry (from Besada, 1996)

Today, the lower part of the profile (up to 52 m) logged by Besada is covered by debris, only the upper part is still exposed.
The sandstone and conglomerate beds have an individual thickness of several meters. As in other sections, they are always interbedded with clay layers.

The south wall shows a wide inventory of sedimentary structures: normal and reverse grading, amalgamation, lamination and cross-bedding. 15 samples of sandstones and conglomerates were taken (figure 26). In addition 10 samples taken by Besada and stored in the collection of the Center for Earth Sciences, University of Vienna, were also studied.

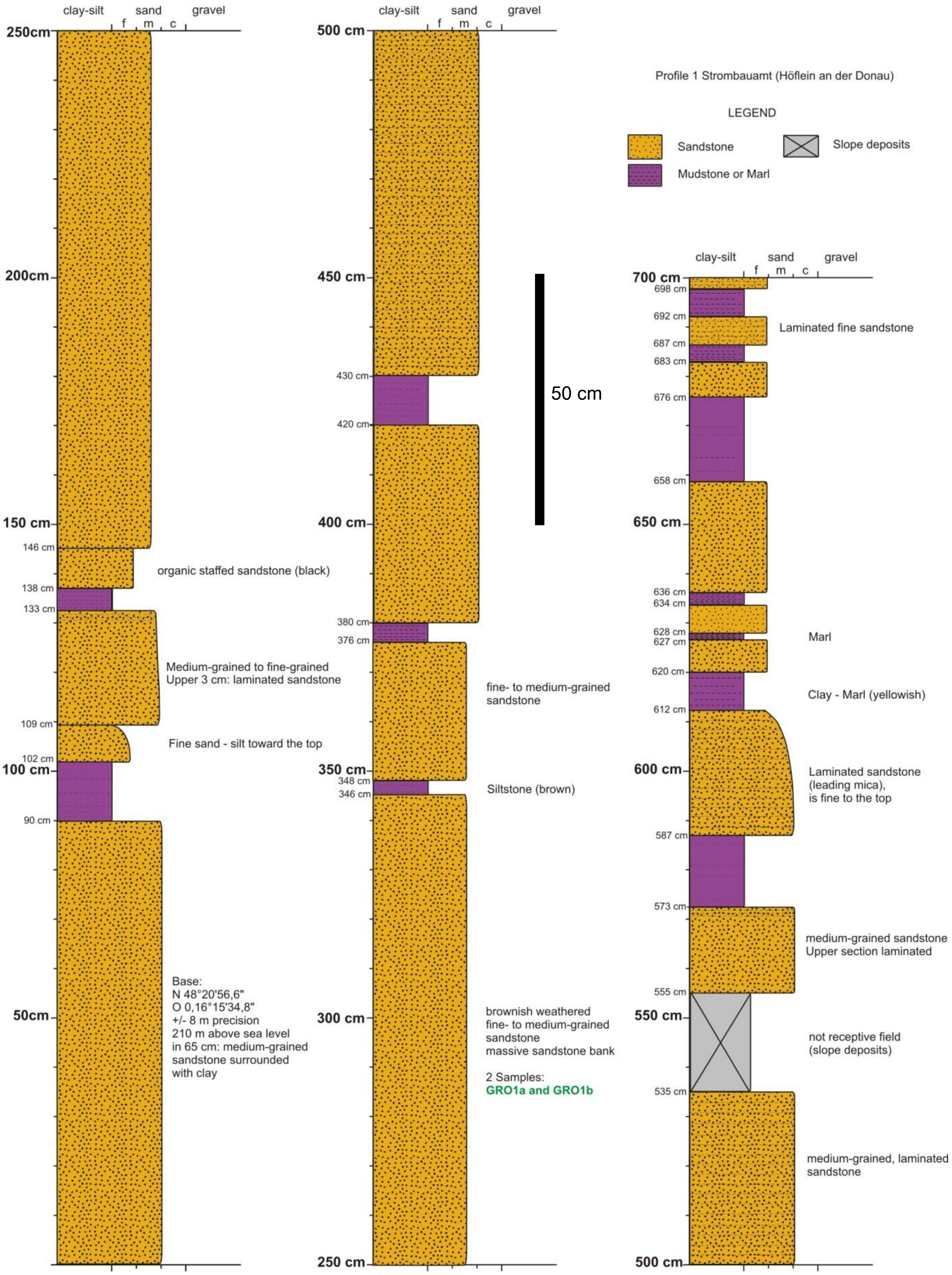

Figure 23 First part of the first profile – East wall quarry Strombauamt

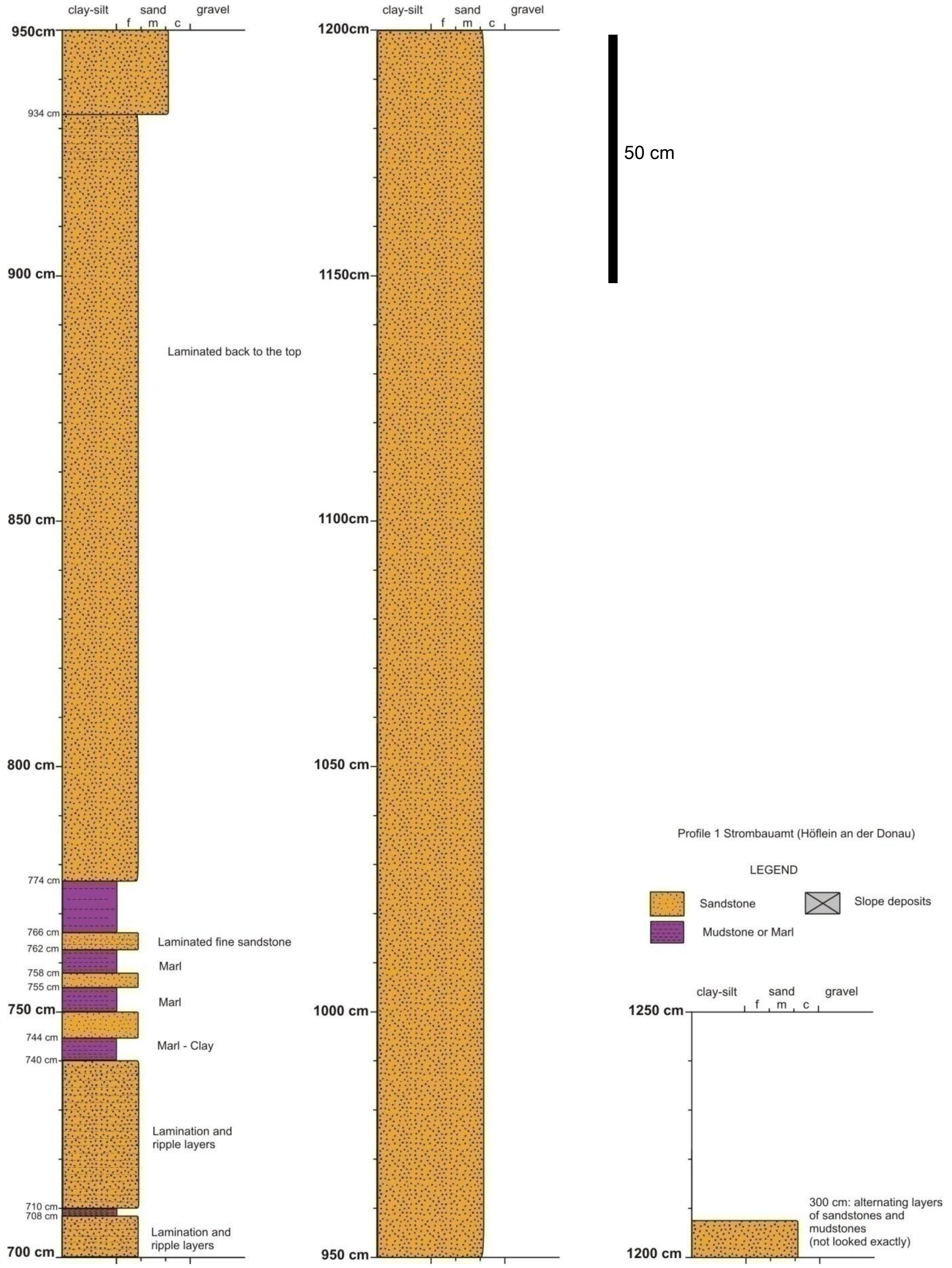

Figure 24 Second part of the first profile – East wall quarry Strombauamt

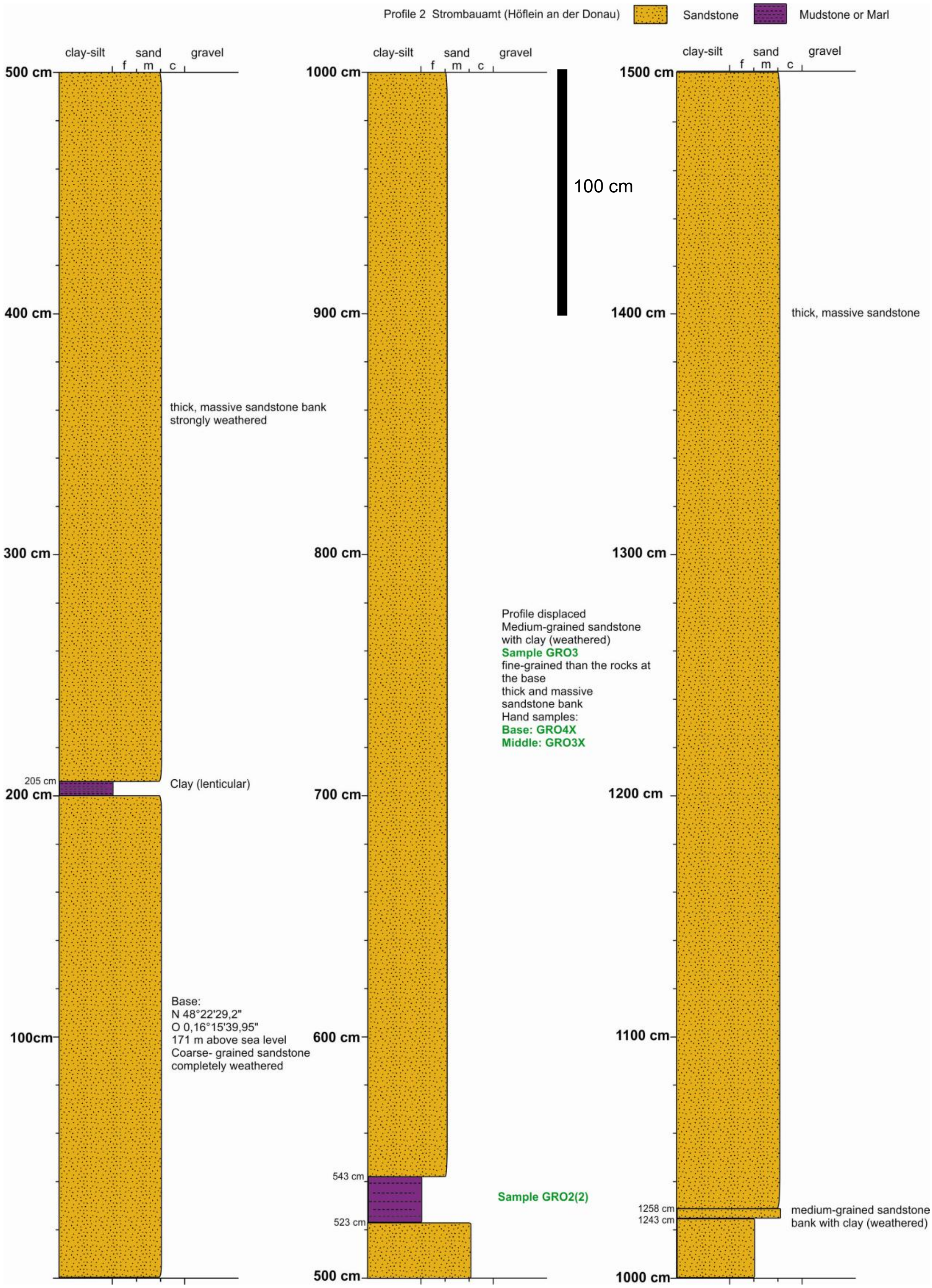

Figure 25 Second profile – East wall quarry Strombauamt

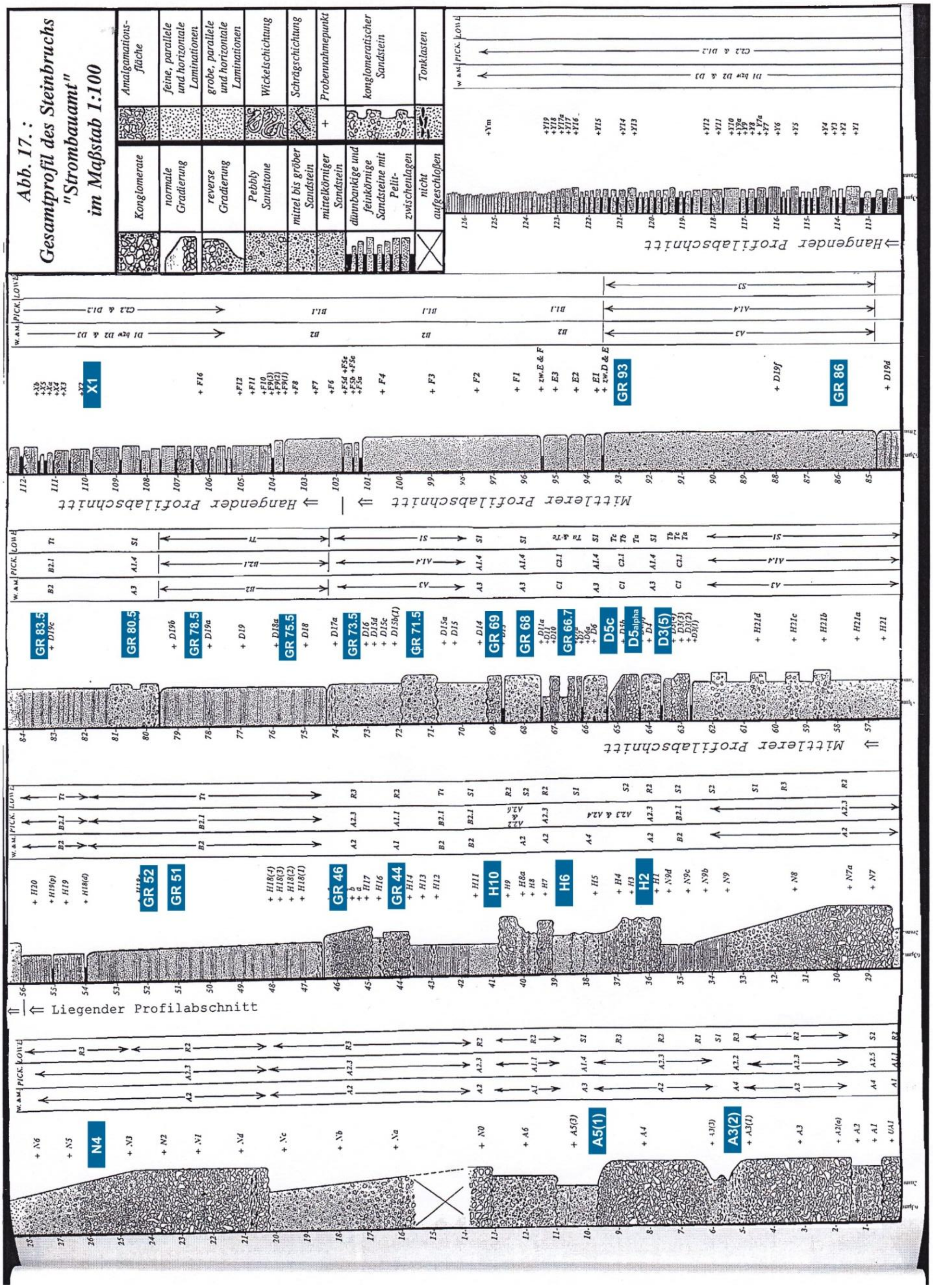

Figure 26 Profile of the south wall quarry Strombauamt (from Besada 1996, modified by Löffler)

4.2 2-D Plot:

A 2-D plot was made from a panoramic image of the east wall of the quarry area (figure 27). Characteristic features of the wall were a fault, channel cuts and their fillings. The latter two can be attributed to the depositional environment. The channels and their fillings could be evidence for poor reservoir properties, as there might be no communication between the different channels. In the clay layers on the south end of the wall one angular unconformity could be found. Otherwise the wall consisted of highly weathered, massive sandstone banks with clay layers. Through constant excavation work at the quarry wall more and more of the wall has been made visible.

Figure 27 2-D Plot of the east wall of the quarry Strombauamt

4.3 Petrographic results:

4.3.1 Point Counting:

The main components are quartz (monocrystalline and polycrystalline), glauconite, carbonate cement, mica (muscovite and biotite), feldspar (plagioclase and orthoclase), rock fragments, and fossil fragments.

The three dominant components in the samples were: quartz, glauconite, and carbonate cement.

Special attention was paid to the high amount of quartz. Figure 28 shows a comparison between the mono- and polycrystalline quartz grains for the individual samples.

The percentage of monocrystalline quartz is much higher than of polycrystalline quartz. Monocrystalline quartz has a percentage twice as high as the polycrystalline quartz.

The content of monocrystalline quartz is much higher in the south wall than in the east wall. The different samples have a similar quartz content. In all rock samples more than 60 % of quartz could be counted.

The similarity between the samples is also evident shown in the diagram in figure 29.

This figure shows the comparison of all rock samples. There are only slight differences in quartz, glauconite and cement between the individual samples. The content of mica, rock fragments and fossil fragments are very low. The amount of glauconite is slightly higher in the samples of the east wall (GRO 1a, GRO 1b, GRO 3, GRO 3X and GRO 4X) than in the samples of the south wall (figure 29).

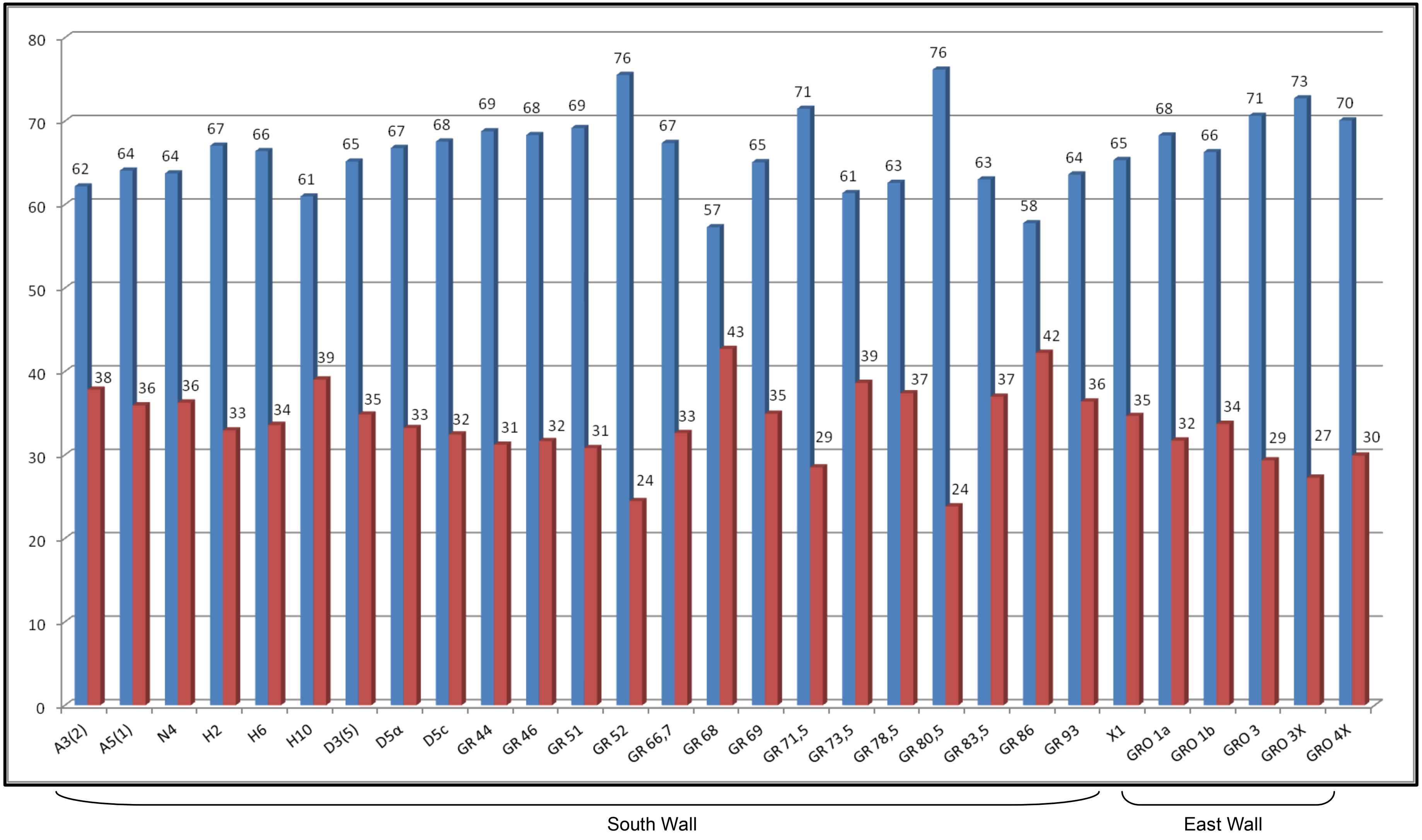

Figure 28 Results of the point counting [%] from quartz – in blue the monocrystalline and in red the polycrystalline quartz. The samples A3(2) to H10 and D3(5) to D5c are samples, which were collected by Besada 1996. It characterizes the profile sequence of the south wall and the east wall from the base (A(3) respectively GRO1a) to the top (X1 respectivley GRO 4X)

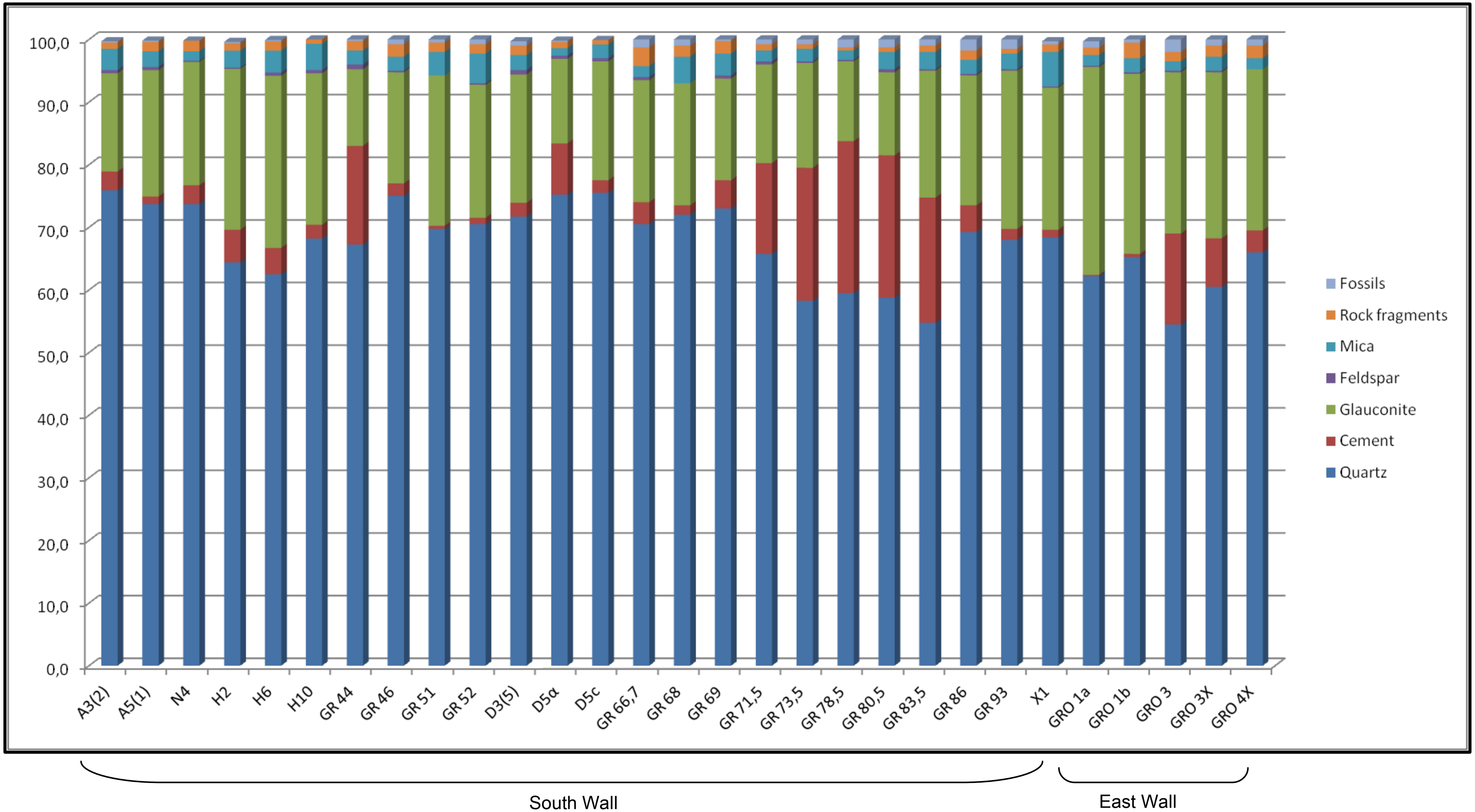

Figure 29 Results of the point counting [in %] from the different components. The samples A3(2) to H10 and D3(5) to D5c are samples, which were collected by Besada 1996. It characterizes the profile sequence of the south wall and the east wall from the base (A(3) respectively GRO1a) to the top (X1 respectivley GRO 4X)

4.3.2 Characterization of the sandstones:

A3(2)

Macroscopic	Microscopic
	
Coarse- grained sandstone Light gray to light brown, quartz grains are visible (most rounded) Compact and no visible porosity	Overview: compact and moderately sorted, coarse sand grains are rounded, medium and fine grains are angular to rounded Components: quartz (monocrystalline and polycrystalline), glauconite (green, round components), mica flakes (biotite and muscovite) - Presence of cement (blue) – Occasional occurrence of fossils and rock fragments

A5(1)

Macroscopic	Microscopic
	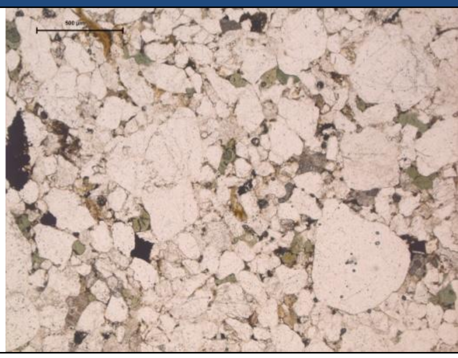
Fine- grained sandstone Light brown, high content of quartz well visible Compact and no visible porosity	Overview: compact and poorly sorted, no coarse grained sand grains, medium and fine grains are angular to rounded Components: quartz (monocrystalline and polycrystalline), glauconite (green, round components), mica flakes (biotite and muscovite) - Presence of cement (blue) – Occasional occurrence of fossils and rock fragments

N4

Macroscopic	Microscopic
	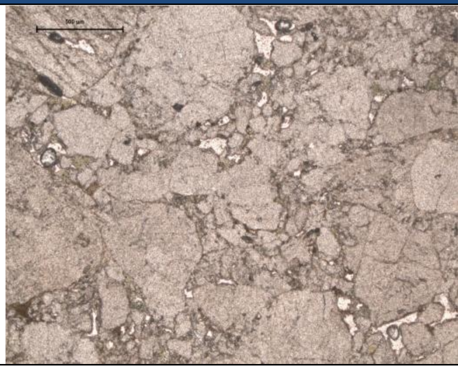
Conglomerate Light brown to light gray Quartz grains are clearly visible Compact and no visible porosity	Overview: Chaotic and poorly sorted, many coarse grains – angular to rounded, fine grains angular and rounded too Components: quartz (monocrystalline and polycrystalline), glauconite (green, round components), mica flakes (biotite and muscovite) - Presence of cement (blue) – Occasional occurrence of fossils and rock fragments

H2

Macroscopic	Microscopic
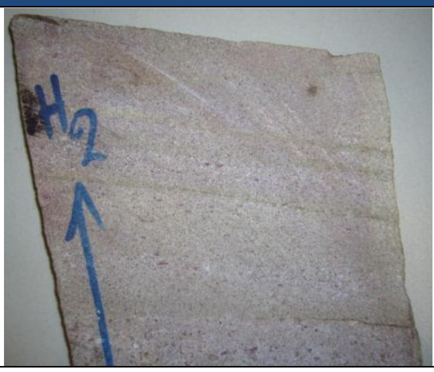	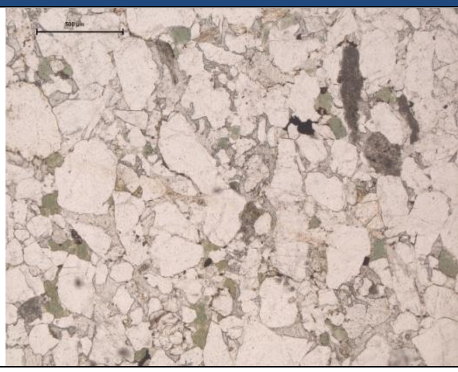
Fine- grained sandstone Light gray to light brown, lamination, quartz grains are clearly visible Compact and no visible porosity	Overview: compact and moderately sorted, few coarse grains (mostly rounded), medium and fine grains are angular to rounded Components: quartz (monocrystalline and polycrystalline), glauconite (green, round components), mica flakes (biotite and muscovite) - Presence of cement (blue) – Sporadic occurrence of fossils and rock fragments

H6

Macroscopic	Microscopic
	
Fine- grained sandstone Light brown Single grains can not be identified Compact and no visible porosity	Overview: compact and poorly sorted, no coarse grains, medium and fine grains are angular to rounded Components: quartz (monocrystalline and polycrystalline), glauconite (green, round components), mica flakes (biotite and muscovite) - Presence of cement (blue) – Occasional occurrence of fossils and rock fragments

H10

Macroscopic	Microscopic
	
Medium- grained sandstone Light gray, alternation between coarse and fine layers, quartz grains are clearly visible Compact and no visible porosity	Overview: very compact and moderately sorted, single coarse grains (rounded), medium and fine grains are angular to rounded Components: quartz (monocrystalline and polycrystalline), glauconite (green, round components), mica flakes (biotite and muscovite) - Presence of cement (blue) – Occasional occurrence of fossils and rock fragments

D3(5)

Macroscopic	Microscopic
	
Medium- grained sandstone Light gray, alternation between fine and coarse layers, quartz grains are clearly visible Compact and no visible porosity	Overview: chaotic and poorly sorted, few coarse components (rounded), medium grains are dominant (angular to rounded), fine grains (angular to rounded) Components: quartz (monocrystalline and polycrystalline), glauconite (green, round components), mica flakes (biotite and muscovite) - Presence of cement (blue) – Occasional occurrence of fossils and rock fragments

D5α

Macroscopic	Microscopic
	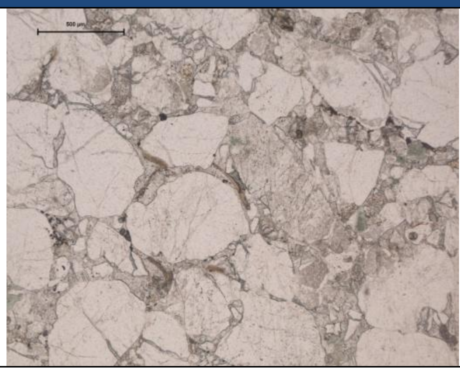
Coarse- grained sandstone Light gray, grains are mostly finer at the top, quartz grains are clearly visible Compact and no visible porosity	Overview: chaotic and poorly sorted, medium and fine grains are angular to rounded Components: quartz (monocrystalline and polycrystalline), glauconite (green, round components), mica flakes (biotite and muscovite) - Presence of cement (blue) – Occasional occurrence of fossils and rock fragments

D5c

Macroscopic	Microscopic
	
Fine- grained sandstone Light grey, middle layer is coarser, quartz grains are clearly visible, lamination Compact and no visible porosity	Overview: fine and poorly sorted, single coarse grains (rounded), medium and fine grains are angular to rounded Components: quartz (monocrystalline and polycrystalline), glauconite (green, round components), mica flakes (biotite and muscovite) - Presence of cement (blue) – Occasional occurrence of fossils and rock fragments

GR 44

Macroscopic	Microscopic
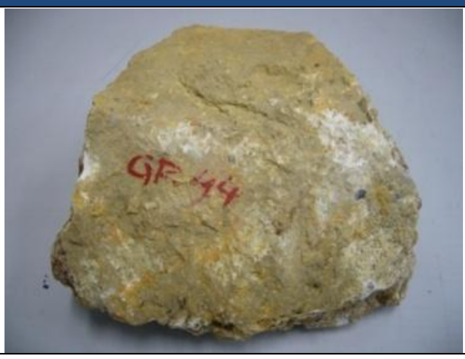	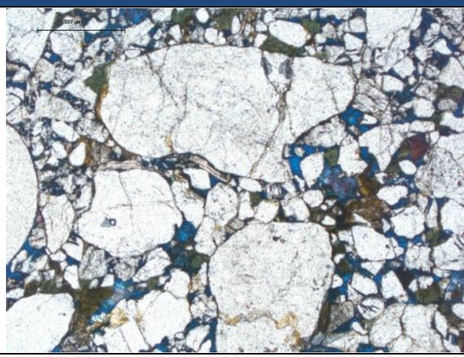
Conglomerate Large components (rounded), brown / orange surface due to weathering Quartz components are large and clearly visible, compact and no visible porosity, contains pebbles	Overview: Extremely coarse grained, moderately sorted, occurrence of coarse rock fragments - usually rounded, occasionally angular grains Components: quartz (monocrystalline and polycrystalline), glauconite (green, round components), mica flakes (biotite and muscovite) - Presence of cement (blue) – Occasional occurrence of fossils and rock fragments

GR 46

Macroscopic	Microscopic
	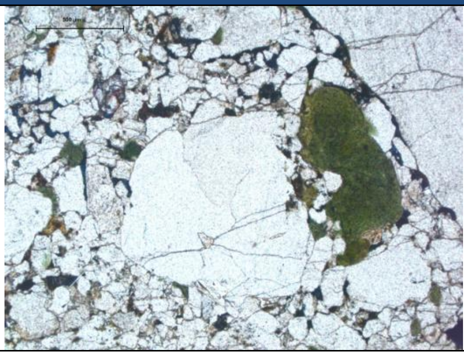
Conglomerate Light brown rock surface, less weathered than GR 44, little or no visible porosity, quartz grains are clearly visible	Overview: finer components, compact and densely arranged, coarse components less than in GR 44 - mostly angular to rounded Components: quartz (monocrystalline and polycrystalline), glauconite (green, round components), mica flakes (biotite and muscovite) - Presence of cement (blue) – Occasional occurrence of fossils and rock fragments

GR 51

Macroscopic	Microscopic
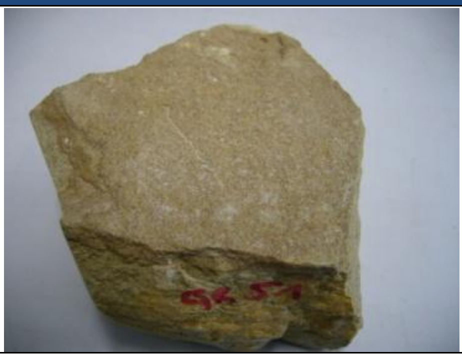	
Fine-grained sandstone Laminated (dark brown layers are intercalated), brownish surface, very fine and compact, little or no visible porosity	Overview: layering (grading) visible on thin-section, very fine and compact, well sorted and ordered, usually round components Components: quartz (monocrystalline and polycrystalline), glauconite (green, round components), mica flakes (biotite and muscovite) - Presence of cement (blue) – Occasional occurrence of fossils and rock fragments

GR 52

Macroscopic	Microscopic
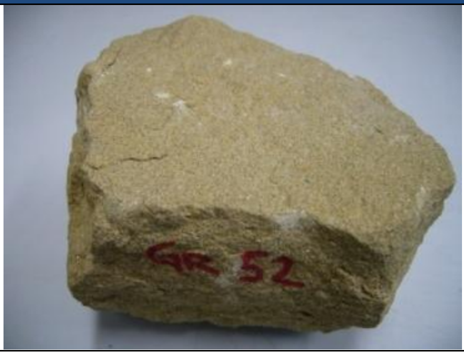	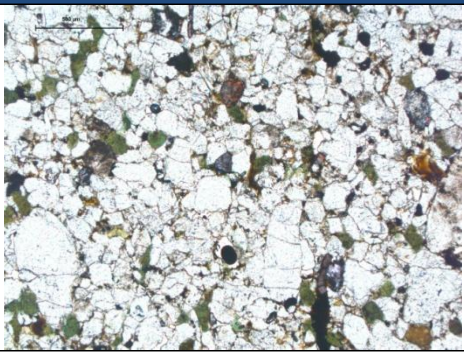
Fine-grained sandstone Not as fine as GR 51, brown surface, very compact with little or no visible porosity	Overview: mostly well-rounded grains, compact and finely arranged, in a small section the grains were more compacted and finer grained, moderately to poorly sorted Components: quartz (monocrystalline and polycrystalline), glauconite (green, round components), mica (biotite and muscovite) - Presence of cement (blue) – Occasional occurrence of fossils and rock fragments

GR 66,7

Macroscopic	Microscopic
	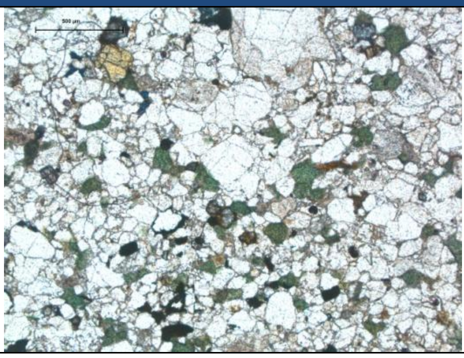
Fine-grained sandstone Light gray / gray stone color, shows lamination, surface is partially weathered orange, little or no visible porosity	Overview: moderately sorted, mostly rounded but occasionally angular components, thin section: lamination is visible Components: quartz (monocrystalline and polycrystalline), glauconite (green, round components), mica (biotite and muscovite) - Presence of cement (blue) – Occasional occurrence of fossils and rock fragments

GR 68

Macroscopic	Microscopic
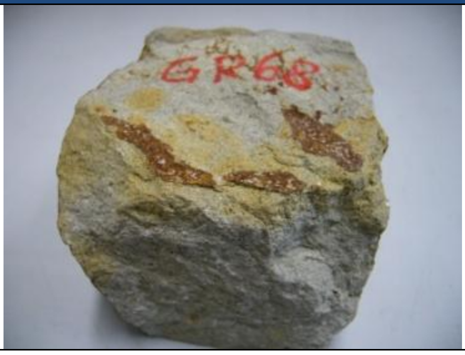	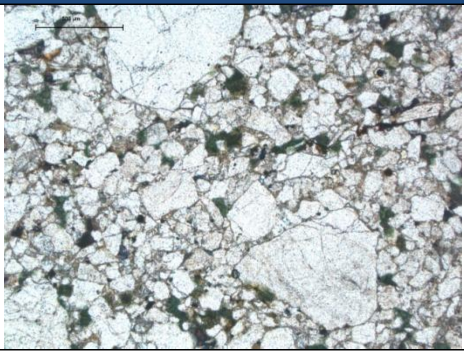
Fine-grained sandstone Dark gray, heavily weathered surface (orange to red-brown), rugged surface, little or no visible porosity	Overview: some larger rounded grains – some of them can also be angular, occasionally small fossil fragments, moderately sorted Components: quartz (monocrystalline and polycrystalline), glauconite (green, round components), mica flakes (biotite and muscovite) - Presence of cement (blue) - Occasional occurrence of fossils and rock fragments

GR 69

Macroscopic	Microscopic
	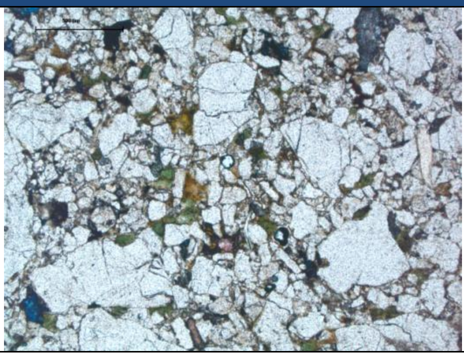
Conglomerate Quartz components are clearly visible, in some places weathered orange to reddish brown, surface carries the color gray / brown, little or no visible porosity	Overview: coarse grains are present (angular to rounded), a lot of small components – poorly sorted Components: quartz (monocrystalline and polycrystalline), glauconite (green, round components), mica flakes (biotite and muscovite) - Presence of cement (blue) - Occasional occurrence of fossils and rock fragments

GR 71,5

Macroscopic	Microscopic
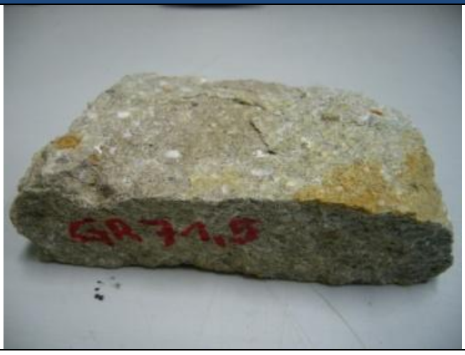	
Conglomerate Gray / brown surface - weathering orange on one side, quartz grains are clearly visible, little or no visible porosity	Overview: Many large and coarse grains - mostly rounded, chaotic arrangement, smaller components are mostly angular, poorly sorted Components: quartz (monocrystalline and polycrystalline), glauconite (green, round components), mica flakes (biotite and muscovite) - Presence of cement (blue) – Occasional occurrence of fossils and rock fragments

GR 73,5

Macroscopic	Microscopic
	
Coarse-grained sandstone Brownish, almost completely weathered, some larger quartz grains can be detected, little or no visible porosity	Overview: Some coarse grains (rounded), medium and fine grains are messy and compact (angular to rounded), poorly sorted Components: quartz (monocrystalline and polycrystalline), glauconite (green, round components), mica flakes (biotite and muscovite) - Presence of cement (blue) – Occasional occurrence of rock fragments, fossil fragments

GR 75,5

Macroscopic

Coarse-grained sandstone Light to dark brown surface, on one side very weathered (brown) - Iron-rich crust, individual quartz grains visible, compact, little or no visible porosity

GR 78,5

Macroscopic	Microscopic
	
Medium-grained sandstone Gray / brown, sometimes reddish brown weathered, individual quartz grains are clearly visible, compact, little or no visible porosity	Overview: few very coarse components (rounded), medium grains very common (angular to rounded), fine grains (angular to rounded) are poorly sorted/compact Components: quartz (monocrystalline and polycrystalline), glauconite (green, round components), mica flakes (biotite and muscovite) - Presence of cement (blue) – Occasional occurrence of fossils and rock fragments

GR 80,5

Macroscopic	Microscopic
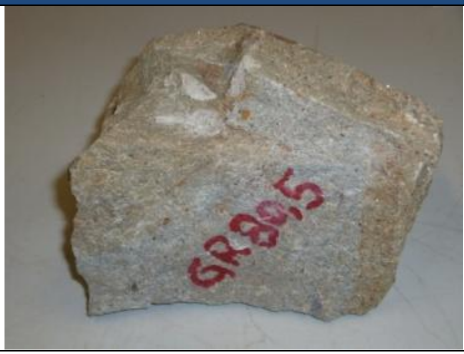	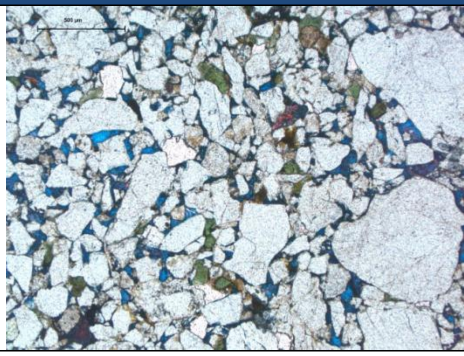
Coarse-grained sandstone Thin calcite vein visible - runs through the rock, light brown to light gray surface - slightly weathered, quartz components are clearly visible, compact, little or no visible porosity	Overview: Occurrence of some medium-sized grains (angular to rounded), finer components are poorly sorted and compact (angular to rounded) Components: quartz (monocrystalline and polycrystalline), glauconite (green, round components), mica (biotite and muscovite) - Presence of cement (blue) – Occasional occurrence of fossils and rock fragments

GR 83,5

Macroscopic	Microscopic
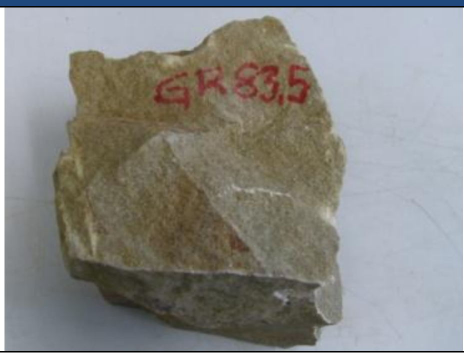	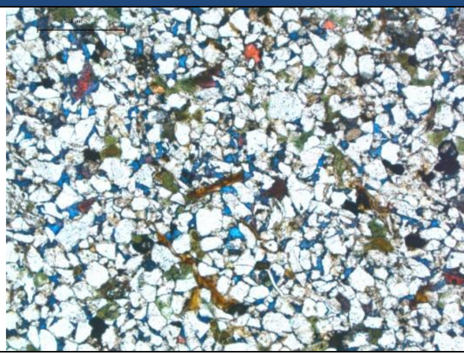
Fine-grained sandstone Strong red-brown weathering - usually light brown to brown rock surface, grains are difficult to detect (rock surface is too fine), compact, little or no visible porosity	Overview: Mostly fine grains (usually rounded - angular), compact, moderately sorted Components: quartz (monocrystalline and polycrystalline), glauconite (green, round components), mica (biotite and muscovite) - Presence of cement (blue) – Occasional occurrence of fossils and rock fragments

GR 86

Macroscopic	Microscopic
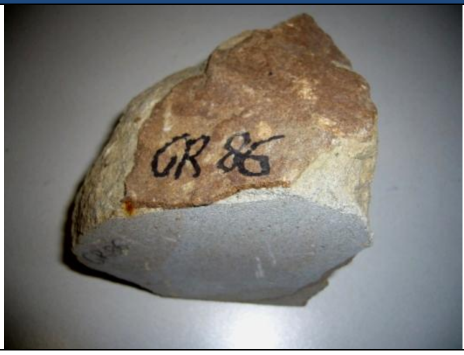	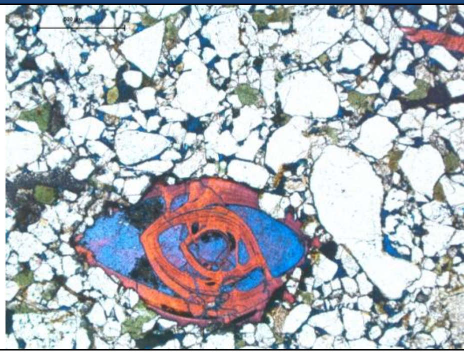
Fine-grained sandstone Some coarse components, strong reddish brown weathered rock on top and bottom, light brown to light gray, compact, little or no visible porosity	Overview: very compact – poorly sorted, occurrence of some very coarse components (rounded) and finer components (rounded to angular) - Components: quartz (monocrystalline and polycrystalline), glauconite (green, round components), mica (biotite and muscovite) - Presence of cement (blue) – Occasional occurrence of fossils (foraminifera) and rock fragments

GR 93

Macroscopic	Microscopic
	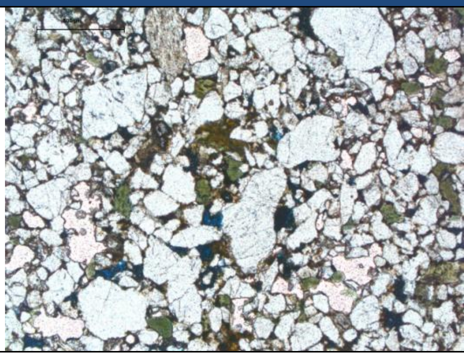
Fine-grained sandstone Strong red-brown weathering, sandstone color brown to light gray, compact, little or no visible porosity	Overview: more compact and finer than GR 86, occasionally medium-sized grains (rounded), larger components missing, fine components are densely arranged (rounded to angular), poorly sorted - Components: quartz (monocrystalline and polycrystalline), glauconite (green, round comp.), mica (biotite and muscovite) - Presence of cement (blue) – Occasional occurrence of fossils and rock fragments

X1

Macroscopic	Microscopic
	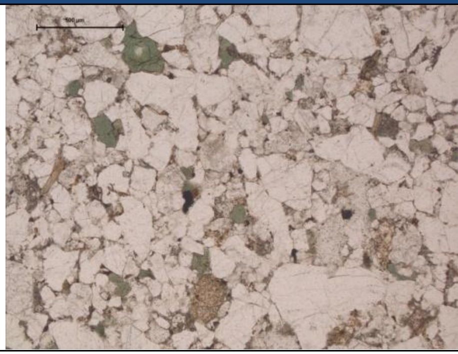
Coarse- grained sandstone Light brown, the deepest part is finer , quartz grains are clearly visible Compact and no visible porosity	Overview: compact and poorly sorted, single coarse grains (rounded), medium and fine components are angular to rounded Components: quartz (monocrystalline and polycrystalline), glauconite (green, round components), mica flakes (biotite and muscovite) - Presence of cement (blue) – Occasional occurrence of fossils and rock fragments

GRO 1a

Macroscopic	Microscopic
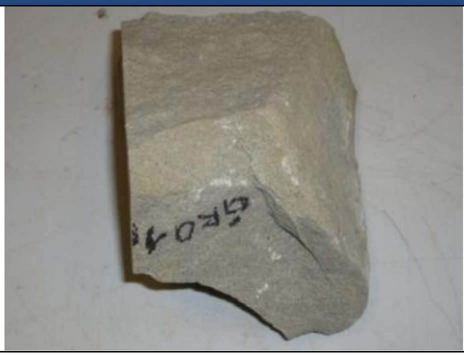	
Fine-grained sandstone Light gray (light brown) surface - not entirely weathered, compact, little or no visible porosity	Overview: extremely fine and moderately sorted, almost medium-sized components (rounded to angular) - fossils, fine components are arranged densely (rounded to angular) Components: quartz (monocrystalline and polycrystalline), glauconite (green, round components), mica flakes (biotite and muscovite) - Presence of cement (blue) – Occasional occurrence of fossils and rock fragments

GRO 1b

Macroscopic	Microscopic
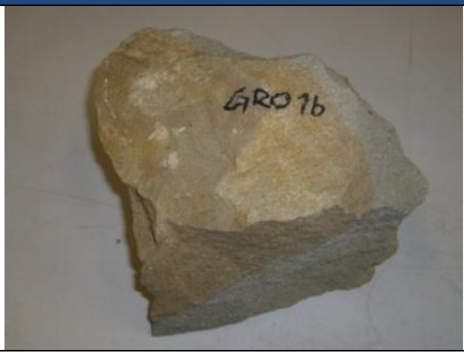	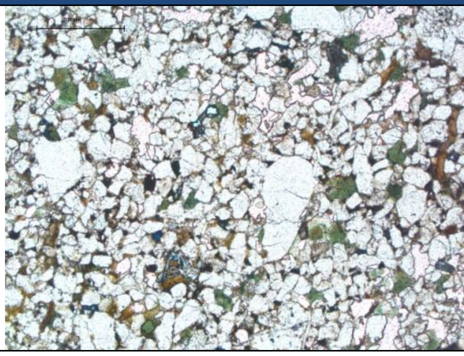
Fine-grained sandstone One-third of the sandstone is partly brownish (weathered), partly gray color, compact, little or no visible porosity	Overview: very compact, finely arranged and poorly sorted, large components are missing - medium-sized components are rounded to angular, fine grains (rounded to angular) Components: quartz (monocrystalline and polycrystalline), glauconite (green, round components), mica flakes (biotite and muscovite) - Presence of cement (blue) – Occasional occurrence of fossils and rock fragments

GRO 3

Macroscopic	Microscopic
	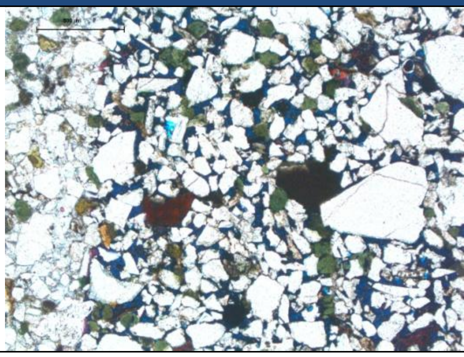
Fine-grained sandstone Very weathered brown surface, normal rock color is dark gray, compact, little or no visible porosity	Overview: not as compact as GRO 1b (still fine), random presence of larger components (rounded to angular), moderately sorted, medium-sized and fine components (rounded to angular) Components: quartz (monocrystalline and polycrystalline), glauconite (green, round components), mica flakes (biotite and muscovite) - Presence of cement (blue) – Sometimes fossils and rock fragments

GRO 3X

Macroscopic	Microscopic
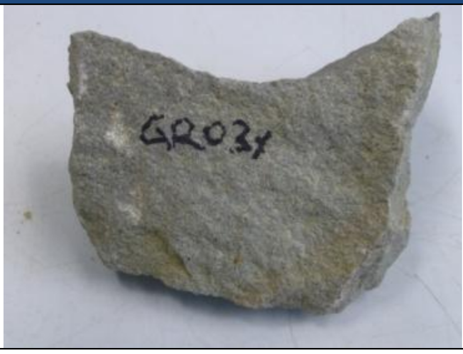	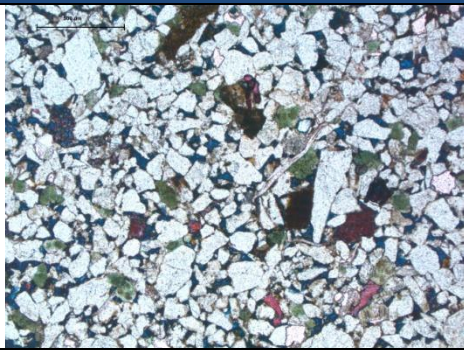
Fine-grained sandstone Gray surface, very fine - grains are not detectable macroscopically, strongly weathered, little or no visible porosity	Overview: very fine and poorly sorted, occurrence of large (rounded to angular), medium and fine components (also rounded to angular) Components: quartz (monocrystalline and polycrystalline), glauconite (green, round components), mica (biotite and muscovite) - Presence of cement (blue) – Occasional occurrence of fossils and rock fragments

GRO 4X

Macroscopic	Microscopic
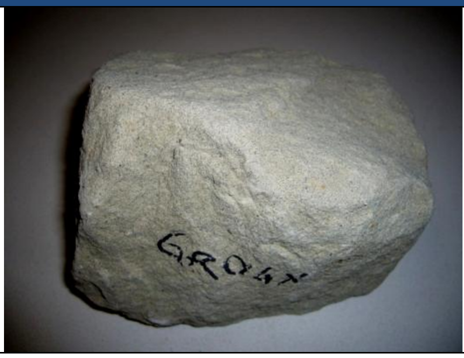	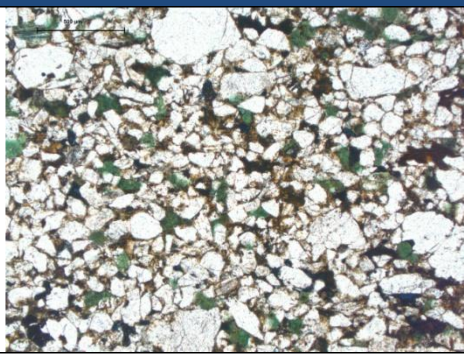
Fine-grained sandstone Gray / brown sandstone (browner, in contrast to GRO 3X), not weathered, very fine components are not visible macroscopically, little or no visible porosity	Overview: fine and compact thin section, medium grains are rounded to angular, many small grains (rounded to angular) Components: quartz (monocrystalline and polycrystalline), glauconite (green, round components), mica flakes (biotite and muscovite) - Presence of cement (blue) – Occasional occurrence of fossils and rock fragments

4.3.3 Classification of the sandstones:

The three components, quartz, feldspar and lithic fragments, were plotted in a triangular plot after Folk (1968) (figure 30 to figure 37). According to this plot, the sandstones can be classified as quartz arenites. All samples consist of more than 98 % quartz. Here poly- and monocrystalline quartz were combined. Since the percentage of glauconite lies between 15-35 %, the sandstones can also be referred to as glauconite bearing quartz arenites (Mount, 1985).

By plotting all the individual samples, the similarity of the rocks can be seen (figure 30 to figure 37). The first seven plots show the results of the south quarry wall and the last one is the plot of the east wall.

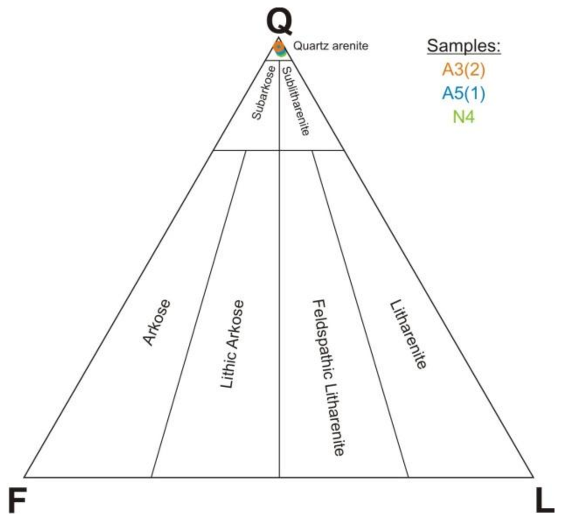

Figure 30 Classification of the sandstones after Folk – South wall: Samples A3(2), A5(1) and N4

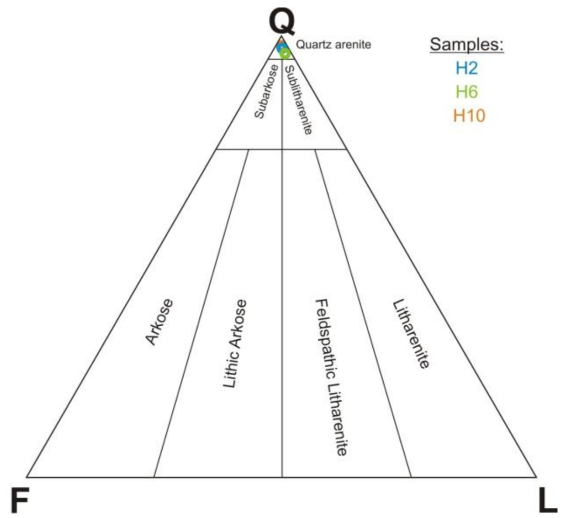

Figure 31 Classification of the sandstones after Folk – South wall: Samples H2, H6 and H10

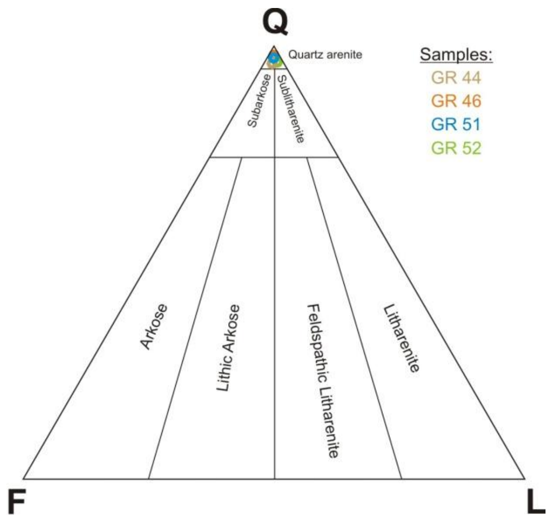

Figure 32 Classification of the sandstones after Folk – South wall: Samples GR 44, GR 46, GR 51, GR 52

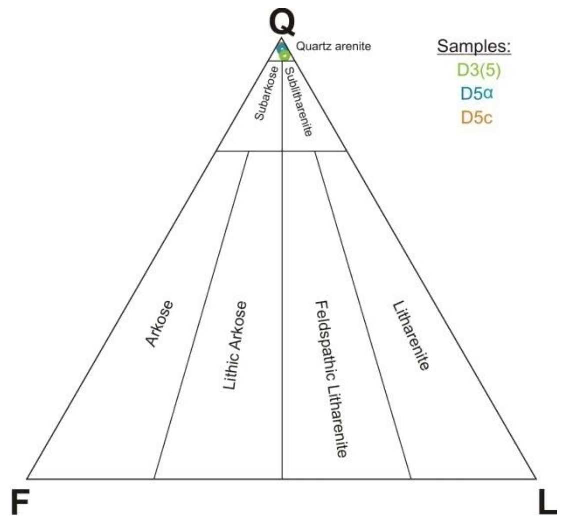

Figure 33 Classification of the sandstones after Folk – South wall: Samples D3(5), D5α and D5c

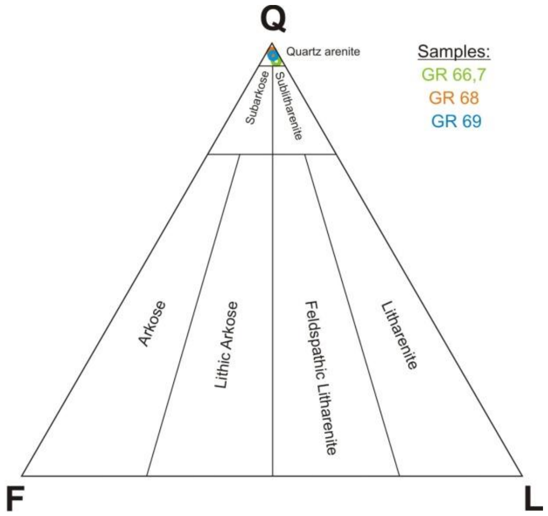

Figure 34 Classification of the sandstones after Folk – South wall: Samples GR 66.7, GR 68 and GR 69

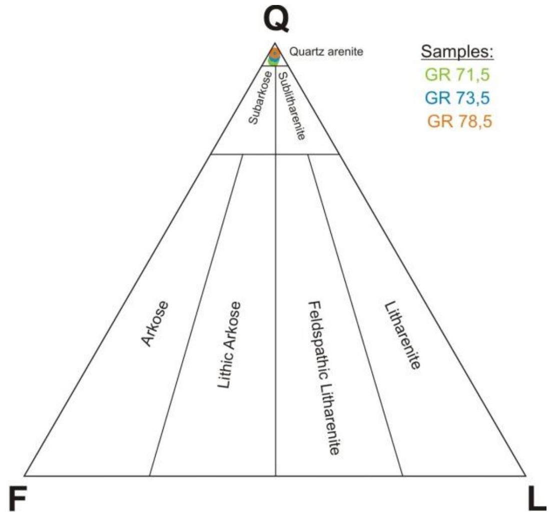

Figure 35 Classification of the sandstones after Folk – South wall: Samples GR 71.5, GR 73.5 and GR 78.5

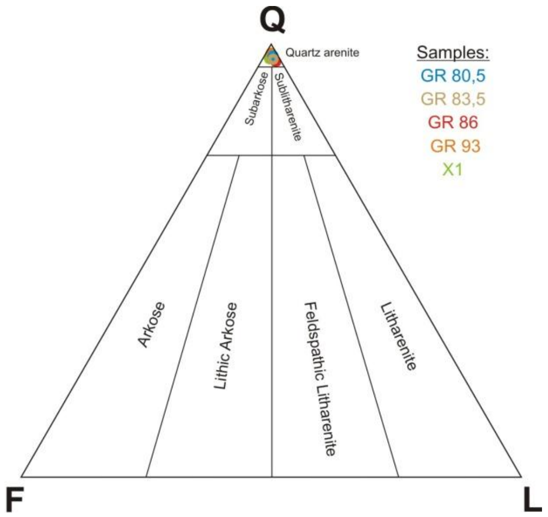

Figure 36 Classification of the sandstones after Folk – South wall: Samples GR 80.5, GR 83.5, GR 86, GR 93 and X1

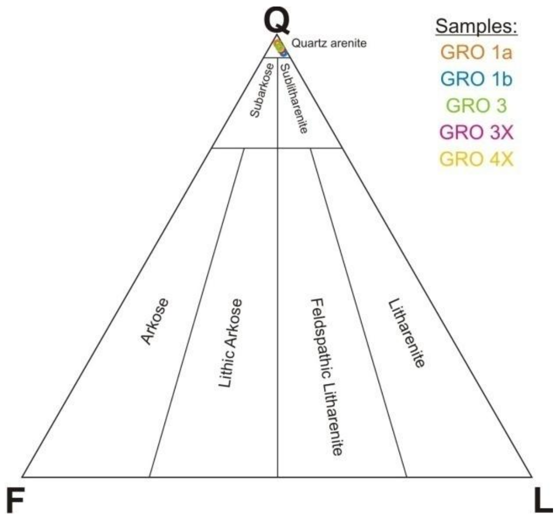

Figure 37 Classification of the sandstones after Folk – East wall: Samples GRO 1a, GRO 1b, GRO 3, GRO 3X and GRO 4X

4.3.4 X-ray diffraction (XRD):

The mineralogical results, which were analyzed with XRD, are comparable with the results of the point counting. The most abundant mineral in most of the samples was quartz. Further, glauconite, calcite, and orthoclase were found (figures 38 to 43).

Calcite is caused by the presence of fossil fragments and calcite cement.

All diffractograms show similar results.

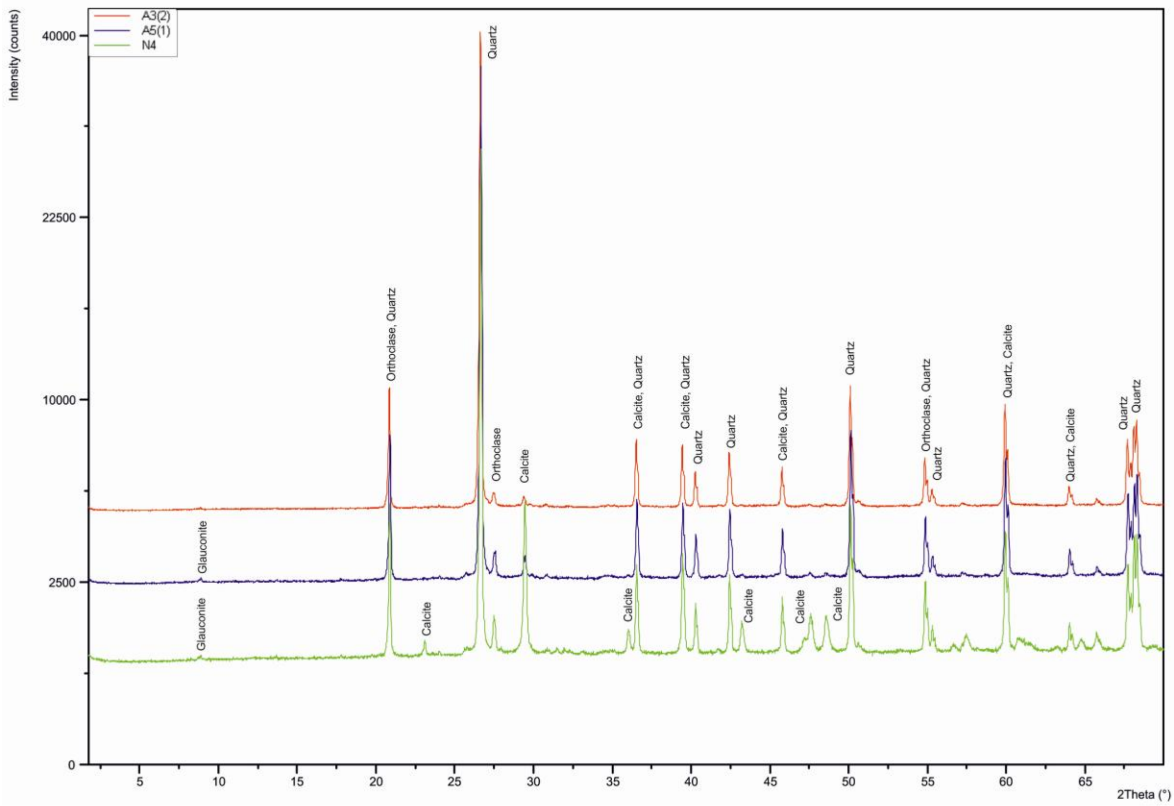

Figure 38 X-ray diffraction patterns of samples A3(2), A5(1) and N4 of the south wall of the quarry

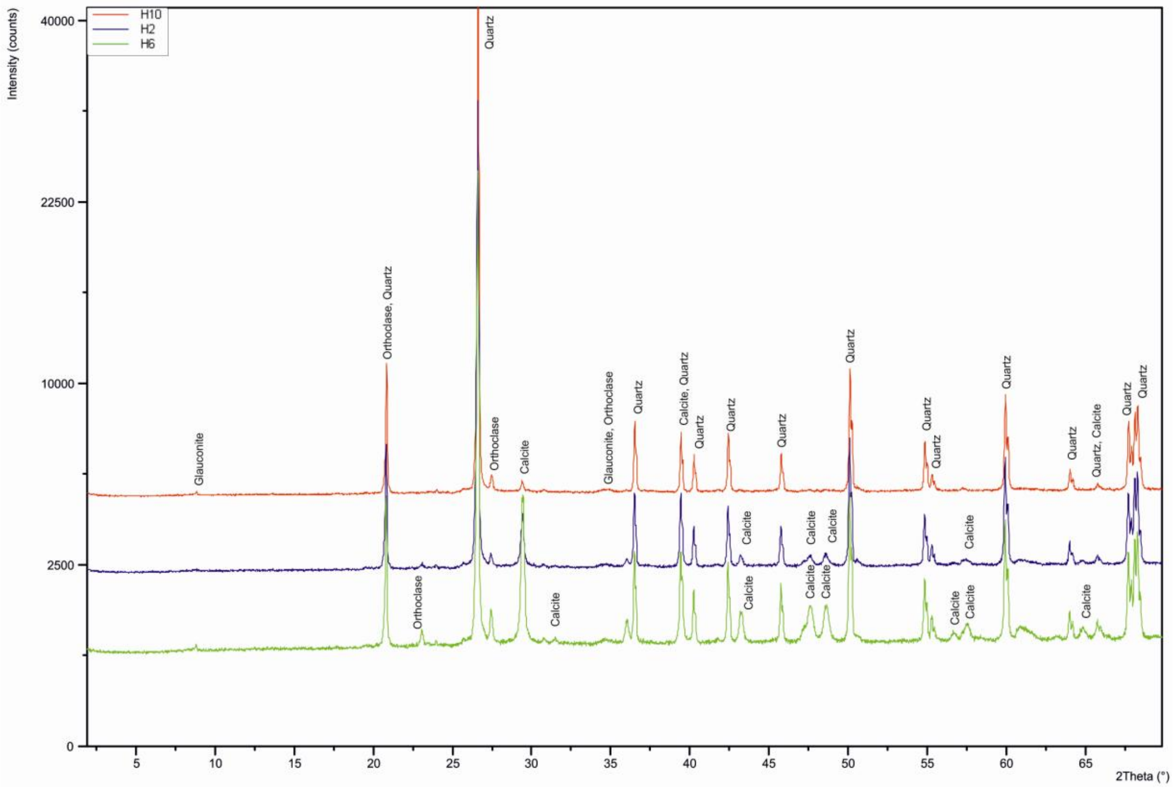

Figure 39 X-ray diffraction patterns of samples H2, H6 and H10 of the south wall of the quarry

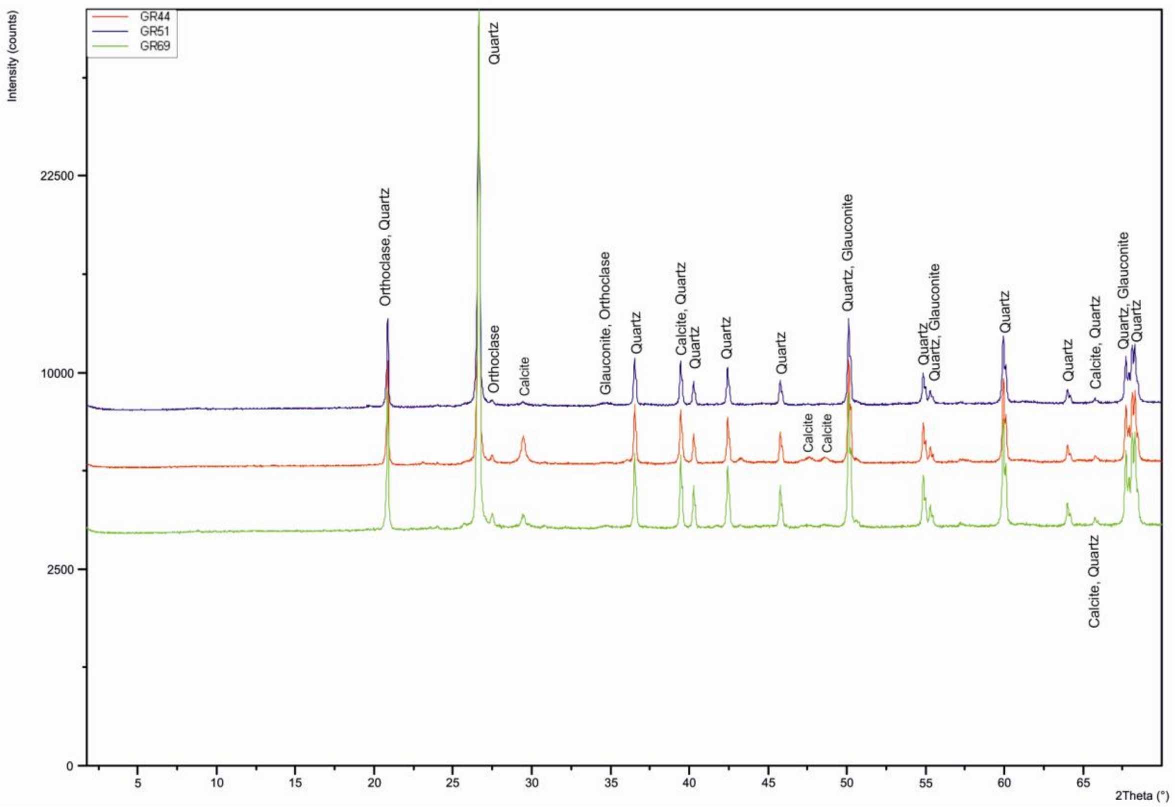

Figure 40 X-ray diffraction patterns of samples GR 44, GR 51 and GR 69 of the south wall of the quarry

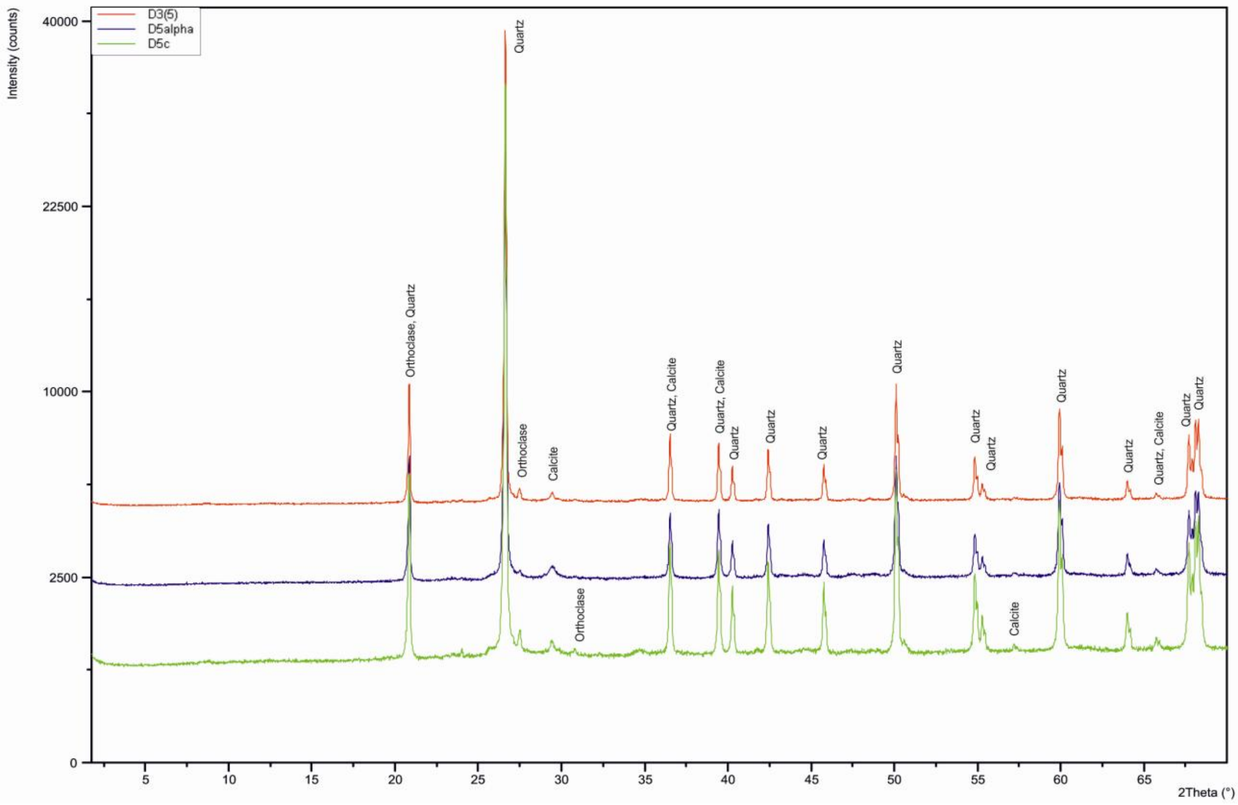

Figure 41 X-ray diffraction patterns of samples D3(5), D5α and D5c of the south wall of the quarry

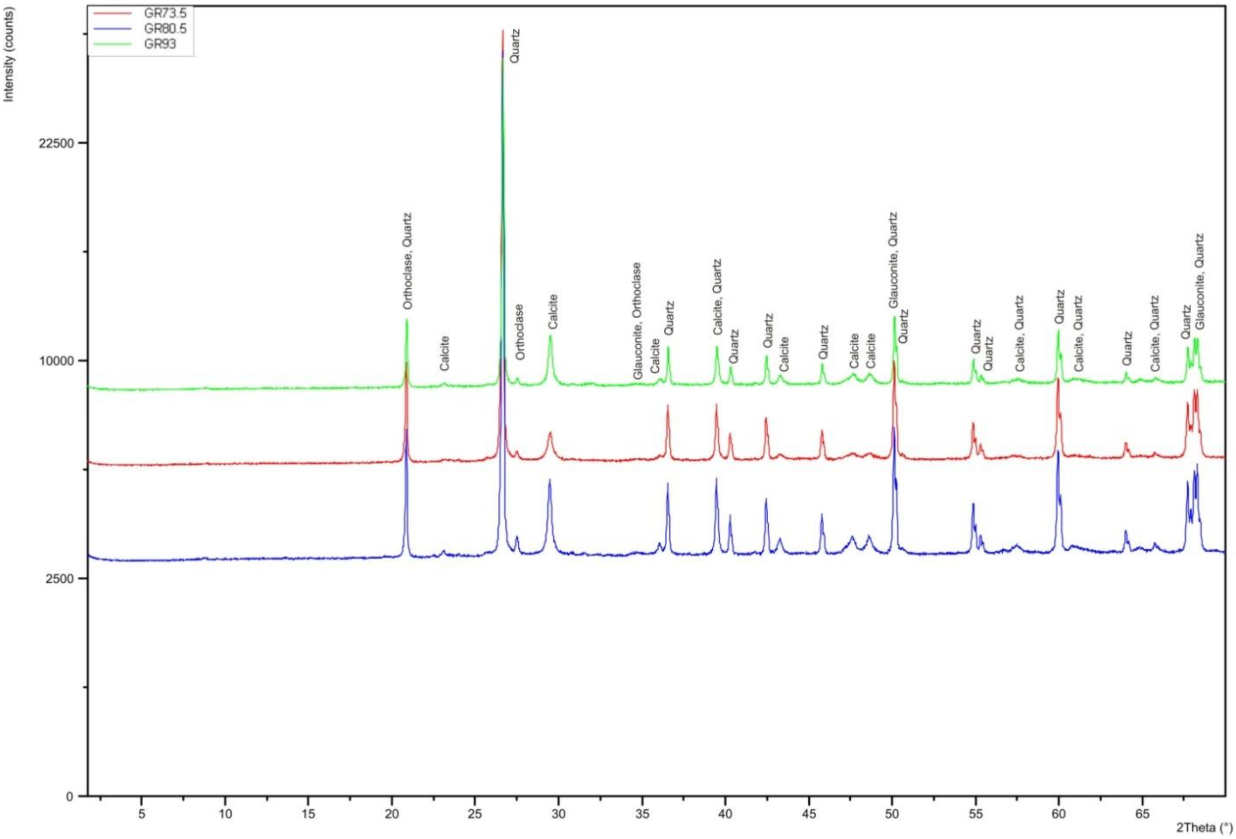

Figure 42 X-ray diffraction patterns of samples GR 73.5, GR 80.5 and GR 93 of the south wall of the quarry

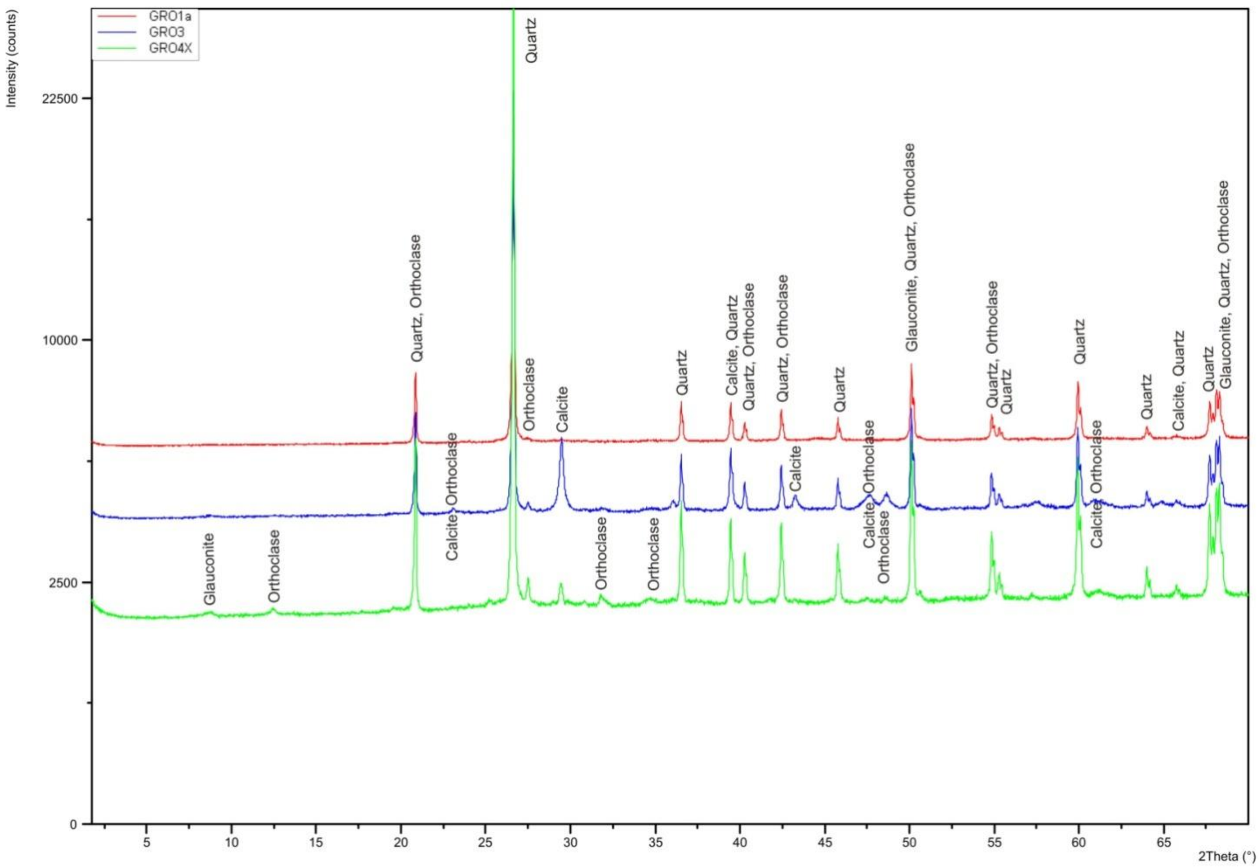

Figure 43 X-ray diffraction patterns of samples GRO 1a, GRO 3 and GRO 4X of the east wall of the quarry

4.3.5 Cathodoluminescence (CL):

By stimulating the samples with an electron beam the minerals show different colors. Quartz is represented by the color dark blue or brown, K-feldspar by light blue and carbonate cement by orange. The carbonate cement is very dominant and starts corroding the individual grain edges (figure 61). Two sandstone samples were selected for this analysis, sample GR 78.5 from the south wall of the quarry and sample GRO 3 of the east wall. The samples were selected according to their glauconite, cement and quartz amount.

Figure 44 is a cathodoluminescence picture of sample GR 78.5. A clear dominance of calcite cement, as well as quartz and feldspar is visible. The yellow-green grain in the upper left side of the thin section represents apatite. The picture on the right side shows the same sample, mainly quartz, in crossed polarized light, XPL (figure 45). In Figure 46 polycrystalline quartz is visible. But the dominant components of cement and K-feldspar are also visible. This is even more evident in crossed polarized light (figure 47).
Figure 46 additionally shows the dominant presence of monocrystalline quartz.

Figure 44 CL Photo of the sample GR 78.5

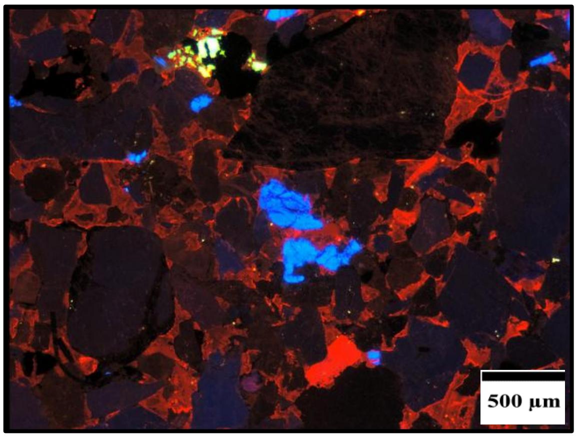

Figure 45 XPL Photo of the sample GR 78.5

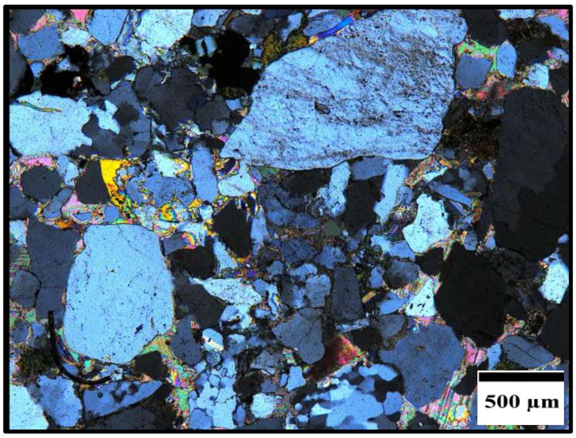

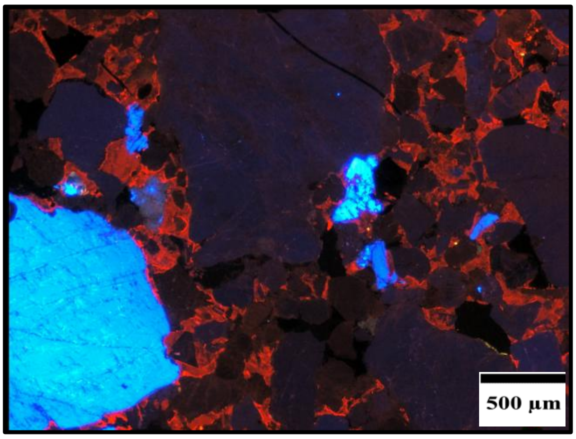

Figure 46 CL Photo of the sample GR 78.5

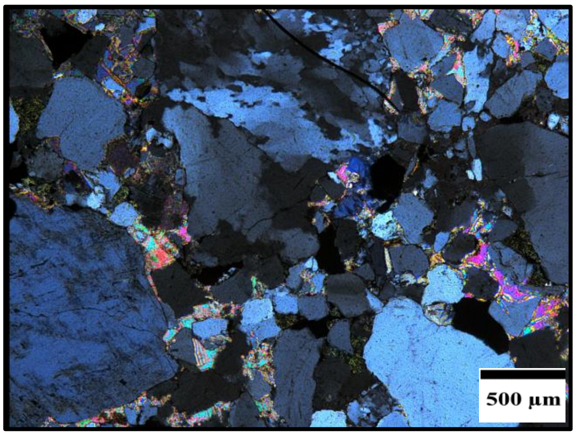

Figure 47 XPL Photo of the sample GR 78.5

Figure 48 shows calcite cement as dominant phase, also quartz and feldspar are present. In the middle of the thin section an apatite is visible. With crossed polarizer the dominance of quartz and k-feldspar are visible (figure 49).

In the middle of Figures 50 and 51 a very big and elongated part of a carbonate fossil fragment can be seen. This fragment has a bright orange color. With XPL (figure 51) the structure of the fossil fragment is very good visible, but also the presence of the monocrystalline quartz grains.

Figure 48 CL Photo of the sample GRO 3

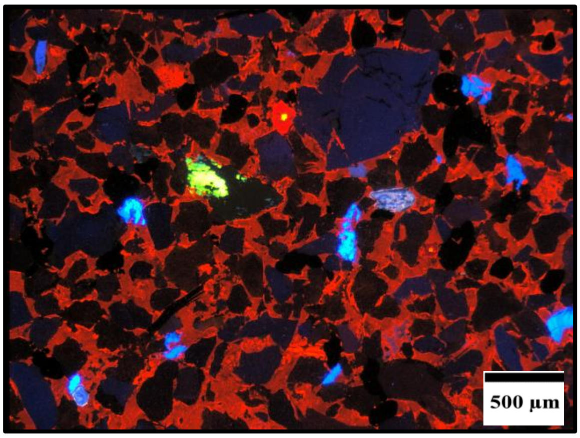

Figure 49 XPL Photo of the sample GRO 3

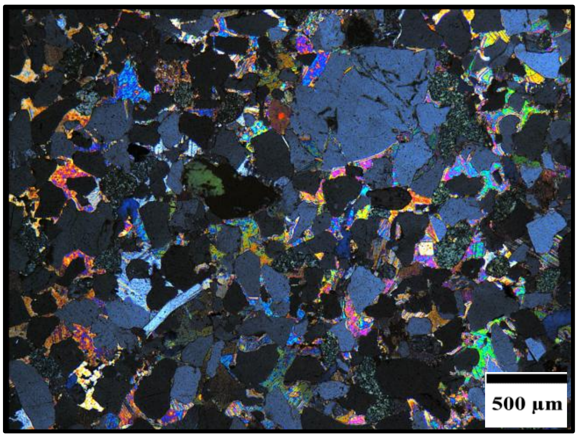

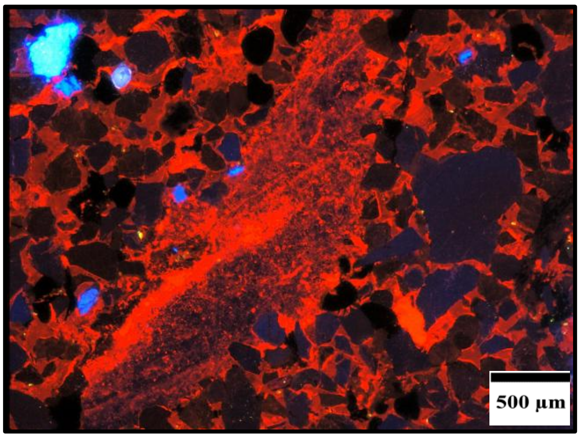

Figure 50 CL Photo of the sample GRO 3

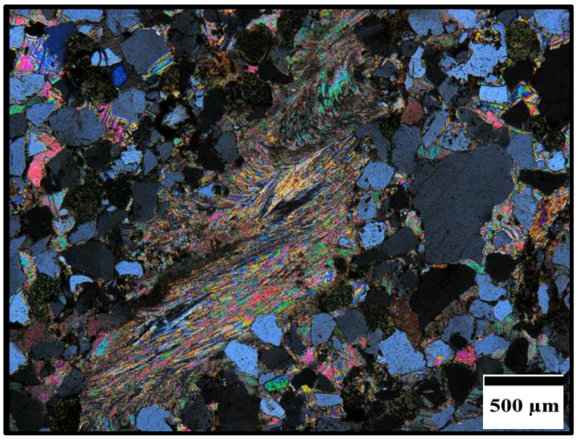

Figure 51 XPL Photo of the sample GRO 3

4.3.6 Electron microprobe (EMP):

The crystal-chemical structural formulae of glauconites of two sandstone samples (GR 78.5 and GRO 3) were calculated using the Marshall method (Marshall, 1949).

The process of calculating is described in chapter 3.2.6. For the formula calculation the results of table 3 were important.

The results of the calculation (mean value) are the formulae:

Glauconites of sandstone sample GR 78.5

$(K_{0.67}\ Na_{0.01}\ Ca_{0.04})\ (Al_{0.68}\ Fe_{0.87}\ Mg_{0.43})\ (Si_{3.59}\ Al_{0.41})\ O_{10}\ (OH)_2$

Glauconites of sandstone sample GRO 3

$(K_{0.72}\ Na_{0.01}\ Ca_{0.04})\ (Al_{0.66}\ Fe_{0.91}\ Mg_{0.42})\ (Si_{3.64}\ Al_{0.36})\ O_{10}\ (OH)_2$

Table 3 Chemical composition (wt % - mean value) and calculated structural formulae (based on $O_{10}\ (OH)_2$)

Chemical composition wt %		
	GR 78.5	GRO 3
SiO_2	50.50	51.19
Al_2O_3	13.01	12.23
Fe_2O_3	16.24	17.04
MnO	0,01	0,01
MgO	4.03	3.95
CaO	0.59	0.46
Na_2O	0.08	0.09
K_2O	7.41	7.94
Tetrahedral position		
Si	3.59	3.64
Al	0.41	0.36
Octahedral position		
Al	0.68	0.66
Fe	0.87	0.91
Mg	0.43	0.42
Interlayer position		
K	0.72	0.72
Na	0.01	0.01
Ca	0.04	0.04

The tetrahedral, octahedral and interlayer charges of each glauconite grain were plotted in the triangular plots in figure 52 and figure 53. In the sample GR 78.5 thirteen points were analyzed and in sample GRO 3 twenty-three.

All analyses (in green results of the rim and in blue results of the centre of the glauconite grains) plot inside of the glauconite field (figure 52 and figure 53). This demonstrates that the composition of the glauconites in the sandstones is evolved (Odin, 1988) and does not contain expandable smectite anymore.

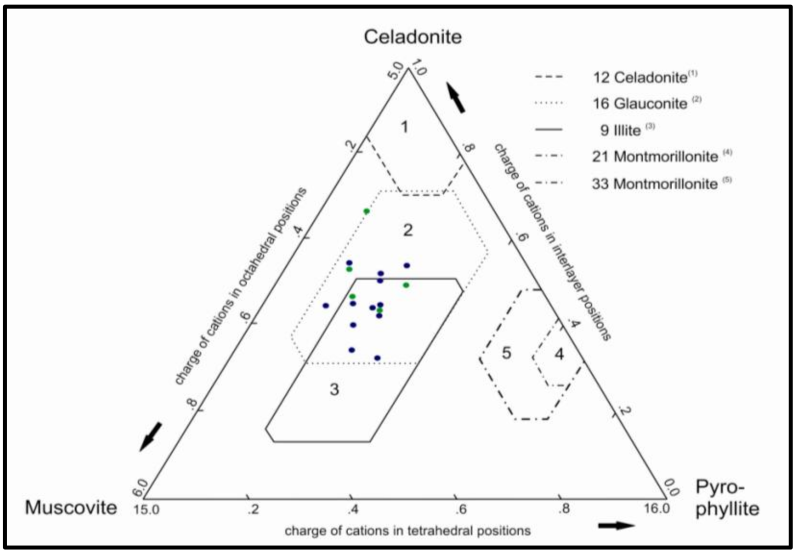

Figure 52 Charge distribution diagram with end-members celadonite, muscovite and pyrophyllite (modified from Köster, 1977) of the sample GR 78.5 – In blue the analyses in the centre (n=15) of the single grains and in green on the rim (n=8)

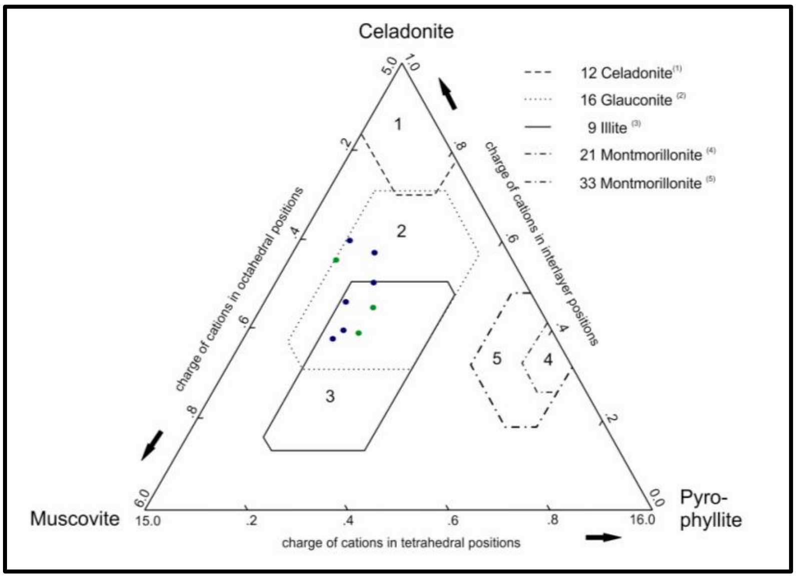

Figure 53 Charge distribution diagram with end-members celadonite, muscovite and pyrophyllite (modified from Köster, 1977) of the sample GRO3 – In blue the analyses in the centre (n=8) of the single grains and in green on the rim (n=5)

The composition of the carbonate cement of the two sandstone samples was also analyzed in the centre and the rim. Fifty-eight points were analyzed.
In the following table, the mean values of the composition of the cements in the centre and on the rim are shown. Complete results are given in appendix (8.).

Table 4 Chemical composition (wt%) of the cement in both samples GR 78.5 and GRO 3

Chemical composition wt %				
	GR 78.5		GRO 3	
	Centre	Rim	Centre	Rim
Na_2O	0.03	0.08	0.03	0.05
SiO_2	0.06	0.29	0.04	0.07
MgO	0.43	0.48	0.45	0.39
Al_2O_3	0.03	0.04	0.02	0.02
K_2O	0	0	0	0
CaO	58.56	58.27	59.02	54.40
MnO	0.10	0.11	0.15	0.13
FeO	1.46	1.55	1.80	1.56

The compositions of the samples show a high amount of 54 to 59 wt % CaO. The amount of FeO is above 1 wt %. The centre and the rim of the samples are very similar. The cement in the sandstone samples are can be classified as Fe-bearing calcite cement. The average composition of calcite cement is 0.4 % MgO, 57.6 % CaO, 0.1 % MnO and 1.6 % FeO.

4.4 Technical results:

4.4.1 Porosity:

To determine the porosity, different methods were used. On one hand, the bulk density was determined by immersion weighing, on the other hand, the true density was determined by using a pycnometer.

In Figure 54 a comparison of these two methods is displayed. The porosity values range from 0.6 to 12.3 %. The comparison shows, that both methods give comparable results. The porosity of most samples ranges between 2-8 %. There are six samples A3(2), GR 52, GR 66.7, GRO 1a, GRO 1b and GRO 4X, which have higher porosity values. The first two samples GR 52 and GR 66.7 are samples of the south wall of the quarry and the samples GRO 1a, GRO 1b and GRO 4X are sandstones samples of the east wall. A low porosity value suggests that the rock samples are not suitable as reservoir rock for oil and natural gas.

In some cases, the methods resulted in different values. This can be explained by the different preparation methods for the sandstone samples. With the pycnometer powdered samples were used and with the immersion weighing the whole sandstone sample. Another reason can be the error range for the measurements.

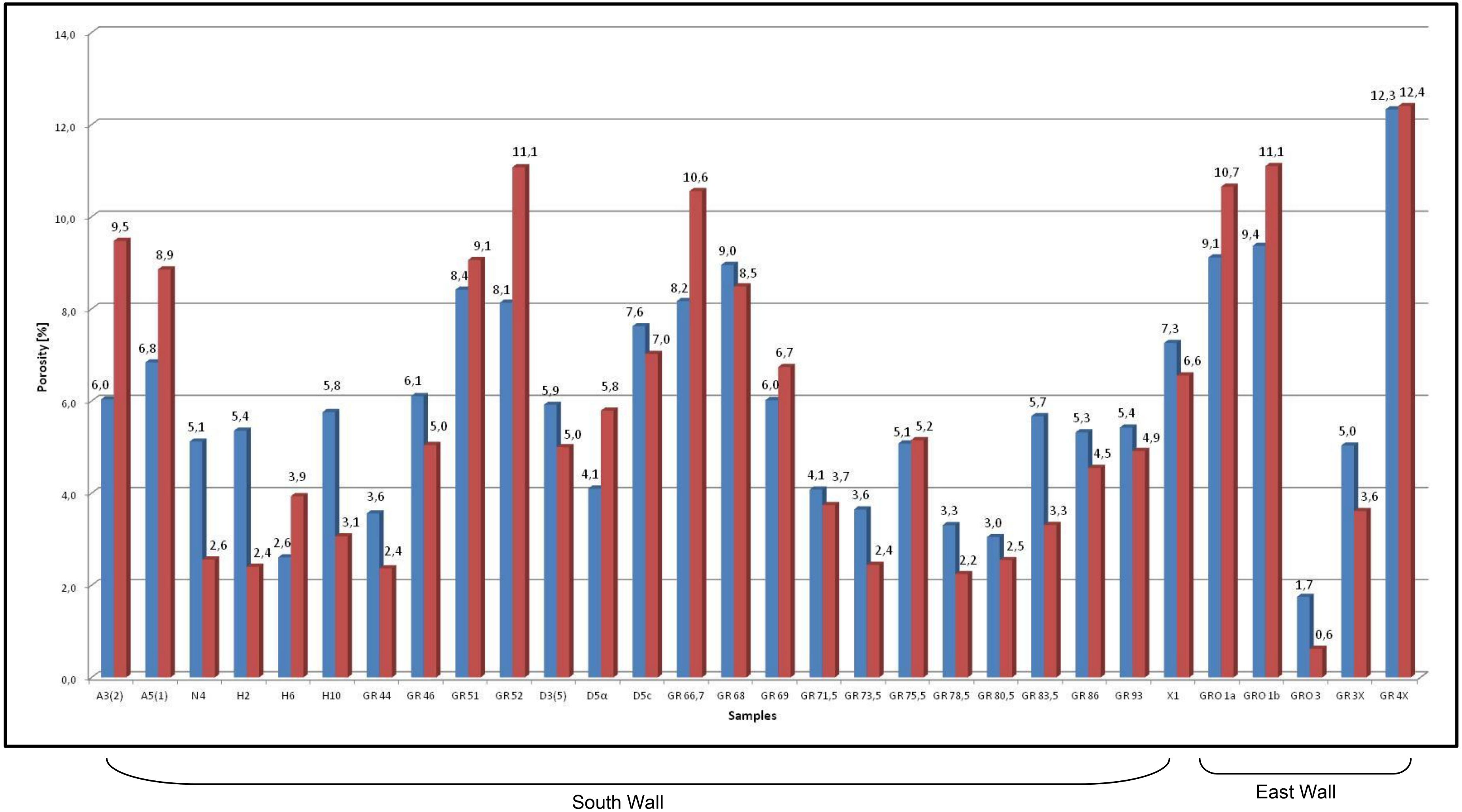

Figure 54 Results of the porosity measuring [%]: The blue bar shows the results of the pycnometer test and the red one the results of the immersion weighing. The samples A3(2) to H10 and D3(5) to D5c are samples, which were collected by Besada 1996. It characterized the profile sequence of the south wall and the east wall from the base (A(3) respectively GRO1a) to the top (X1 respectivley GRO 4X)

Bulk density vs. Net density:

The bulk density was determined with the immersion weighing and the net density with a pycnometer. The measuring method was described in chapter 3.3.1.

Most of the sandstone samples plot near the regression line (r = 0.908), but some of them show a strong difference between the different measuring methods (figure 55). The sample GRO 4X is outside of the line, with porosity values over 12 %. The other sandstone samples with values between 2 % and 8 % porosity plot near the line, there are not really significant differences.

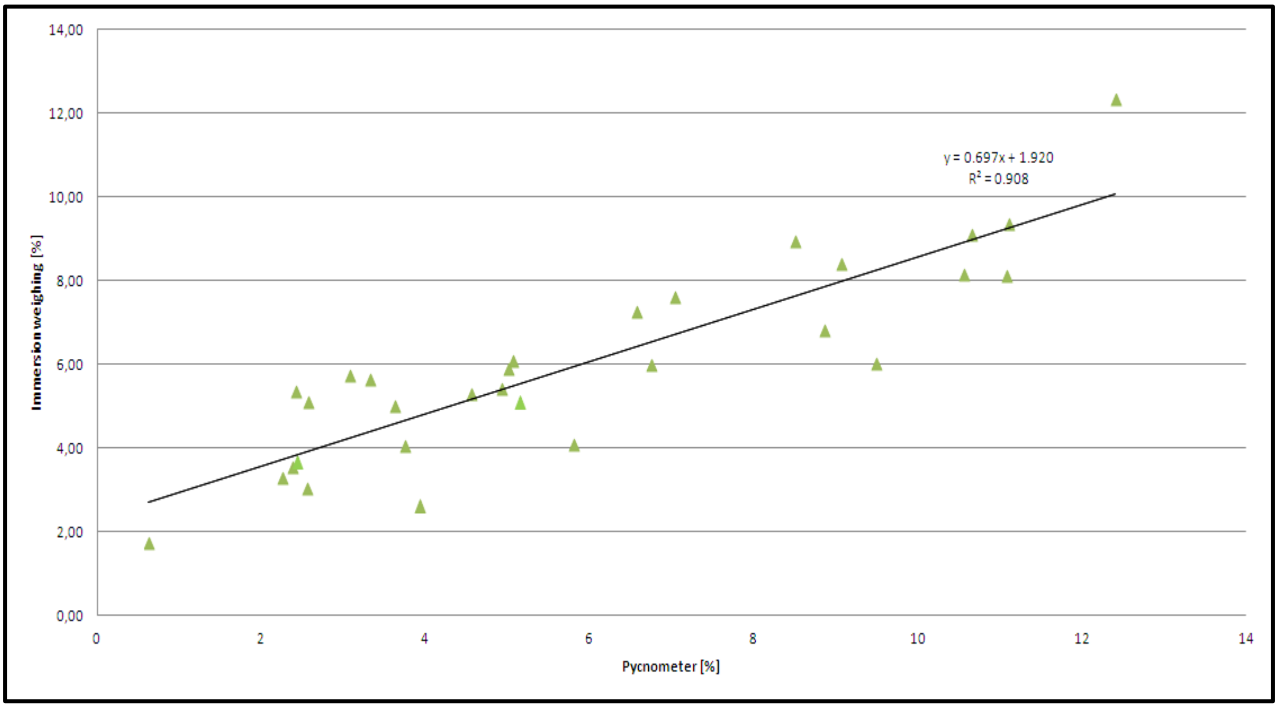

Figure 55 Bulk density measured with an immersion weighing vs. net density measured with a pycnometer

4.4.2 Permeability:

The permeability was determined using a micropermeameter at OMV in Gänserndorf. For the measurement, it was particularly important to use a fresh, smooth surface otherwise the nitrogen could not be pressed right through the rock. For the same reason it is important to ensure that the micropermeameter sits tightly on the sample with no gap in between. Unfortunately, this could not be achieved by all rock samples. From the east wall two sandstone samples could be analyzed, because the other rock samples were too big for measuring with micropermeameter. The results range from 4.5 to 6.5 mD (figure 56). Samples GR 52, GR 66.7 and GRO 1a have slightly higher permeabilities with 9.04 to 10.01 mD (figure 56).

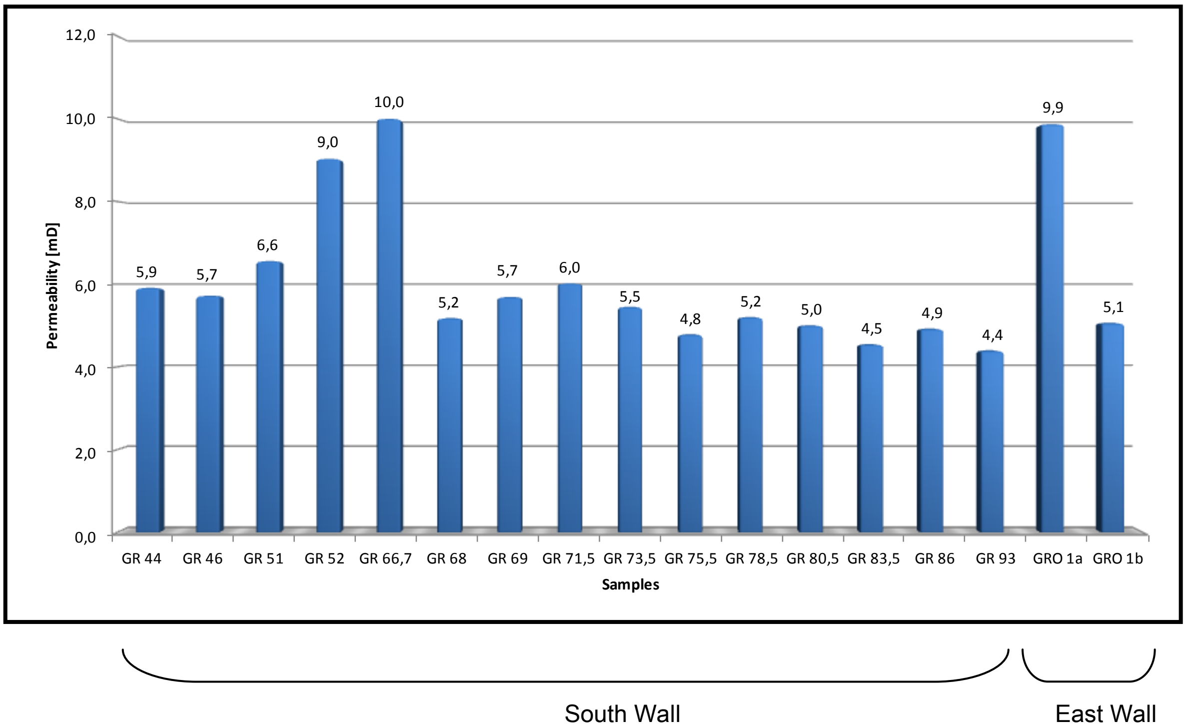

Figure 56 Results of the permeability measurements [mD]

4.4.3 Porosity vs. Permeability:

In Figure 57 the porosity is plotted against the permeability. The porosities and permeabilities are positively correlated with $R^2 = 0.372$ (correlation coefficient). Samples with porosities of 2-6 % and permeabilities of 4-6 mD (figure 54 and figure 56) plot near the regression line. Samples GR 51, GR 52, GR 66.7, GR 68 (green triangles) and samples GRO 1a and GRO 1b (blue triangles) plot further away from the regression line.

The other samples from the east wall could not be plotted in figure 57 as they could not be measured with the micropermeameter. Also the samples, which were taken by Besada from the south wall, were not measured.

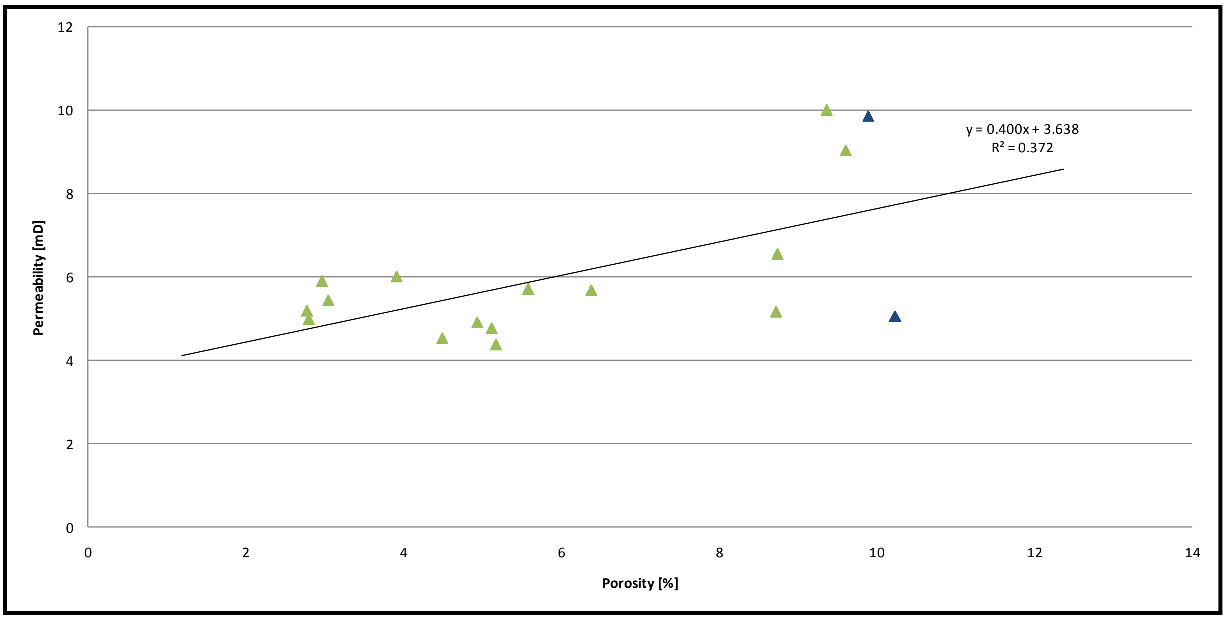

Figure 57 Porosity vs. Permeability of the different samples – In green the samples of the south wall of the quarry and in blue the samples of the east wall

5. Discussion

This master thesis studies the reservoir properties of the Greifenstein Formation from the quarry Strombauamt (Lower Austria). For this study, outcrop samples were collected and analyzed for their porosity and permeability. Also the chemical and mineralogical compositions of the sandstone samples were determined.

In this chapter the results will be discussed and compared with literature, such as Besada (1996), Rammel (1989) and Hösch (1985).

5.1 Outcrop Sedimentology

Two walls of the quarry were studied; the east wall and the south wall. The profile on the south wall is stratigraphically older than the profile on the east wall. This is based on the general dip orientation of the beds and the thickness of the sandstone banks.
In addition samples of Besada (1996) from (now covered parts of) the south wall were also analyzed.

In the counterpart of the profile of the west wall (logged by Stephanie Neuhuber, figure 58), sandstones can be seen with thin layers of pelites. Similar layers are present on the top of the south wall (figure 26). Only the macroscopic lithology was determined on the west wall. The observation confirmed a good correlation between the profile walls (east, south and west wall). By comparing lithology and layer thickness of sandstone banks, it could be confirmed that the profiles of the quarry Strombauamt belong to one continuous formation, although the Greifenstein Formation is not fully exposed at the quarry.

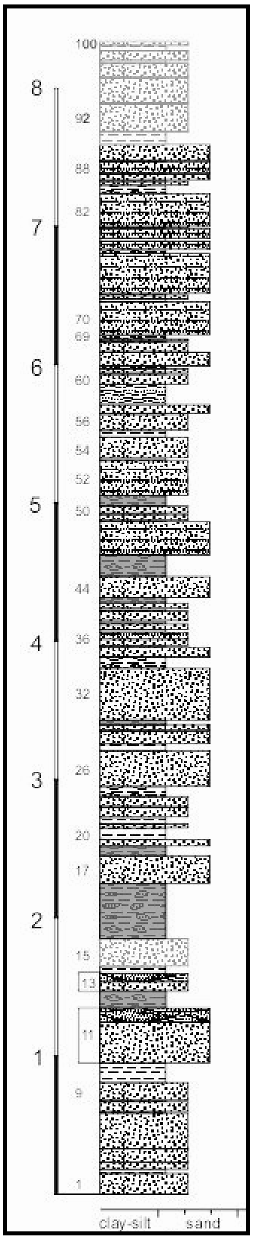

Figure 58 Profile of the west wall of the quarry (from Dr. Stephanie Neuhuber)

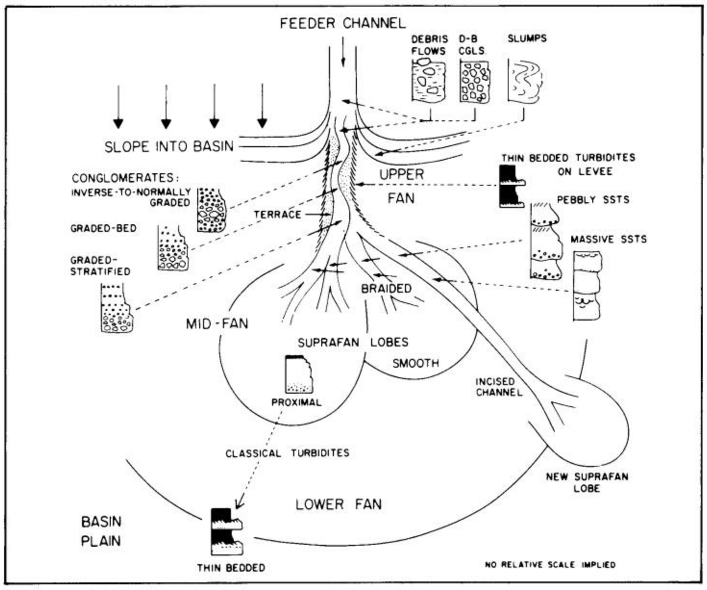

Figure 59 Submarine/deep-sea fan model: Delivery of the sediments from the continent to the deep sea. Sediments are deposited on the slope or on the basin floor. Fan geometries develop where the depositional system enters the basin floor. First, coarser components like conglomerates are deposited. In a more distal position, sandstones are deposited. Classical turbidites are deposited in the lower fan (after Walker 1980). The red arrow in the figure shows, where the deposition of the studied profile could have taken place in such a model.

Figure 59 shows the submarine/deep-sea fan model after Walker (1980).
This model can be used to explain, in what depositional environments and systems the deposition of the sediments of the quarry Strombauamt took place. Following this model it can be interpreted, that the sediments, which were sourced from the Bohemian Massif (Besada, 1996 and Hösch 1985), were transported through a canyon into the deep sea. Grain size and thickness allow an interpretation of the depositional environment. A canyon cut into the slope allowed transport of sediments to the upper fan (Walker, 1980).
Thin bedded turbidites were deposited on levees of the channel. Channel fillings consist of massive sandstones and conglomerates (Besada, 1996).
By comparing Walker´s model (1980) and the profiles, it can be said that the sediments in the area were deposited in a channel. Overall, deposition can be interpreted to have taken place in an upper to mid fan environment. In addition figure 59 shows that braided channel systems occur in the middle fan. They are filled with massive sandstone banks at the channel base and with thin and fine-grained sedimentary material in the upper part (Besada, 1996).
In the distal part of the deep-sea fan model, the lower fan is characterized by an absence of channels and the appearance of fine sediments. Classical turbidite sequences are visible there (Walker, 1980). Such *classical "distal" turbidite* sediments were not found in the profiles of the quarry Strombauamt (Besada, 1996).

From the south wall Besada (1996) recorded conglomerates at the base, massive sandstone banks with *classical turbidites* in the middle part, and a thin-bedded sandstone

bank from the top of the wall. Sedimentary features of this wall are: normal and reverse grading, amalgamation, lamination and cross-bedding (figure 26).
The conglomerates, which were found in the lower part of the south wall, could be interpreted as upper fan deposits, which were caused by debris flows. According to Schäfer (2005) the components of sand and pebbles were held in suspension during transport. Massive sandstones could be deposited in the upper fan. The turbidites, they could be finer-grained turbidites, which were deposited on the wall of major feeder channels in continuation of the canyon (Walker, 1980). Occasionally turbidites that can be described with the Bouma sequence (figure 3) are present.

Recognizable structures in the eastern outcrop wall were also channel lenses and channel fills (figure 27 and figure 60). They allow a reconstruction of the depositional environment. The channels in figure 60 could be part of a deep sea fan system (figure 27 and figure 59).

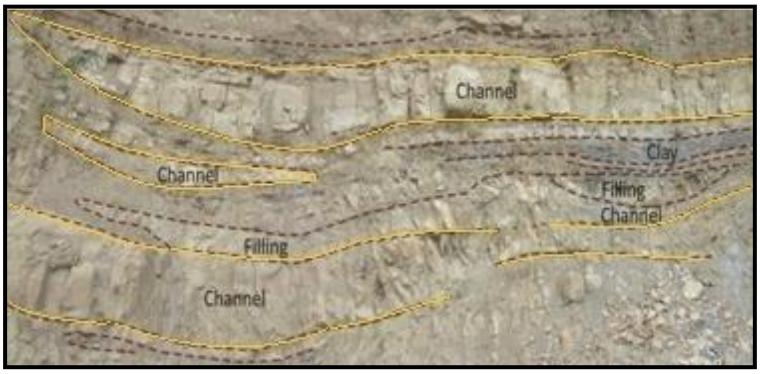

Figure 60 Channel systems of the east quarry wall

A precise classification of the east wall according to the Walker model is difficult, since the wall consists of only largely and fairly dense sandstone.
In the fan models of Walker (1980) it can be interpreted as upper to middle fan, consisting of thick bedded sandstones as channel fills.
At the height of 600 and 700 cm in the first profile of the east wall, lamination and cross bedding is found. This could indicate the occurrence of turbidites.

The channels represent individual units, with slightly different porosity and composition, even if they come from the same source area.
Based on these observations, the sediments of the eastern quarry wall were deposited in the upper fan, as already described by Besada (figure 59).

At the east wall of the quarry it is difficult to say whether the thick-bedded, solid and partially weathered sandstones found in the quarry represent parts of a classical Bouma sequence (described in figures 20, 21 and 22).
In general the sediments have a fining upward trend with a massive sandstone bed at the base, indicating a Ta sequence. Occasionally ripple lamination and stratification are found in profile 1 (figure 23 and figure 24), which indicate the presence of sequences Tb (lamination) and Tc (ripples) (figure 3) respectively.
These three sequences represent the actual turbidite body. The missing sections, which would complement the Bouma sequences are Tef (massive and graded turbiditic pelites) and Tep (pelagic/hemipelagic pelites). These could not be observed in the eastern profile wall.

These results show that these could be again an upper fan deposits. However, this is only based on fairly dense sandstones with no further evidence.

Hans Egger and Michael Wagreich (personal communication) have the opinion that an interpretation in the context of a fan system is unlikely and that the Greifenstein Formation may represent a deep-sea channel system based on the predominance of channels and channel-fills. One reason may be that in the quarry or in the area no further outcrops exist, where missing parts of a deep-sea fan model are visible.
And since in the quarry Strombauamt not sufficient information is available, except on the east wall channel system, a classification based on Walker´s fan model (1980) is not possible.

Besada (1996), Rammel (1989) and Hösch (1985) have already studied the provenance of the sediments. By studying transport direction, grain size distribution, as well as mineralogy (especially heavy minerals) and sedimentology they interpreted the sediment provenance to be from north-northwest. It can thus be interpreted, that the sediments are derived from the Bohemian Massif. This thesis focused on other subjects, but was also dealing with the mineralogy and rock composition. On the basis of chemical and mineralogical evidence within the quarry Strombauamt their interpretation can be supported. These chemical and mineralogical evidences include, for example, similar quartz contents (mono-and polycrystalline quartz), occurrence of glauconite and iron bearing calcite cement.

5.2 Sandstone Petrology

Under the microscope it can be seen that the samples are well cemented with carbonate cement (calcite) which fills all former porosity. This tight cementation minimizes the possibility to store hydrocarbons.

This is obviously not good for the reservoir quality of the formation. Oil and natural gas are normally reservoired in communicating pores; in the sediments under study, the grains are tightly cemented together with no apparent pore space.

This is supported by mineralogical and chemical analytical methods (XRD, CL and EMP). With these methods, the exact composition of the cement and the composition of the individual mineral grains were determined.

With the result that it is Fe-bearing calcite cement in the collected samples. One reason for the presence of calcite cement could be the increased occurrence of fossil fragments, which may partly dissolve lateron during diagenesis.

This can be explained, that the fossils were transported with a turbidity current in the depth and deposited there. In the thin sections often fossil fragments (such as foraminifera) could be found. However, the sediments were probably deposited below the CCD (calcite compensation depth 3000-5000 m, e.g. Faupl, 1996) and only the fast turbidite sedimentation prevented them from being dissolved.

The cement was formed after the deposition and during the diagenesis of the sandstones. During the diagenesis process the sediment was compacted after deposition. Acidic pore waters dissolved the carbonatic cases and fragments, transported the ions in solution, and carbonate cements were precipitated when the conditions were favorable (high pH).

With microprobe the chemistry of the carbonate cement of two samples (GR 78.5 and GRO3) was analyzed. The composition of 58 wt % CaO and more than 1.4 wt % FeO showed that it is calcite cement with slightly elevated iron content.

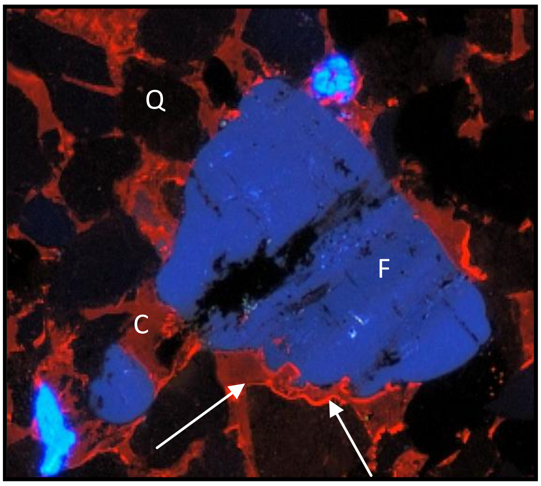

Figure 61 Corroded edge (white arrows) of a feldspar grain in blue (F), calcite cement in orange (C) and a quartz grain in brown (Q)

Thin sections under CL show that the cement (C) begins to corrode individual grains (white arrows in figure 61). This applies to feldspars (F), but also to quartz components (Q) (figure 61).

Figure 61 shows feldspar (blue), quartz (black) and in orange the calcite cement, which fills the former pore space. If these pore spaces had not been filled by cement, it could be that these samples are good reservoir rocks.

The presence of calcite cement was also demonstrated by Rammel (1989) in the Flysch of the Vienna Basin. She has found out that there is in addition to calcite cement also dolomite cement. One reason for the dolomite cement could be that the weathering of Mg-rich minerals resulted in fluids with an elevated Mg content in the underground.

Since there are results of only two samples for the chemical composition, the results might not be fully significant.

Also the composition of glauconite was analyzed. According to Odin and Matter (1981), glauconites are mixed-layer minerals composed of smectite and glauconitic mica. The results of the chemical composition were plotted in a charge distribution diagram after Köster (1977). All samples plot in the glauconite field (figure 52 and figure 53). The stage of maturation of the glauconite is well developed and compact. This demonstrates that the composition of the glauconites in the sandstones is evolved (Odin, 1988) and does not contain expandable smectite anymore.

The glauconite in thin sections has the form of pellets. Glauconite is of marine origin and is in particularly abundant on the upper slope and outer shelf between 200 and 300 m water depth (Odin and Matter, 1981). At water depths of more than 500 m, the green grains are usually interpreted as perigenic being transported downslope (Odin and Fullagar, 1988). Thus it can be assumed that the glauconites in the sandstones were transported.

To determine the composition of the samples, the point counting method was used. The aim of this was to compare the composition of both quarry walls, but also with those of Rammel (1989) from the subsurface of the Vienna basin.

Quartz is the dominant component, as well as glauconite (figure 28).

In the thesis of Rammel (1989) 80 % quartz was counted in a depth of 1187 m.

This correlates well with the quartz content of the outcrop samples (more than 60 %). The amount of glauconite in the same depth (1187 m) is below 8 %.

In general, the results of Rammel and the results of the outcrop show similar values. The samples are from the same formation and from the same tectonic unit, which can be traced into the subsurface of the Vienna Basin.

Sandstone classification after Folk shows that the outcrop samples and the samples of Rammel (1989) are quartz arenites. This is because the Folk classification does not consider components like glauconite. Based on the high content of glauconite in the outcrop samples they should be classified as glauconite bearing quartz arenite.

Based on OMV information from different wells, where core samples were analyzed, the Greifenstein Formation in the Vienna Basin is a fractured reservoir. This means that the hydrocarbons are stored in fractures and not in pore space. This correlates well with the findings of this study, which show that no porosity is present anymore due to tight cementation.

5.3 Porosity and Permeability

The main question in this work was: „Are the rocks suitable to store hydrocarbons?"

The answer is: "Generally no, except for the partially elevated porosity values reaching almost 12 %, which could make it suitable as a gas reservoir."

Applying two different methods of reservoir property determination it could be shown that the outcrop samples have poor features for a reservoir rock.

Most results range between 2-8 % porosity. For comparison, a good sandstone reservoir could have porosities of more than 20 %.

Five samples GR 52, GR 66.7, GRO 1a, GRO 1b and GRO 4 X, have higher porosity values (8-12 %) (figure 54 and figure 62) which are still quite low.

These higher porosity values are still not suitable for being a good oil reservoir, but sufficient for the storage of natural gas.

The permeability values of the sample GR 44 to GR 93 range between 4.5 to 6.5 mD, which are also quite low.

Only three samples (GR 52, GR 66.7 and GRO 1a) show higher permeabilities between 9.04 and 10.01 mD (figure 54 and figure 62). The permeability is positively correlated with porosity. The three samples with higher porosity values had also higher permeabilites.

Generally, no comparison is possible between the measured porosity and permeability values and data from the literature in an upper fan. Therefore, the results are excessively influenced by formation conditions. This is mainly caused by diagenetic effects, which resulted in a tight cementation of the sediments. Individual channel systems may behave different, because they may have been independent systems. Different particle sizes and compositions were found, thus, also different porosity and permeability could be expected.

Usually well sorted sandstones could be a good reservoir for hydrocarbons (Press and Siever, 2008). As in these rock samples, a strong percentage of calcite cement was visible, also accordingly the results of porosity and permeability were quite low.

The conclusion of this master thesis is that the outcrop Strombauamt and the Greifenstein Formation in the subsurface of the Vienna Basin have a very limited potential to reservoir hydrocarbons. Data from the Vienna Basin show that fracturing can enhance reservoir properties.

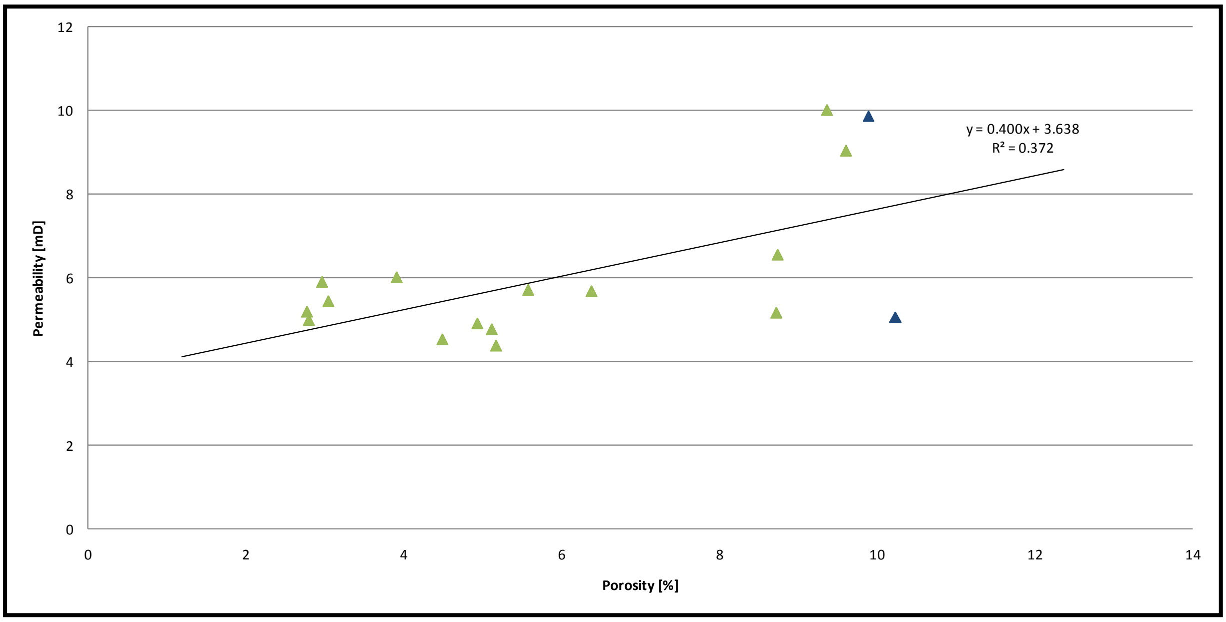

Figure 62 Porosity vs. Permeability of the different samples – In green the samples of the south wall of the quarry and in blue the samples of the east wall

6. Conclusion

The porosities and permeabilities of the sandstone samples collected in the quarry Strombauamt (Lower Austria) are poor. The dominant pore occluding phase is carbonate cement. In addition, the sandstone samples are strongly compacted. Due to this, it can be demonstated, that sandstones of the exposed Greifenstein Formation represent poor reservoirs for the storage of crude oil and gas. The reservoir properties of analogous sediments in the subsurface of the Vienna Basin are enhanced by fractures.

7. References

7.1 Lists of Figures

7.2 Web dictionary

13.02.2012: 12:44 – Picture „Pycnometer“

http://de.wikipedia.org/w/index.php?title=Datei:Pyknometer.jpg&filetimestamp=20100427213155

14.02.2012: 11:03 – Picture „Classification after Folk“

http://www.kgs.ku.edu/Publications/OFR/1988/OFR88_22/05_petr.html

17.02.2012: 09:26 – Information about quarry Strombauamt

http://www.igm-dschungeldorf.at/chronik/hhhirschchronik.pdf

22.02.2012: 16:03 – Wikipedia Flyschzone

http://de.wikipedia.org/wiki/Flyschzone

10.03.2012: 10:59 – Geology map about Höflein an der Donau - GBA (Geologischen Bundesanstalt)

http://geomap.geolba.ac.at/GEO/GEO_main.cfm?Init=false

10.03.2012: 11:00 – Geology from Austria - Rocky Austria

http://www.geologie.ac.at/RockyAustria/geologie_und_landschaft.htm

12.03.2012: 17:27 – Bouma Sequence

http://www.sepmstrata.org/Deepwater/DeepWatClasticSediments.html

17.07.2012: 12:09 – Coordinates of the quarry Strombauamt

http://www.mapcoordinates.net/

7.3 Reference list

Besada A.N., 1996: Sedimentologie der Greifensteiner Schichten im Steinbruch "Strombauamt", Höflein an der Donau (Untereozän, Rhenodanubische Flyschzone, Wienerwald). Unveröffentlichte Diplomarbeit Universität Wien, p. 5-59

Bouma A. H., 1962: Sedimentology of some flysch deposits: A graphic approach to facies interpretation. Elsevier, p. 168

Dengler A.T. & Wilde P., 1983: Turbidity currents generated by hurricane Iwa. Geological Society America Abstr. 15, p. 556

Egger H., 1992: Zur Geodynamik und Paläogeographie des Rhenodanubischen Flysches (Neokom-Eozän der Ostalpen). Zeitung der Geologischen Gesellschaft 143, p. 41-65

Egger H., 1995: Die Lithostratigraphie der Altlengbach-Formation und der Anthering-Formation im Rhenodanubischen Flysch (Ostalpen, Penninikum). Neues Jahrbuch für Geologie und Paläontologie Abhandlungen 196, p. 69-91

Egger H. & Schwerd K., 2008: Stratigraphy and sedimentation rates of Upper Cretaceous deep-water systems of the Rhenodanubian Group (Eastern Alps, Germany). Cretaceous Research 29, p. 405-416

Faupl P., 1996: Tiefwassersedimente und tektonischer Bau der Flyschzone des Wienerwaldes. Berichte der Geologischen Bundesanstalt 33, p. 1-32

Folk R.L., 1968: Petrology of sedimentary rocks. Hephill´s, Austin TX, p. 107

Götzinger G. & Becker H., 1932: Zur geologischen Gliederung des Wienerwaldflysches (Neue Fossilfunde). Jahrbuch der Geologischen Bundesanstalt 82, p. 343-369

Götzinger G., 1954: Die Flyschzone. In: Erläuterung zur geologischen Karte der Umgebung Wien 1:75.000, p. 43-93 (Wien, Geologischen Bundesanstalt)

Grün W., 1984: Die Erschließung von Lagerstätten im Untergrund der alpin-karpatischen Stirnzone, Niederösterreich. Erdöl, Erdgas 100/9, p. 292-295

Grün W., Kittler G., Lauer G., Papp A., & Schnabel W., 1972: Studien in der Unterkreide des Wienerwaldes. Jahrbuch der Geologischen Bundesanstalt 82, p. 103-186

Hösch K., 1985: Zur lithofaziellen Entwicklung der Greifensteiner Schichten in der Flyschzone des Wienerwaldes. Unpublished Thesis University of Vienna, p. 12-92

Jäger R., 1914: Grundzüge der stratigraphischen Gliederung der Flyschbildungen des Wienerwaldes. Mitteilungen der Geologischen Gesellschaft in Wien 7, p. 122-172

Johnson S.D., Flint S., Hinds D., & De Ville Wickens H. (2001): Anatomy, geometry and sequence stratigraphy of basin floor to slope turbidite systems, Tanqua, Karoo, South Africa. Sedimentology 48, p. 987-1023

Köster, H.M., 1977: Die Berechnung kristallchemischer Strukturformeln von 2:1-Schichtsilikaten unter der Berücksichtigung der gemessene Zwischenschichtladungen und Kationenumtauschkapazitäten, sowie die Darstellung der Ladungsverteilung in der Struktur mittels Dreieckskoordinaten. Clay Minerals, 12, p. 45-54

Kuenen Ph. H. & Migliorini C. L., 1950: Turbidity currents as a cause of graded bedding. p. 91-127 (J.Geol. 66)

Marshall, C. E., 1949: The structural interpretation of chemical analyses of the clay minerals. – In: The colloid chemistry of the silicate minerals. Academic Press, New York, p. 159

Marshall D.J., 1988: Cathodoluminescence of Geological Materials. Unwin Hyman Boston, p. 1-146

Mattern F., 2005: Ancient sand-rich submarine fans: depositional systems, models, identification and analysis. Earth-Science Revies 70, p. 167-202

Moore D.M. & Reynolds R.C. Jr., 1997: X-ray Diffraction and the Identification and Analysis of Clay Minerals. Oxford University Press, p. 1-378

Mount J., 1985: Mixed siliciclastic and carbonate sediments: a proposed first-order textural and compositional classification. Sedimentology, 32, p.435-442.

Mutti E. & Ricci Lucchi F., 1975: Turbidite facies and facies associations – Guide to Field trip A-11. International Congress Association of Sedimentologist, p. 21-36

Odin G.S., 1988: Green Marine Clays, Oxford (Elsevier), p. 22-441

Odin G. S. & Fullagar P. D., 1988: Geological significance of the glauconite facies. In Odin, G. S. Green Marine Clays. p. 295-332, Amsterdam (Elsevier).

Odin G. S. & Matter A., 1981: De glauconiarum origine. Sedimentology, 28, p. 611-641

ÖNORM B3121 (Prüfung von Naturstein – Reindichte, Rohdichte, Schüttdichte / Testing of natural stone; density, apparent density, bulk density) 1978

ÖNORM EN 1936 (Prüfverfahren für Naturstein – Bestimmung der Reindichte, der Rohdichte, der offenen Porosität und der Gesamtporosität / Natural stone test methods - Determination of real density and apparent density, and of total and open porosity) 2007

OMV Report 2011/2012: Flysch Vienna Basin- Tectonics, Stratigraphy, Lithofacies, Reservoir Properties and Clay Mineralogie of the Rhenodanubic Flysch Units in the subcrop of the Vienna Basin

Press F. & Siever R., 2008: Allgemeine Geologie (5. Auflage), Spektrum Akademischer Verlag, p. 635

Prey S., 1950: Geologie der Flyschzone im Gebiete des Pernecker Kogels westlich Kirchdorf a.d. Krems (Oberösterreich). Jahrbuch der Geologischen Bundesanstalt 94, p. 93-165

Prey S., 1952: Aufnahme in der Flyschzone auf den Blättern Gmunden-Schafberg (4851) und Kirchdorf-Krems (4852) (Gschliefgraben), sowie den Blättern Ybbs (4754) und Gaming-Mariazell (4854) (Rogatsboden) (Bericht 1951). Verhandlungen der Geologischen Bundesanstalt, p. 41-45

Prey S., 1962: Neue Gesichtspunkte zur Gliederung des Wienerwaldflysches. Verhandlungen der Geologischen Bundesanstalt 1962, p. 258-262

Prey S., 1980: Helvetikum, Flysch und Klippenzone von Salzburg nach Wien – In: R. Oberhauser: Der geologische Aufbau Österreichs – p. 189-217

Rammel M., 1989: Zur Kenntnis der Flyschzone im Untergrund des Wiener Beckens. Die Glaukonitsandsteinserie. Unveröffentlichte Dissertation Universität Wien, p. 8-135

Sauer R., Seifert P. & Wessely G., 1992: Guidebook to Excursion in the Vienna Basin and the Adjacent Alpine-Carpathian Thrustbelt in Austria (Wandertagung 14.-18. September 1992). Mitteilung der Österreichischen Gesellschaft 85, p. 100-137

Schäfer A., 2005: Klastische Sedimente – Fazies und Sequenzstratigraphie, Elsevier Spektrum Akademischer Verlag, ISBN 3-8274-1361-6, p. 303-320

Schnabel W., 1997: Geologische Karte der Republik Österreich 1:50.000, Blatt 58 Baden. Wien, Geologische Bundesanstalt

Tucker M., 1988: Techniques in Sedimentology, Blackwell Scientific Publications. p. 394

Wagreich M., 2008: Lithostratigraphic definition and despositional model of the Hütteldorf Formation (Upper Albian – Turonian, Rhenodanubian Flyschzone, Austria). Austrian Journal of Earth Science 101, p. 70-80

Walker R.G., 1980: Facies Models, Geoscience Canada, Reprint Series 1 (Geological Association Canada, Toronto), p. 211

Wessely G., 2006: Geologie der Österreichischen Bundesländer – Niederösterreich. Geologische Bundesanstalt Wien, ISBN 3-85316-23-9, p. 85-103

Wortmann U.G., Herrle J.O. & Weissert H., 2004: Altered carbon cycling and coupled changes in early Cretaceous weathering patterns: Evidence from integrated carbon isotopes and sandstone records of the western Tethys. Early Planetary Science Letters 220, p. 69-82

8. Appendix

8 .1 Results of the point counting

	Quartz				Feldspar		Mica				
Sample	Poly Quartz	Mono Quartz	Glauconite	Cement	Orthoclase	Plagioclase	Muscovite	Biotite	Rock fragments	Fossils	Lithology
A3(2)	115	189	63	12	2	0	7	7	4	1	Glauconite-bearing
%	28,7	47,2	15,7	3	0,5	0	1,7	1,7	1	0,2	Quartz arenite
A5(1)	106	189	81	5	2	0	6	4	6	1	Glauconite-bearing
%	26,5	47,2	20,2	1,2	0,5	0	1,5	1	1,5	0,2	Quartz arenite
N4	107	188	79	12	1	0	2	4	7	0	Conglomerate
%	26,7	47	19,7	3	0,2	0	0,5	1	1,7	0	
H2	85	173	103	21	1	0	4	7	5	1	Glauconite-bearing
%	21,2	43,2	25,7	5,2	0,2	0	1	1,7	1,2	0,2	Quartz arenite
H6	84	166	110	17	2	0	6	8	6	1	Glauconite-bearing
%	21	41,5	27,5	4,2	0,5	0	1,5	2	1,5	0,2	Quartz arenite
H10	105	164	97	9	2	0	9	8	4	2	Glauconite-bearing
%	26,2	41	24,2	2,2	0,5	0	2,2	2	1	0,5	Quartz arenite
D3(5)	100	187	82	9	3	0	5	5	6	3	Glauconite-bearing
%	25	46,7	20,5	2,2	0,7	0	1,2	1,2	1,5	0,7	Quartz arenite
D5α	100	201	54	33	2	0	3	2	4	1	Glauconite-bearing
%	25	50,2	13,5	8,2	0,5	0	0,7	0,5	1	0,2	Quartz arenite
D5c	98	204	76	8	2	0	6	3	3	0	Glauconite-bearing
%	24,5	51	19	2	0,5	0	1,5	0,7	0,7	0	Quartz arenite

GR 44	84	185	49	2	3	0	4	5	6	1	Conglomerate
%	21	46,25	12,25	0,5	0,75	0	1	1,25	1,5	0,25	
GR 46	95	205	71	8	1	0	4	5	8	3	Conglomerate
%	23,75	51,25	17,75	2	0,25	0	1	1,25	2	0,75	
GR 51	86	193	96	2	0	0	6	9	6	2	Glauconite-bearing
%	21,5	48,25	24	0,5	0	0	1,5	2,25	1,5	0,5	Quartz arenite
GR 52	69	213	85	4	1	0	9	10	6	3	Glauconite-bearing
%	17,25	53,25	21,25	1	0,25	0	2,25	2,5	1,5	0,75	Quartz arenite
GR 66,7	92	190	78	14	2	0	1	6	12	5	Glauconite-bearing
%	23	47,5	19,5	3,5	0,5	0	0,25	1,5	3	1,25	Quartz arenite
GR 68	123	165	78	6	0	0	5	12	7	4	Glauconite-bearing
%	30,75	41,25	19,5	1,5	0	0	1,25	3	1,75	1	Quartz arenite
GR 69	102	190	65	18	2	0	7	7	8	1	Conglomerate
%	25,5	47,5	16,25	4,5	0,5	0	1,75	1,75	2	0,25	
GR 71,5	75	188	63	58	2	0	4	3	4	3	Conglomerate
%	18,75	47	15,75	14,5	0,5	0	1	0,75	1	0,75	
GR 73,5	90	143	67	85	1	0	5	3	3	3	Glauconite-bearing
%	22,50	35,75	16,75	21,25	0,25	0	1,25	0,75	0,75	0,75	Quartz arenite
GR 78,5	89	149	51	97	1	0	4	2	2	5	Glauconite-bearing
%	22,25	37,25	12,75	24,25	0,25	0	1	0,50	0,50	1,25	Quartz arenite
GR 80,5	56	179	53	91	2	0	5	6	3	5	Glauconite-bearing
%	14	44,75	13,25	22,75	0,5	0	1,25	1,5	0,75	1,25	Quartz arenite
GR 83,5	81	138	81	80	1	0	6	5	4	4	Glauconite-bearing
%	20,25	34,5	20,25	20	0,25	0	1,5	1,25	1	1	Quartz arenite

GR 86	117	160	83	17	1	0	4	5	6	7	Glauconite-bearing
%	29,25	40	20,75	4,25	0,25	0	1	1,25	1,5	1,75	Quartz arenite
GR 93	99	173	101	7	1	0	5	5	3	6	Glauconite-bearing
%	24,75	43,25	25,25	1,75	0,25	0	1,25	1,25	0,75	1,5	Quartz arenite
X1	95	179	91	5	1	0	12	10	5	2	Glauconite-bearing
%	23,7	44,7	22,7	1,2	0,2	0	3	2,5	1,2	0,5	Quartz arenite
GRO 1a	79	170	133	1	1	0	4	3	5	4	Glauconite-bearing
%	19,7	42,5	33,2	0,2	0,2	0	1	0,7	1,2	1	Quartz arenite
GRO 1b	88	173	115	2	1	0	4	5	10	2	Glauconite-bearing
%	22	43,25	28,75	0,5	0,25	0	1	1,25	2,5	0,5	Quartz arenite
GRO 3	64	154	103	58	1	0	4	2	6	8	Glauconite-bearing
%	16	38,5	25,75	14,5	0,25	0	1	0,5	1,5	2	Quartz arenite
GRO 3X	66	176	106	31	1	0	5	4	7	4	Glauconite-bearing
%	16,5	44	26,5	7,75	0,25	0	1,25	1	1,75	1	Quartz arenite
GRO 4X	79	185	103	14	0	0	4	3	8	4	Glauconite-bearing
%	19,75	46,25	25,75	3,5	0	0	1	0,75	2	1	Quartz arenite

8.2 Results of the porosity measuring with immersion weighing

Sample	Dry mass of the sample [g] 24h	48h	Average	Mass of water-saturated body [g] 24h	48h	Average	mass of the body dipped in water [g] 24h	48h	Average	Bulk density	Open porosity	%
A3(2)	265,7	265,6	265,65	272,1	272,6	272,35	161,1	161,6	161,35	2,39	0,06	6,0
A5(1)	344,05	344	344,03	353,8	354,15	353,98	208,05	208,9	208,475	2,36	0,07	6,8
N4	343,1	342,9	343	350	350,1	350,05	212,6	212,1	212,35	2,49	0,05	5,1
H2	823,5	823,4	823,45	841	842,1	841,55	502,8	504,3	503,55	2,44	0,05	5,4
H6	507,7	507,8	507,75	512,9	512,8	512,85	317,3	317,1	317,2	2,60	0,03	2,6
H10	944,7	944,8	944,75	966,7	967,4	967,05	580	579,6	579,8	2,44	0,06	5,8
GR 44	1513,2	1513,1	1513,15	1533,9	1534,6	1534,25	941,6	942	941,8	2,55	0,04	3,6
GR 46	1067,3	1067,2	1067,25	1093,4	1094,5	1093,95	656,3	657,15	656,725	2,44	0,06	6,1
GR 51	1071,55	1071,4	1071,475	1109,6	1110,2	1109,9	652,9	653,8	653,35	2,35	0,08	8,4
GR 52	1047,1	1047,2	1047,15	1083,3	1083,5	1083,4	636,2	639,2	637,7	2,35	0,08	8,1
D3(5)	349,7	349,7	349,7	358,1	358,3	358,2	214,5	214,7	214,6	2,44	0,06	5,9
D5α	164,4	164,5	164,45	167,1	167,1	167,1	102,2	102,7	102,45	2,54	0,04	4,1
D5c	329,15	329,3	329,225	339,8	339,85	339,825	200,5	201,1	200,8	2,37	0,08	7,6
GR 66,7	964,2	964,2	964,2	997,7	997,9	997,8	586,1	587	586,55	2,34	0,08	8,2
GR 68	1302,1	1302,1	1302,1	1350,8	1351,3	1351,05	803,5	805,3	804,4	2,38	0,09	9,0
GR 69	765,9	765,95	765,925	785	784,5	784,75	471,9	472,1	472	2,45	0,06	6,0
GR 71,5	403,7	403,6	403,65	410	410,2	410,1	251,9	252	251,95	2,55	0,04	4,1
GR 73,5	677,5	677,5	677,5	687,2	687	687,1	423,7	424	423,85	2,57	0,04	3,6
GR 75,5	1104,5	1104,2	1104,35	1126,5	1127	1126,75	685,7	685,7	685,7	2,50	0,05	5,1
GR 78,5	918,9	918,6	918,75	930,6	930,5	930,55	573,4	573,4	573,4	2,57	0,03	3,3
GR 80,5	1215,8	1215,7	1215,75	1230,1	1230,1	1230,1	759	759	759	2,58	0,03	3,0

GR 83,5	1997,8	1996,6	1997,2	2041,4	2043,3	2042,35	1246	1246	1246	2,51	0,06	5,7
GR 86	983,3	983,1	983,2	1003,8	1004,2	1004	612,9	612,9	612,9	2,51	0,05	5,3
GR 93	2514	2512,7	2513,35	2566,9	2567,6	2567,25	1573,5	1573,5	1573,5	2,53	0,05	5,4
X1	252,05	252,1	252,075	259,7	259,65	259,675	154,75	155,25	155	2,41	0,07	7,3
GRO 1a	782,8	782,7	782,75	812,7	813,3	813	481,2	481,2	481,2	2,36	0,09	9,1
GRO 1b	1837,6	1837,1	1837,35	1909,8	1911,2	1910,5	1129,55	1129,55	1129,55	2,35	0,09	9,4
GRO 3	1292,9	1291,8	1292,35	1300,4	1301,5	1300,95	809,25	809,25	809,25	2,63	0,02	1,7
GR 3X	920,7	920,6	920,65	938,9	938,7	938,8	578,3	578,4	578,35	2,55	0,05	5,0
GR 4X	1805,7	1805,6	1805,65	1900,8	1901,6	1901,2	1125,9	1126,7	1126,3	2,33	0,12	12,3

8.3 Results of the porosity measuring with pycnometer

Sample	Bulk density	A	B	C	D	Net density	Porosity	%
A3(2)	2,39	30,8675	81,5981	34,0765	83,5933	2,64	0,09476	9,5
A5(1)	2,37	30,8675	81,5981	34,2038	83,64865	2,59	0,08857	8,9
N4	2,49	30,8675	81,5981	34,2651	83,6666	2,56	0,02558	2,6
H2	2,44	30,8675	81,5981	34,0292	83,4932	2,50	0,02402	2,4
H6	2,60	30,8675	81,5981	34,0077	83,5759	2,70	0,03934	3,9
H10	2,44	30,8675	81,5981	35,0938	84,1451	2,52	0,03062	3,1
GR 44	2,55	30,8675	81,5981	35,0926	84,2081	2,62	0,02368	2,4
GR 46	2,44	30,8675	81,5981	35,1904	84,2394	2,57	0,05047	5,0
GR 51	2,35	30,8675	81,5981	35,2715	84,2956	2,58	0,09060	9,1
GR 52	2,35	30,8675	81,5981	35,0409	84,1919	2,64	0,11075	11,1
D3(5)	2,44	30,8675	81,5981	34,8202	84,0088	2,56	0,04998	5,0
D5α	2,40	30,8675	81,5981	34,2094	83,6282	2,55	0,05793	5,8
D5c	2,37	30,8675	81,5981	34,29085	83,67845	2,55	0,07024	7,0
GR 66,7	2,34	30,8675	81,5981	35,2091	84,2834	2,62	0,10556	10,6
GR 68	2,38	30,8675	81,5981	35,5277	84,4679	2,60	0,08487	8,5
GR 69	2,45	30,8675	81,5981	35,7717	84,6347	2,63	0,06738	6,7
GR 71,5	2,55	30,8675	81,5981	35,0341	84,1933	2,65	0,03741	3,7
GR 73,5	2,57	30,8675	81,5981	35,5782	84,5231	2,64	0,02442	2,4
GR 75,5	2,50	30,8675	81,5981	35,9923	84,7816	2,64	0,05151	5,2
GR 78,5	2,57	30,8675	81,5981	35,086	84,2135	2,63	0,02243	2,2
GR 80,5	2,58	30,8675	81,5981	35,5666	84,5227	2,65	0,02548	2,5
GR 83,5	2,51	30,8675	81,5981	35,3026	84,3233	2,59	0,03309	3,3
GR 86	2,51	30,8675	81,5981	35,1275	84,2406	2,63	0,04547	4,5
GR 93	2,53	30,8675	81,5981	35,3787	84,4133	2,66	0,04916	4,9
X1	2,41	30,8675	81,5981	34,85625	84,04025	2,58	0,06555	6,6
GRO 1a	2,36	30,8675	81,5981	34,5534	83,888	2,64	0,10651	10,7
GRO 1b	2,35	30,8675	81,5981	35,71	84,6108	2,65	0,11100	11,1
GRO 3	2,63	30,8675	81,5981	35,2831	84,3441	2,64	0,00619	0,6
GR 3X	2,55	30,8675	81,5981	33,2193	83,06238	2,65	0,03611	3,6
GR 4X	2,33	30,8675	81,5981	35,0107	84,1838	2,66	0,12405	12,4

A	weight of the pycnometer	[g]
B	weight of the pycnometer with water (volume)	[g/cm^3]
C	weight of the pycnometer with ground sample	[g]
D	Weight of the pycnometer with water and ground sample	[g/cm^3]

8.4 Results of the permeability measuring with micropermeameter

Sample	Permeability [mD]
GR 44	5,91
GR 46	5,72
GR 51	6,56
GR 52	9,04
GR 66,7	10,01
GR 68	5,18
GR 69	5,69
GR 71,5	6,02
GR 73,5	5,45
GR 75,5	4,78
GR 78,5	5,20
GR 80,5	5,00
GR 83,5	4,54
GR 86	4,92
GR 93	4,39
GRO 1a	9,88
GRO 1b	5,06

8.5 Results of the XRD method

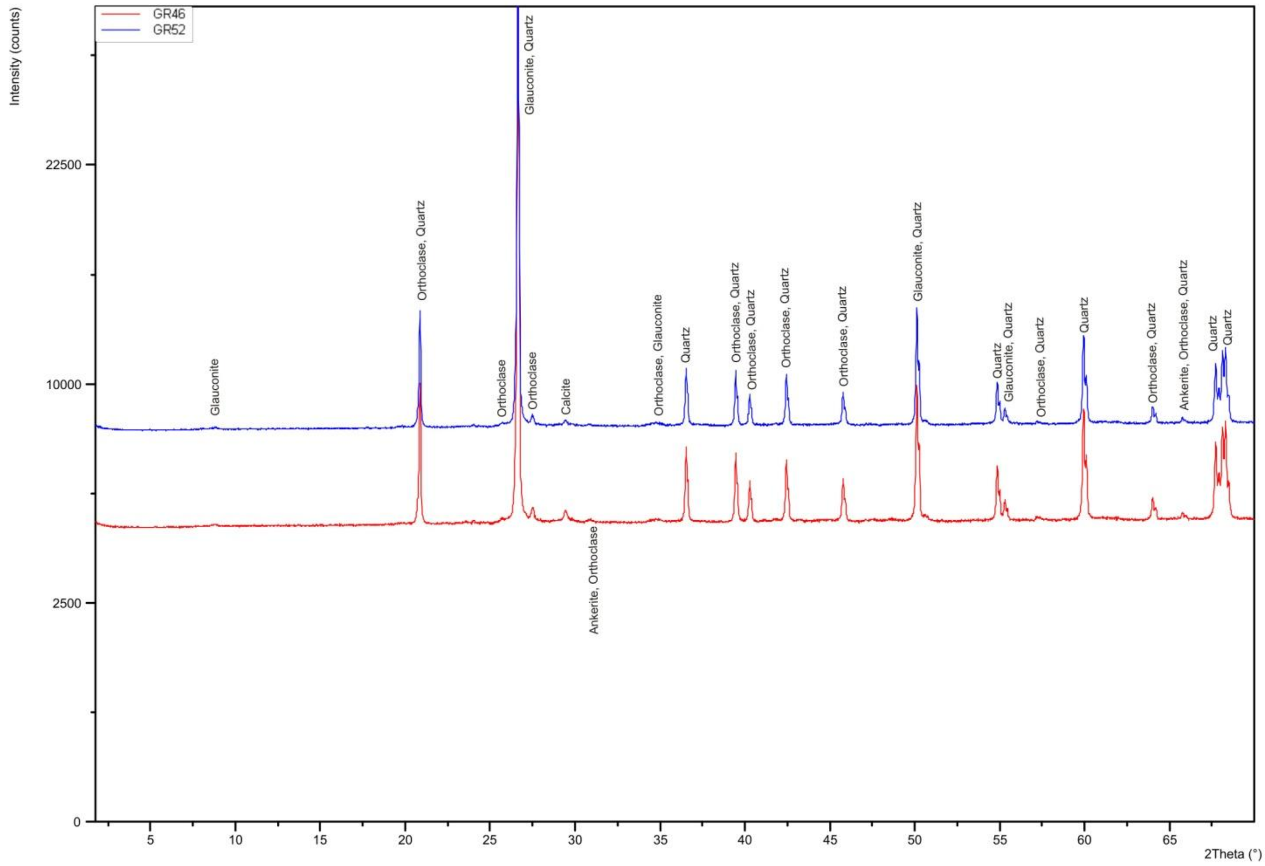

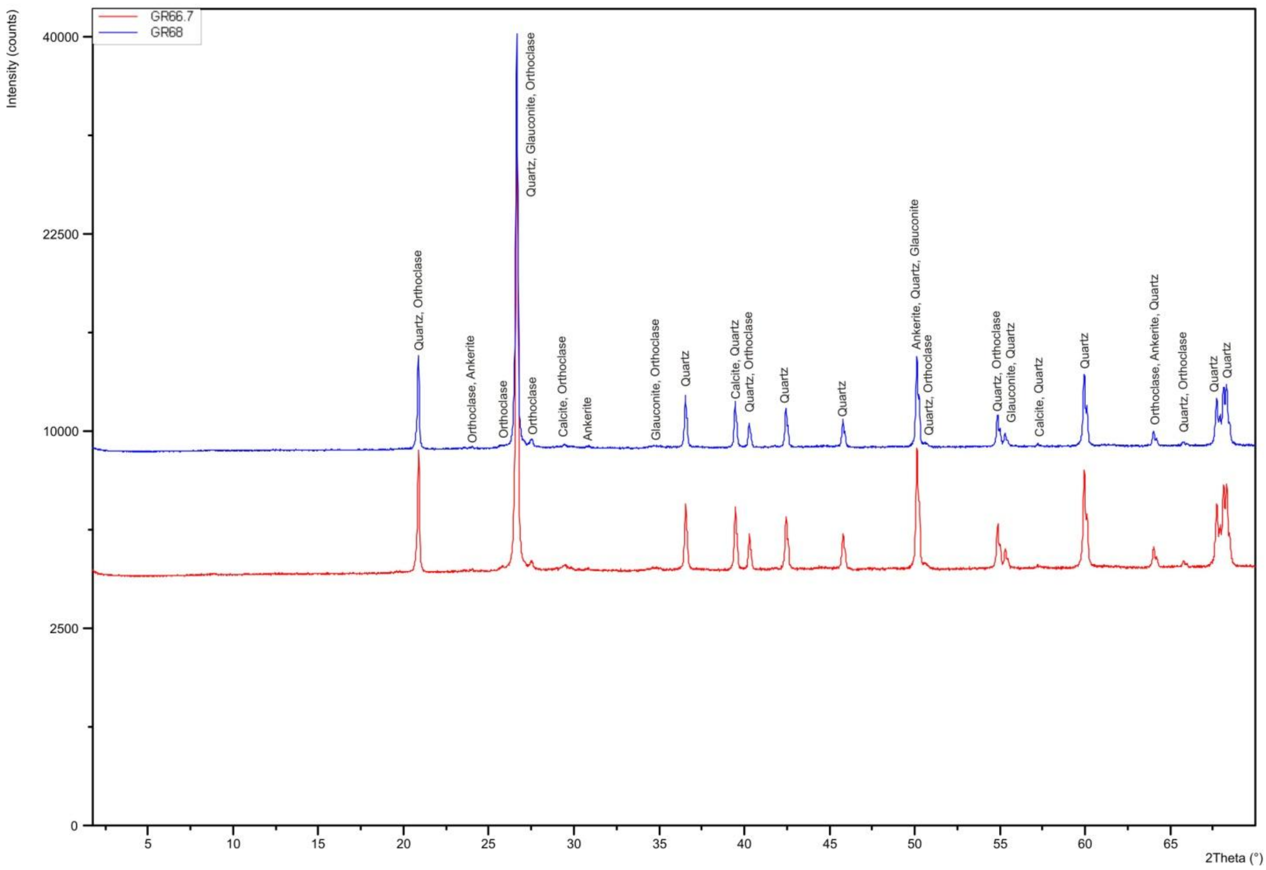

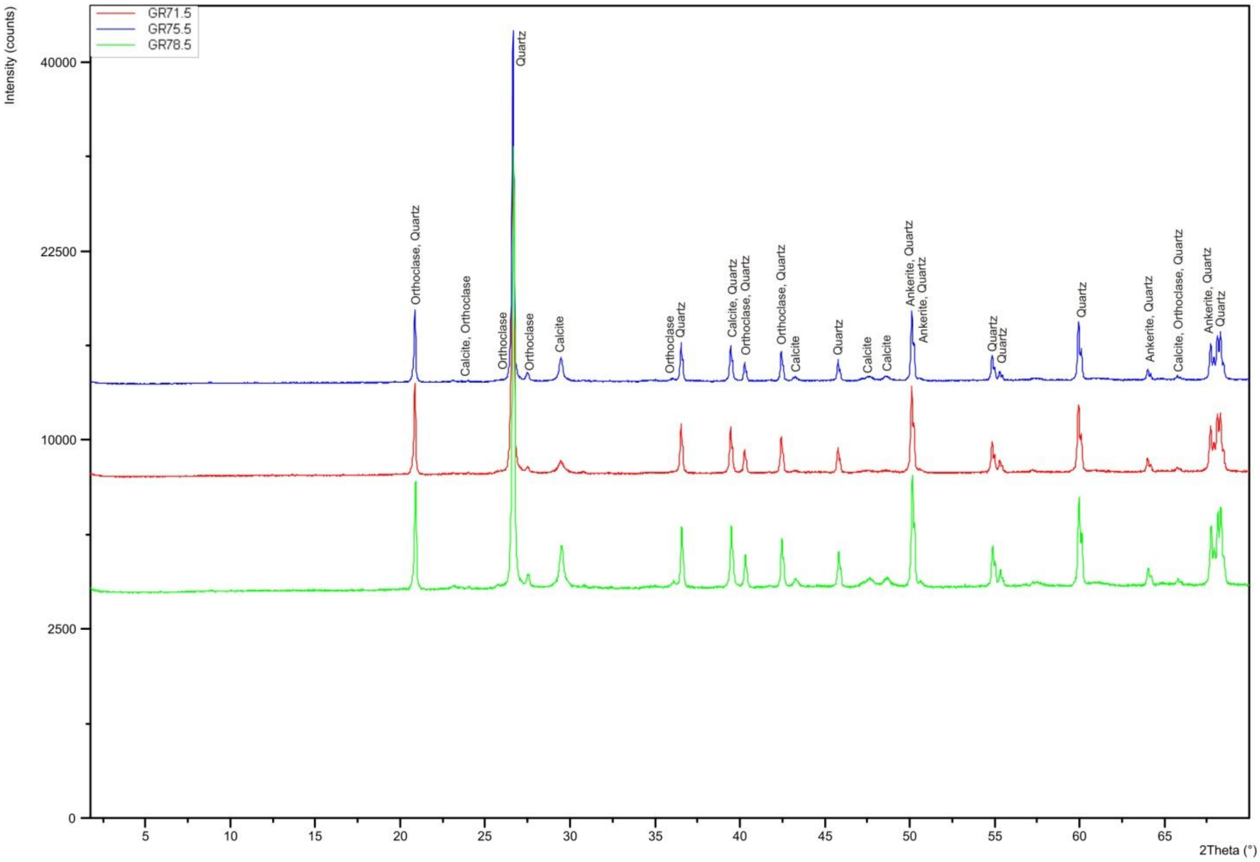
GR71.5
GR75.5
GR78.5
Intensity (counts)
40000
22500
10000
2500
0
5
10
15
20
25
30
35
40
45
50
55
60
65
2Theta (°)
Quartz
Orthoclase, Quartz
Calcite, Orthoclase
Orthoclase
Orthoclase
Calcite
Orthoclase
Quartz
Calcite, Quartz
Orthoclase, Quartz
Orthoclase, Quartz
Calcite
Quartz
Calcite
Calcite
Ankerite, Quartz
Ankerite, Quartz
Quartz
Quartz
Quartz
Ankerite, Quartz
Calcite, Orthoclase, Quartz
Ankerite, Quartz
Quartz

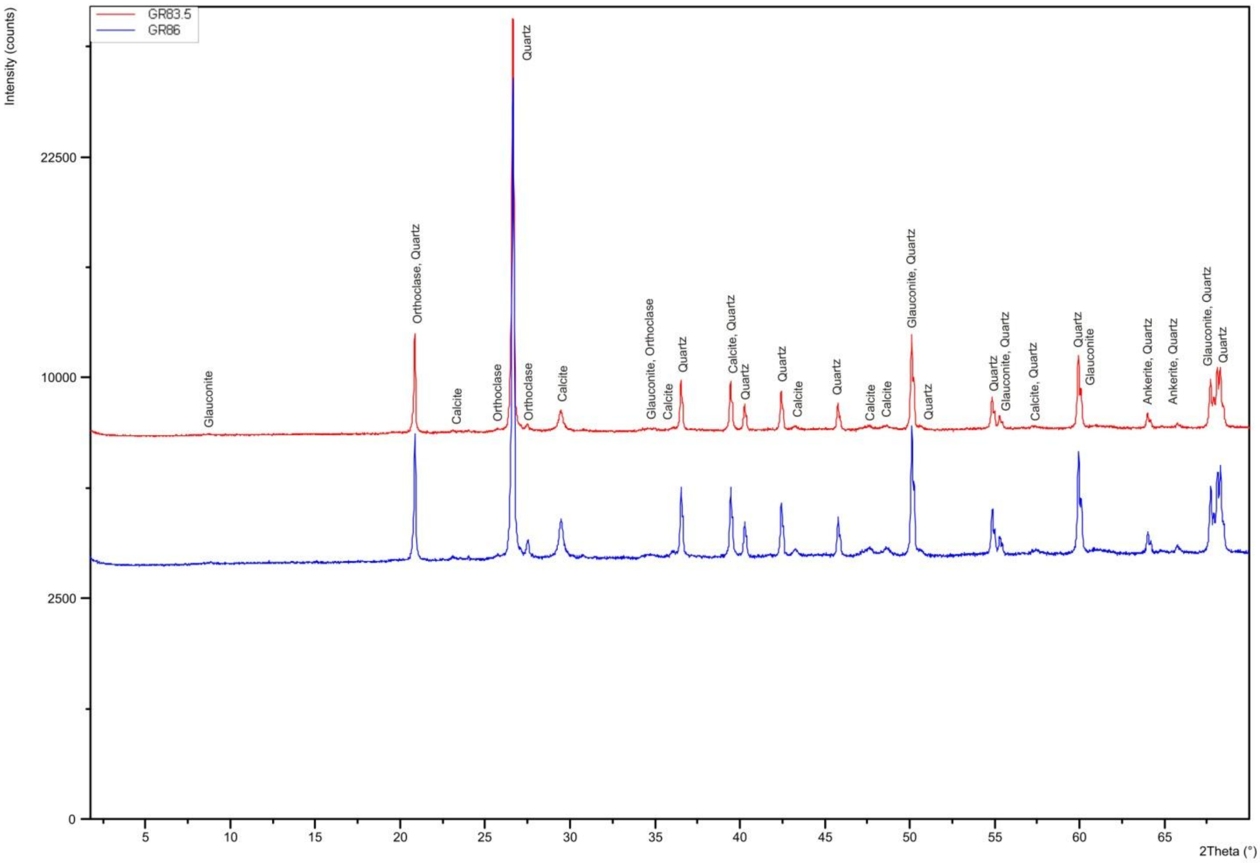
GR83.5
GR86
Intensity (counts)
22500
10000
2500
0
5
10
15
20
25
30
35
40
45
50
55
60
65
2Theta (°)
Quartz
Glauconite
Orthoclase, Quartz
Calcite
Orthoclase
Orthoclase
Calcite
Glauconite, Orthoclase
Calcite
Quartz
Calcite, Quartz
Quartz
Quartz
Calcite
Quartz
Calcite
Calcite
Glauconite, Quartz
Quartz
Quartz
Glauconite, Quartz
Calcite, Quartz
Quartz
Glauconite
Ankerite, Quartz
Ankerite, Quartz
Glauconite, Quartz
Quartz

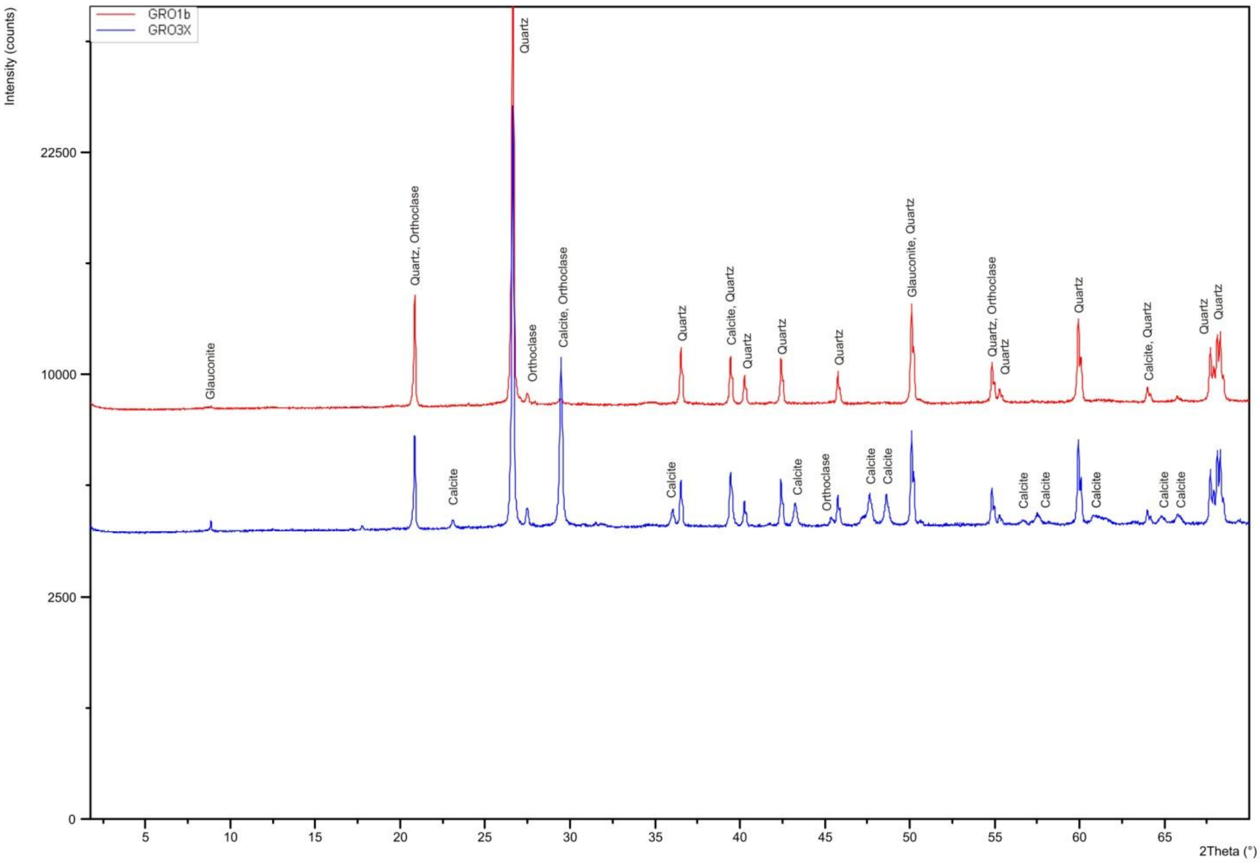
GRO1b
GRO3X
Intensity (counts)
22500
10000
2500
0
5
10
15
20
25
30
35
40
45
50
55
60
65
2Theta (°)
Quartz
Quartz, Orthoclase
Glauconite
Orthoclase
Calcite, Orthoclase
Calcite, Quartz
Glauconite, Quartz
Quartz, Orthoclase
Calcite, Quartz
Calcite
Orthoclase

8.6 Results of the cement analysis with electron microprobe

	DataSet/Point	Na_2O	SiO_2	MgO	Al_2O_3	K_2O	CaO	MnO	FeO
GRO 3	1 / 1 .	0,004	0,03	0,405	0,005	0	59,231	0,127	1,639
	2 / 1 .	0,034	0,053	0,37	0,014	0	59,158	0,136	1,493
	3 / 1 .	0,008	0,014	0,393	0	0,017	60,649	0,148	1,833
	4 / 1 .	0,012	0,01	0,457	0,001	0	60,52	0,163	1,837
	5 / 1 .	0	0,021	0,447	0,002	0	58,918	0,136	1,764
	6 / 1 .	0,064	0,081	0,453	0,024	0	59,625	0,149	1,753
	7 / 1 .	0	0,09	0,518	0,015	0	60,114	0,166	1,987
	8 / 1 .	0,009	0,053	0,434	0,015	0,012	56,838	0,149	1,837
	9 / 1 .	0,125	0,109	0,37	0,005	0	57,624	0,214	1,682
	10 / 1 .	0,199	0,103	0,424	0,01	0	59,721	0,172	1,709
	11 / 1 .	0,103	0,093	0,437	0,003	0,007	59,635	0,146	1,804
	12 / 1 .	0,028	0,037	0,458	0,022	0	59,955	0,177	1,827
	13 / 1 .	0	0,128	0,376	0,008	0,002	60,574	0,157	1,401
	14 / 1 .	0	0,012	0,348	0,037	0	52,636	0,029	0,136
	22 / 1 .	0	0,021	0,536	0,069	0,001	58,981	0,182	1,977
	23 / 1 .	0,14	0,099	0,438	0,009	0,007	59,31	0,183	1,8
	24 / 1 .	0	0,008	0,465	0,007	0,001	58,284	0,128	1,712
	25 / 1 .	0,038	0,12	0,376	0,008	0,003	58,812	0,124	1,687
	26 / 1 .	0,122	0,033	0,473	0,031	0	57,696	0,115	1,81
	27 / 1 .	0	0,095	0,394	0,083	0,003	58,946	0,076	1,545
	28 / 1 .	0,041	0,056	0,442	0,048	0	58,863	0,17	1,749
	29 / 1 .	0,08	0,074	0,481	0,081	0,002	58,713	0,102	1,814

	30 / 1 .	0	0,481	0,263	0,298	0,026	55,541	0,049	0,65
	31 / 1 .	0	0,008	0,498	0,008	0,009	59,833	0,164	1,944
	Mean Value Centre	**0,03**	**0,04**	**0,45**	**0,02**	**0,00**	**59,02**	**0,15**	**1,80**
	Mean Value Rim	**0,05**	**0,07**	**0,39**	**0,02**	**0,00**	**54,40**	**0,13**	**1,56**
GRO 78.5	38 / 1 .	0	0,016	0,527	0	0,004	60,826	0,112	1,688
	39 / 1 .	0,039	0,082	0,593	0	0	60,525	0,16	1,866
	40 / 1 .	0	0,032	0,378	0,034	0	58,51	0,054	1,286
	41 / 1 .	0	0,076	0,343	0,079	0	55,146	0,071	0,989
	42 / 1 .	0	0,059	0,323	0,027	0	61,044	0,098	1,313
	43 / 1 .	0,003	0,097	0,486	0,001	0	59,78	0,146	1,744
	44 / 1 .	0,062	0,117	0,499	0,047	0	60,105	0,103	1,828
	45 / 1 .	0	0,068	0,551	0,009	0,002	59,571	0,133	1,685
	46 / 1 .	0	0,003	0,568	0,052	0	60,062	0,108	1,898
	47 / 1 .	0	0,024	0,177	0,017	0,008	53,992	0,087	0,688
	48 / 1 .	0,043	0,07	0,49	0,02	0,002	59,858	0,115	1,799
	49 / 1 .	0	0,038	0,392	0,028	0,004	60,776	0,105	1,655
	50 / 1 .	0,02	0,133	0,586	0	0	59,242	0,128	1,737
	64 / 1 .	0,011	0,031	0,533	0,014	0	57,855	0,145	1,568
	65 / 1 .	0	0,025	0,515	0,018	0,002	58,572	0,103	1,492
	66 / 1 .	0	0,102	0,545	0	0,009	57,784	0,121	1,581
	67 / 1 .	0,019	0,047	0,525	0,023	0,003	59,524	0,078	1,624
	68 / 1 .	0,157	0,101	0,356	0,017	0,008	58,526	0,087	1,245
	69 / 1 .	0,024	0,024	0,361	0,032	0,014	55,995	0,109	1,091
	70 / 1 .	0	0,108	0,564	0,044	0,009	59,59	0,13	1,666

71 / 1 .	0,02	0,244	0,545	0,026	0,004	60,112	0,127	1,913
72 / 1 .	0	0,023	0,353	0,004	0	53,513	0,068	1,014
73 / 1 .	0	0,049	0,381	0,02	0	58,91	0,097	1,131
74 / 1 .	0	0,081	0,517	0,009	0,005	58,987	0,101	1,648
75 / 1 .	0,147	0,078	0,503	0	0	59,84	0,126	1,727
76 / 1 .	0,066	0,376	0,528	0,224	0,008	56,858	0,099	1,713
77 / 1 .	0,053	0,031	0,268	0,023	0,002	54,123	0,024	0,758
78 / 1 .	0,198	0,103	0,506	0,019	0,005	58,789	0,079	1,542
79 / 1 .	0	0,006	0,327	0,015	0	59,345	0,078	1,279
80 / 1 .	0,285	2,094	0,314	0,01	0	56,898	0,102	1,266
81 / 1 .	0,136	0,032	0,37	0	0	59,185	0,082	1,314
82 / 1 .	0,188	0,169	0,413	0,022	0,01	58,068	0,108	1,542
83 / 1 .	0,183	0,251	0,403	0,12	0,034	57,166	0,08	1,804
84 / 1 .	0,022	0,136	0,568	0,02	0	58,606	0,165	1,612
Mean Value Centre	**0,03**	**0,06**	**0,43**	**0,03**	**0,00**	**58,56**	**0,10**	**1,46**
Mean Value Rim	**0,08**	**0,29**	**0,48**	**0,04**	**0,00**	**58,27**	**0,11**	**1,55**

Eidesstattliche Erklärung

Ich versichere hiermit, dass ich die vorliegende Arbeit selbstständig verfasst und keine anderen, als die im Literaturverzeichnis angegebenen, Quellen benutzt habe.

Die Zeichnungen oder Abbildungen in dieser Arbeit sind von mir selbst erstellt worden oder mit einem entsprechenden Quellennachweis versehen.

Diese Arbeit ist in gleicher oder ähnlicher Form noch bei keiner anderen Prüfungsbehörde eingereicht worden.

Wien, Jänner 2013

Curriculum Vitae

Persönliche Daten:

Name: Raffaela Löffler

E-Mail: raffaela.loeffler@gmx.at

Geburtsdatum: 29.04.1985

Geburtsort: Wien

Staatsbürgerschaft: Österreich

Schulische Laufbahn:

2001- 2006	HLA für Umwelt und Wirtschaft im Ypsertal
1995- 2001	Gymnasium der Stadt Wien
1991-1995	Volkschule Grünentorgasse

Universitätsausbildung:

2006-2007	Universität Wien: Studium Biologie
2007-2010	Universität Wien: Bachelorstudium Erdwissenschaften Titel der Bachelorarbeit: ”Chesapeake Bay Impaktstruktur – Petrographische Analyse von Exmore Breccien“ Betreuer: Univ.- Prof. Dr. Christian Köberl
2010-2013	Universität Wien: Masterstudium Erdwissenschaften Titel der Masterarbeit: „Reservoir properties of glauconite sandstones (Greifenstein Formation) in the quarry Strombauamt“ Betreuerin: Ao. Univ. Prof. Mag. Dr. Susanne Gier

Sprachkenntnisse:

Englisch: Gut in Wort und Schrift

Französisch: Schulkenntnisse

Berufserfahrungen und Ferialjobs:

Seit August 2006	Geringfügige Angestellte bei Metro Cash&Carry Langenzersdorf
Juli 2009	OMV Auersthal
Juli, August 2008	OMV Exploration & Produktion Raffinerie Schwechat und OMV Auersthal
September 2007	OMV Exploration & Produktion Raffinerie Schwechat

Juli 2005	OMV Exploration & Produktion Raffinerie Schwechat
Juni, Juli, August 2004	OMV Exploration & Produktion Raffinerie Schwechat
Juli 2003:	Raiffeisen Zentralbank Landstraße
Juli 2002:	Raiffeisen Zentralbank Landstraße

Qualifikationen:

Gefahrgutbeauftragte

Qualitätsbeauftragte für kleine und mittlere Betriebe

Sicherheitsvertrauensperson

B - Führerschein

Sprengbefugte (Sprengkurs TU-Wien)

EDV- Kenntnisse:

Windows Office (Word, Excel, Front Page, Power Point, Acsess) MathLab, Tectonics FP, Modflow, PhreeqC, Mathematica, Photoshop, CorelDraw, AutoCad